Sensing Inorganic Phosphate Starvation by the Phosphate-Responsive (PHO) Signaling Pathway of Saccharomyces cerevisiae

Sensing Inorganic Phosphate Starvation by the Phosphate-Responsive (PHO) Signaling Pathway of *Saccharomyces cerevisiae*

A dissertation presented

by

Joonhyuk Choi

to

The Department of Chemistry and Chemical Biology

in partial fulfillment of the requirements

for the degree of

Doctor of Philosophy

in the subject of

Chemistry

Harvard University

Cambridge, Massachusetts

April 2013

Dissertation Advisor: Professor Erin K. O'Shea **Author: Joonhyuk Choi**

Sensing Inorganic Phosphate Starvation by the Phosphate-Responsive (PHO) Signaling Pathway of *Saccharomyces cerevisiae*

Abstract

Inorganic phosphate (P_i) is an essential nutrient whose intracellular levels are maintained by the PHO pathway in *Saccharomyces cerevisiae*. P_i limitation triggers upregulation of the PHO genes whose gene products primarily function to counterbalance the P_i deficiency. Despite a growing catalogue of genes that are involved in signaling of the PHO pathway, little is known about how cells actually sense P_i limitation.

To better characterize the P_i sensing mechanism, I exploited two comprehensive and orthogonal approaches: 1) genome-wide genetic screening to identify novel genes involved in signaling P_i limitation through the PHO pathway and characterization of genetic interactions among these genes and 2) liquid chromatography /mass spectrometry (LC/MS)-based metabolic profiling to characterize the metabolomic response to changes in P_i availability.

In genome-wide screening, I found that the *aah1* mutant constitutively activated the PHO pathway and showed that *AAH1* is involved in regulating PHO pathway activity. Moreover, I identified several novel genetic interactions of genes involved in inositol

polyphosphate metabolism with those involved in purine metabolism and mitochondrial fatty acid biosynthesis.

Through metabolomic profiling, I showed that all adenine nucleotides were downregulated in the constitutively induced *ado1*, *adk1*, and *aah1* mutants in high P_i as well as in the wild type strain in low P_i. These observations led to the hypothesis that downregulation of adenine nucleotides triggers activation of the PHO pathway. However, I find that decreases in adenine nucleotides appear to be the consequence of downregulation of glycolysis and of the pentose phosphate pathway rather than an activation signal for the PHO pathway.

Among all the detected metabolites, S-adenosyl-L-homocysteine (SAH) responded the most quickly and significantly to changes in P_i concentration. It was known that SAH is an inhibitor of *de novo* synthesis of phosphatidylcholine (PC). I showed that overall PC levels were downregulated in low P_i, suggesting that phospholipid metabolism is downregulated in low P_i conditions. Furthermore, I observed that exogenous SAH induces activation of the PHO pathway in high P_i implying a possible role of SAH as an initiating activation signal of the PHO pathway.

Table of Contents

Abstract …… iii

Acknowledgements ……..…….. vii

Chapter 1. Introduction to the Phosphate-responsive Signaling (PHO) Pathway in *Saccharomyces cerevisiae*……. 1

Chapter 2. Genome-wide Genetic Screening to Identify Novel Genes Involved in Signaling of the PHO Pathway …… 10

Rationale ……..... 11

Results...…… 13

Discussion ……..... 27

Materials and methods ……. 33

Chapter 3. Metabolomic Measurements in Response to Changes in P_i Availability ……... 41

Rationale…… 42

Results...…… 43

Discussion……..... 63

Materials and methods…….. 67

Chapter 4. Conclusion…….. 72

Appendix 1. Supplementary Tables..……..……. 76

References ……..…… 108

Acknowledgements

I would not be able to finish my doctoral training if it were not for the support of people I met at Harvard. First and foremost, I would like to thank my adviser Dr. Erin K. O'Shea for giving me an opportunity to study biology even though I did not have any background in biology when I joined her lab. Our discussions helped me to think about my projects very critically and develop an ability to solve problems. I believe that the training I got from Erin will be tremendously useful as I pursue my scientific career in the future.

Moreover, I have been very lucky to have all our lab members during my graduate studies. They are very talented people and have been intellectually stimulating me to focus on right questions and solve numerous problems I encountered in my projects. Especially, Harold Kim helped me a lot to learn how to use fluorescence microscope and supported me when I experienced some difficulties during my graduate studies. Endless discussions with Joe Markson at late night were precious experiences. We talked about all kinds of topics including not only our own projects but also other interesting sciences we could pursue in the future. He helped me to think about science more broadly and creatively. I would like to thank personally Christopher Chidley, Andrian Gutu, Shankar Mukherji , Tim Peterson and Brian Zid for their enormous help when I prepared my thesis and defense presentation.

In the course of my graduate studies I could collaborate with many excellent people. When I tried to develop an inorganic phosphate sensor, Drs. Wolf Frommer and Sakiko Okumoto generously shared their phosphate sensor construct with me. Thanks

to them, I could learn basic ideas about how sensors should be designed. Drs. Jeff Hasty and Mike Ferry kindly provided me with their microfluidics device when I tried to characterize Pho4 translocation dynamics. For the genetic screening project described in Chapter 2, I would like to thank Drs. Jonathan Weissman and Martin Jonikas for sharing their yeast library with me and our previous lab member Dr. Abbhirami Rajagopal for measuring single mutant phenotypes with me. For the metabolomic measurements described in Chapter 3, I would not be able to finish this project if it were not for collaboration with the Rabinowitz lab at Princeton. I would like to thank Dr. Joshua Rabinowitz and Yifan Xu for helping me to perform metabolomic profiling.

I would like thank Drs. Andrew Murray and Vlad Denic for serving on my dissertation advisory committee. They provided fresh insights into what should be done and what directions are more promising than others and their comments were very helpful to get things done properly.

Finally, I would like to thank my family. My parents have never lost faith in me even if I have. My brother has been a great listener and good friend whenever I need to discuss my problems. Without their unconditional love, I would not have been able to be a Ph.D. I cannot overexpress my gratitude to my family. Thank you so much.

Joonhyuk Choi

April 2013

Chapter 1

Introduction to the Phosphate-responsive Signaling (PHO) Pathway in *Saccharomyces cerevisiae*

In order for microorganisms to survive in an unpredictable environment, they must monitor changes in environmental conditions and respond to maintain relatively constant intracellular conditions for growth. Given that nutrient availability is one of the most important environmental factors, cells have developed elaborate networks capable of sensing changes in the nutrient availability inside cells or in the environment, transferring the signals containing information about the fluctuations, and inducing transcriptional response to cope with the changes in nutrient levels. The proper regulation of these signaling pathways is essential for fulfilling cellular nutrient needs.

The regulation of the PHO pathway in response to changes in P_i availability

Inorganic phosphate (P_i) is an essential nutrient required for the synthesis of cellular constituents such as phospholipids as components of the plasma membrane and synthesis of ATP that is widely used as a carrier of chemical energy in cells. Therefore, it is crucial for cells to maintain P_i concentrations *in vivo* even in low extracellular P_i conditions. In *Saccharomyces cerevisiae* (budding yeast), the phosphate-responsive (PHO) signaling pathway is responsible for P_i homeostasis and responds to changes in extracellular P_i availability. The first cellular response to a decrease in extracellular P_i availability is to increase the uptake rate of P_i from the environment by secreting the acid phosphatase Pho5 (Oshima, 1997, To et al., 1973) and upregulating transcription of the high-affinity P_i transporter Pho84 (Bun-Ya et al., 1991). This cellular response is regulated by a core regulator cyclin Pho80 / cyclin-dependent kinase (CDK) Pho85 / CDK inhibitor Pho81 complex (Figure 1.1.) (Schneider

et al., 1994, O'Neill et al., 1996, Kaffman et al., 1994). The Pho80/85 complex phosphorylates the transcription factor Pho4 and regulates Pho4 subcellular localization depending on the P_i availability. Pho81 is bound to the Pho80/85 complex and required for the inhibition of Pho80/85 kinase activity in response to P_i starvation. In P_i limited conditions, *myo*-D-inositol heptakisphosphate (IP_7) levels increase and bind to the CDK inhibitor Pho81 causing it to inhibit Pho80/85 complex kinase activity (Lee et al., 2007, Lee et al., 2008). The loss of Pho80/85 kinase activity allows Pho4 to be dephosphorylated (Kaffman et al., 1994), resulting in nuclear localization (Kaffman et al., 1998b). Nuclear Pho4 binds cooperatively with another transcription factor Pho2 to PHO promoters (Vogel et al., 1989) and induces transcription of the PHO genes, including *PHO5* and *PHO84*. In high extracellular P_i conditions, Pho81's activity as a CDK inhibitor is repressed due to low levels of IP_7. This allows Pho4 to be multiply phosphorylated by the Pho80/85 complex and excluded from the nucleus (Kaffman et al., 1998a). The export of Pho4 from the nucleus turns off transcription induction of the PHO regulon.

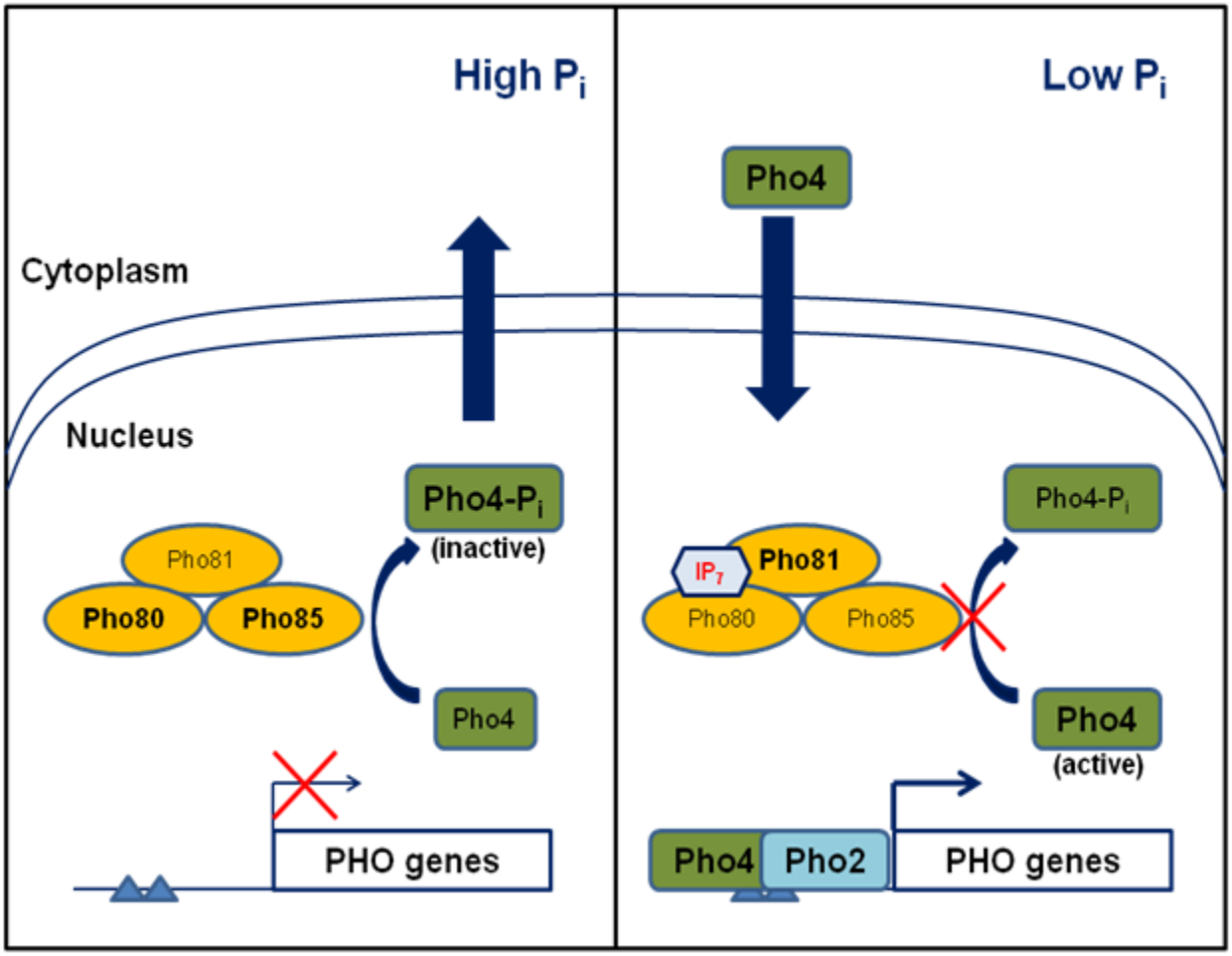

Figure 1. 1. Regulation of the PHO pathway in response to changes in P_i concentration.

Identification of the PHO regulon with microarray analysis

The advent of genome-wide technologies made it possible to define a comprehensive list of genes involved in the PHO regulon. Microarray data comparing the expression profiles of cells grown in high and no P_i conditions identified 22 genes regulated by the PHO pathway (Ogawa et al., 2000). In addition to the previously identified genes such as *PHO5* and *PHO84*, this study identified eight novel genes

PHM1-PHM8 that had no previously defined function in P_i metabolism. Those genes were involved in maintaining a pool of polyphosphate, a linear polymer of P_i, within the vacuole (Neef and Kladde, 2003) and these stores are mobilized during P_i starvation (Thomas and O'Shea, 2005).

Identification of upstream signaling components of the PHO pathway

While the PHO pathway downstream of Pho80/Pho85/Pho81 had been well characterized through biochemical studies and microarray measurements, little was known about genes acting upstream of Pho80/Pho85/Pho81. Historically, the high affinity P_i transporter Pho84 has been long considered the putative P_i sensor based on the constitutive activation of the PHO pathway of the *pho84* mutant and genetic evidence that *PHO84* acts upstream of the core Pho80/Pho85/Pho81 complex (Bun-Ya et al., 1991). The idea that a nutrient transporter acts as a regulating sensor was strengthened by its precedence in other signaling contexts. For example, the plasma membrane proteins Snf3 and Rgt2 sense a decrease in extracellular glucose concentration and regulate glucose transport in a glucose limited environment (Ozcan et al., 1996a, Ozcan et al., 1998, Ozcan et al., 1996b). However, overexpression of the low affinity transporters Pho87 and Pho89 that do not share significant amino acid similarity with Pho84 repressed the constitutive phenotype of the *pho84* mutant (Wykoff and O'Shea, 2001) indicating that an increase in P_i uptake represses the PHO pathway and it can occur independent of *PHO84* . Therefore, it appeared unlikely that Pho84 is a key P_i sensor for the PHO pathway.

To identify missing factors involved upstream signaling of the PHO pathway, Huang *et al.* performed a high-throughput and quantitative enzymatic screen of a yeast deletion collection (Winzeler et al., 1999) searching for novel mutants defective in expression of *PHO5* (Huang and O'Shea, 2005). From this screening, nine genes that had not been previously known to regulate *PHO5* expression were identified. Five genes were functioned downstream of the Pho80/Pho85/Pho81 complex and were known to be involved in other cellular signaling pathways such as alanine metabolism and glucose repression. However, other genes, such as those encoding the adenosine kinase Ado1 (Lecoq et al., 2001) and the adenylate kinase Adk1(Konrad, 1988), acted upstream of *PHO81* and negatively regulated *PHO5* expression. The observation that the novel genes required for regulation of *PHO5* expression were involved in other cellular activities suggested that the PHO pathway might be networked with other pathways including those involved in purine metabolism.

As the genetic screening was not enough to explain how cells sense P_i starvation to activate the PHO pathway, a biochemical strategy was employed as a complementary approach to the genetic screening (Lee et al., 2007). A series of biochemical assays narrowed down the identity of a regulatory factor for Pho80/Pho85/Pho81; IP_7, one of inositol polyphosphate metabolites, was identified as a signaling molecule for the PHO pathway. The cellular concentration of IP_7 increased in P_i starvation conditions and an isomer of IP_7 generated by the inositol hexakisphosphate kinase Vip1 binds to Pho81 and inhibits the kinase activity of the Pho80/Pho85 complex both *in vivo* and *in vitro*. In the *vip1* mutant, Pho4 was not localized into the nucleus in P_i starvation conditions, whereas it was constitutively

nuclear in the *ddp1* (IP_7 phosphatase) mutant, which has high levels of IP_7 (York et al., 2005). Pho4 was constitutively in the nucleus in the *vip1 pho80* double mutant, but it was not detected in the nucleus in the *ddp1 pho81* double mutant in P_i starvation conditions suggesting that IP_7 acts upstream of *PHO80* and upregulation of IP_7 is required for activation of the PHO pathway.

Although *ADO1*, *ADK1*, and *VIP1* were identified as genes involved in signaling in the PHO pathway, we still do not understand how they work together to sense P_i availability. It was shown that Vip1-synthesized IP_7 is upregulated and required for inducing the PHO regulon in P_i starvation conditions. However, the initiation signal for an increase in IP_7 production during P_i starvation is still unknown. Given that IP_7 levels are determined by a balance between Vip1 kinase activity and Ddp1 phosphatase activity during P_i starvation (York et al., 2005, Lee et al., 2007), there should be a signal upstream of IP_7 that perturbs the balance between them to make IP_7 levels increase in low P_i conditions. Furthermore, the molecular mechanism by which *ADO1* and *ADK1* repress the PHO pathway in high P_i is unknown and possible connections between these kinases' activities and Vip1 for regulating the PHO pathway have not been investigated.

The properties of signaling components of the PHO pathway

To elucidate how cells sense P_i availability, more signaling factors need to be identified. These factors may include small molecules and proteins and should meet two criteria. First, their relative abundance or activities should be altered in response to changes in P_i concentration. Secondly, they must respond quickly to changes in P_i

concentration given that the PHO pathway is activated within 10 minutes in no P_i conditions (Zhou and O'Shea, unpublished data).

As signaling factors, small molecules such as IP_7 could interact directly with regulatory proteins of the PHO pathway in order to modify their activities. Alternatively, these small molecules could regulate proteins that interact with other regulatory proteins of the PHO pathway. For example, P_i enhances the kinase activity of Ado1 (Maj et. al., 2000) that represses the PHO pathway in high P_i conditions. In low P_i conditions, however, its kinase activity could be lower than in high P_i due to decreases in P_i concentration within the cells resulting from Pi-limited conditions. This decrease in Adk1 kinase activity could then be a signal for depression of the PHO pathway. It is also possible that proteins involved in signaling could generate small molecules regulating the PHO pathway. For example, Vip1 synthesizes IP_7 whose upregulation is required for activating the PHO pathway low P_i conditions. Therefore, to better characterize the molecular mechanism of sensing P_i availability, we need to explore both small molecules and proteins as signaling factors.

I sought new components of the PHO pathway using genome-wide genetic screening. However, as previous genome-wide genetic screens (Huang and O'Shea, 2005) identified only a few genes as signaling candidates, I need to design screening experiments to cover as much of the genome as possible and utilize a more reliable and sensitive phenotype as a screening readout. In chapter 2, I will describe the design of a genome-wide genetic screen using a more sensitive and quantitative reporter than that of Huang et al. As the outcome of this screening, I report a list of novel genes defective in regulation of the PHO pathway and the functional relationships among them.

To identify any novel small molecules that regulate the PHO pathway, I investigated the metabolic responses to changes in extracellular P_i concentration. Given that deletion of *ADO1*, *ADK1,* and *AAH1* – genes involved in the purine metabolism - constitutively activates the PHO pathway, regulation of the PHO pathway may be associated with changes in purine metabolism. Furthermore, it was previously shown that an increase in IP_7 abundance regulates the PHO pathway in P_i-limited conditions. Recent technical advances in mass spectrometry (MS) coupled with liquid chromatography (LC) enable me to detect many metabolites simultaneously (Fiehn et al., 2000, Raamsdonk et al., 2001, Ejsing et al., 2009) and to generate a comprehensive picture of how the metabolome is rearranged under conditions in which environmental nutrient levels vary (Brauer et al., 2006). Based on the response times and amplitudes of metabolites in changing P_i concentrations, I provide insights into which metabolites could be regulatory signals for the PHO pathway. In chapter 3, I will describe how the metabolome of *Saccharomyces cerevisiae* varied over time in P_i-starved and replenished conditions.

Chapter 2

Genome-wide Genetic Screening to Identify Novel Genes Involved in Signaling of the PHO Pathway

Rationale

In response to P_i limitation, *Saccharomyces cerevisiae* induces the transcription of a set of genes that are essential for maintaining intracellular P_i concentrations. The PHO pathway mediates this response through a cyclin/cyclin-dependent kinase (CDK) /CDK inhibitor complex, Pho80/Pho85/Pho81 complex. While the molecular mechanism by which the core complex regulates the transcription of the PHO regulon in response to changes in extracellular P_i concentration is well understood, little is known about how cells sense changes in environmental P_i availability. Previous work identified three signaling factors upstream of the Pho80/Pho85/Pho81 complex: the adenosine kinase Ado1, the adenylate kinase Adk1, and the inositol hexakisphosphate kinase Vip1 (Lee et al., 2007, Huang and O'Shea, 2005). However, it is still not known how these signaling factors are interconnected to regulate the PHO pathway. Specifically, we do not know how Ado1 and Adk1 regulate the PHO pathway depending on the P_i concentration or how IP_7 is upregulated in P_i-limited conditions. Given that Ado1, Adk1, and Vip1 appear to be under the control of other regulatory proteins that are not known, it is desirable to screen for those additional genes and identify the functional relationships among them.

To address these issues, I exploited synthetic genetic interaction screens as a means of identifying functional relationships among the genes of interest (Jonikas et al., 2009, Collins et al., 2007). The relationships can be inferred by comparing the phenotype of a double mutant and its constituent single mutants and estimating the extent to which deletion of one gene modulates the phenotype of a second deletion. For

example, synthetic lethality occurs when each mutant is viable and the combination of two mutations leads to an inviable organism. This interaction between the two genes suggests that their gene products buffer one another for the essential function. Because this screening technique allows us to generate double mutants carrying all possible combinations of single mutations of interest by crossing them in parallel (Tong et al., 2004), a large-scale mapping of functional relationships between genes can be obtained.

In this chapter, I described how I performed genome-wide genetic screening and report a list of novel genes whose deletion leads to defects in the regulation of the PHO pathway. Furthermore, I identified unappreciated genetic interactions among the identified genes.

Results

Determination of mutants defective in *PHO84* expression levels acting upstream of *PHO80* or *PHO81* from genome-wide genetic screening

Genome-wide screens with a yeast deletion library were performed to identify genes that affect PHO pathway activity and act upstream of *PHO80* or *PHO81*. The activity of the PHO pathway in each mutant was monitored by a fluorescent gene expression reporter driven by the *PHO84* promoter, which is induced in low P_i (see “Quantification of *PHO84* expression level of the single mutant“). The phenotypes of all the mutants in the library were measured in both low and high P_i conditions to determine if the PHO pathway is misregulated in the mutant strain - either less activated than the wild type strain in low P_i (weakly inducible mutant) or inappropriately activated in high P_i (constitutively induced mutant), (see “P_i concentrations for screening”). Statistical analysis was performed to quantify how significantly each sample’s phenotype deviated from that of the wild type strain (see "p-value analysis to determine the first hits” in Material and Methods). From this initial screening, 445 weakly inducible mutants and 280 constitutively induced mutants with a p-value< 0.001 were identified (Figure 2.1).

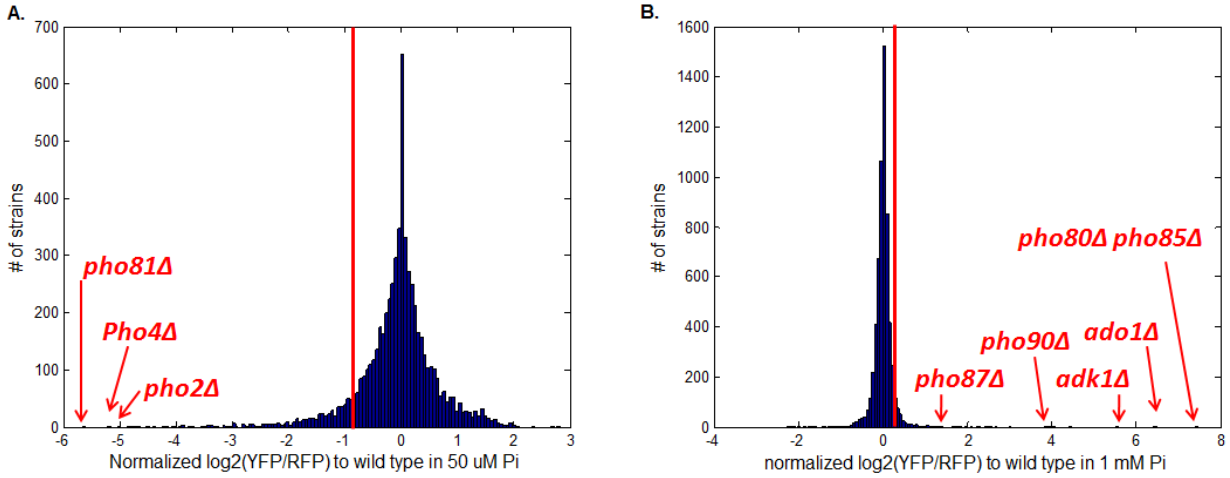

Figure 2.1. Identification of mutants showing phenotypes deviating from wild type in low and high P_i. (A) The distribution of *PHO84* expression levels of all the single mutants in 50 uM P_i. All the phenotypes are normalized to wild type in 50 uM P_i. The mutants showing lower *PHO84* expression levels than wild type in 50 uM P_i are defined as weakly inducible hits. (B) The distribution of *PHO84* expression levels of all the single mutants in 1 mM P_i. All the phenotypes are normalized to wild type in 1 mM P_i. The mutants showing higher PHO84 expression levels than wild type in 1 mM P_i are defined as constitutively induced hits. The red bars in each diagram indicate the maximum and minimum *PHO84* expression levels satisfying the p-value of measurement errors <0.001. The mutants in red are previously identified as uninducible (A) and constitutively induced mutants (B), respectively.

To identify genes acting upstream of *PHO80* or *PHO81*, a double mutant analysis was performed on all 725 hits identified in the initial screening. It is known that the *pho80* mutant constitutively activates the PHO pathway, whereas the *pho81* mutant is uninducible in low P_i conditions (Schneider et al., 1994, Kaffman et al., 1994). In principle, if the weakly inducible mutants act upstream of *PHO80,* the 445 double mutants carrying the *pho80* mutant are expected to have the same phenotype as the *pho80* single mutant. Given that the *pho80* mutant phenotype is so strong, it was difficult to detect a decrease in *PHO84* expression levels due to deletion of the weakly

inducible genes even if the defect exists. To circumvent this potential problem, I used a partial loss of function *pho80* DAmP allele – instead of the *pho80* deletion mutant - which reduces the stability of *PHO80* transcripts significantly. (See "Double mutant analysis to identify genes upstream of *PHO80* and *PHO81"*). From this analysis, 362 of the 445 weakly inducible mutants appeared to act upstream of *PHO80* (Figure 2.2.A). Similarly, if the constitutively induced mutants act upstream of *PHO81,* I expect the 280 double mutants carrying the *pho81* mutant to show the same phenotype as the *pho81* single mutant. For the constitutively induced mutants, most of them showed very similar *PHO84* expression levels to the *pho81* single mutant (Figure 2.2.B). Therefore, all of the 280 constitutively induced mutants appeared to act upstream of *PHO81*. In view of the high number of genes identified as acting upstream of *PHO80* and *PHO81*, the stringency of the initial genome-wide screen was increased to focus on the genes having a profound effect. I selected only genes showing at least a two-fold decrease or increase in the *PHO84* expression levels compared to the wild type in low and high Pi conditions, respectively. Among the 362 weakly inducible and 280 constitutively induced mutants, 310 weakly inducible and 30 constitutively induced mutants met those criteria, respectively (Supplementary table 2.1 and 2.2).

Among the top 30 constitutively induced mutants, there are seven genes whose deletion leads to more than a 10-fold induction of *PHO84* expression compared to the wild type in high P_i conditions. Interestingly, three of the seven genes are involved in purine metabolism (*AAH1*, *ADO1* and *ADK1*; Supplementary table 2.1). It was previously reported that deletion of *ADO1* and *ADK1* leads to a constitutively induced PHO phenotype in high P_i (Huang and O'Shea, 2005). In this screen, both of the *ado1*

and *adk1* mutants induced *PHO84* expression about 45 times more than the wild type strain in high P_i conditions (Figure 2.1. B, Supplementary table 2.1). Deletion of *AAH1*, a gene encoding a deaminase that converts adenine into hypoxanthine, induced *PHO84* expression about 30 times more than the wild type strain in high P_i conditions (Figure 2.3.B). The identification of another gene involved in purine metabolism highlights the potential importance of this pathway in the P_i starvation response. For this reason, in chapter 3, I measured the abundances of purine metabolites in purine metabolism mutants affecting the PHO pathway (*AAH1*, *ADO1* and *ADK1*) in high P_i as well as the wild type in low $P_{i.}$

Huang et al. have shown that both *ADO1* and *ADK1* act upstream of *PHO81* (Huang and O'Shea, 2005). To determine if this is also the case for the *aah1* mutant, the *aah1 pho81* double mutant was generated and its *PHO84* expression levels were measured. As expected, the constitutively activated phenotype of *aah1* mutant was suppressed in the *aah1 pho81* double mutant suggesting that *AAH1* also acts upstream of *PHO81* (Figure 2.3.E).

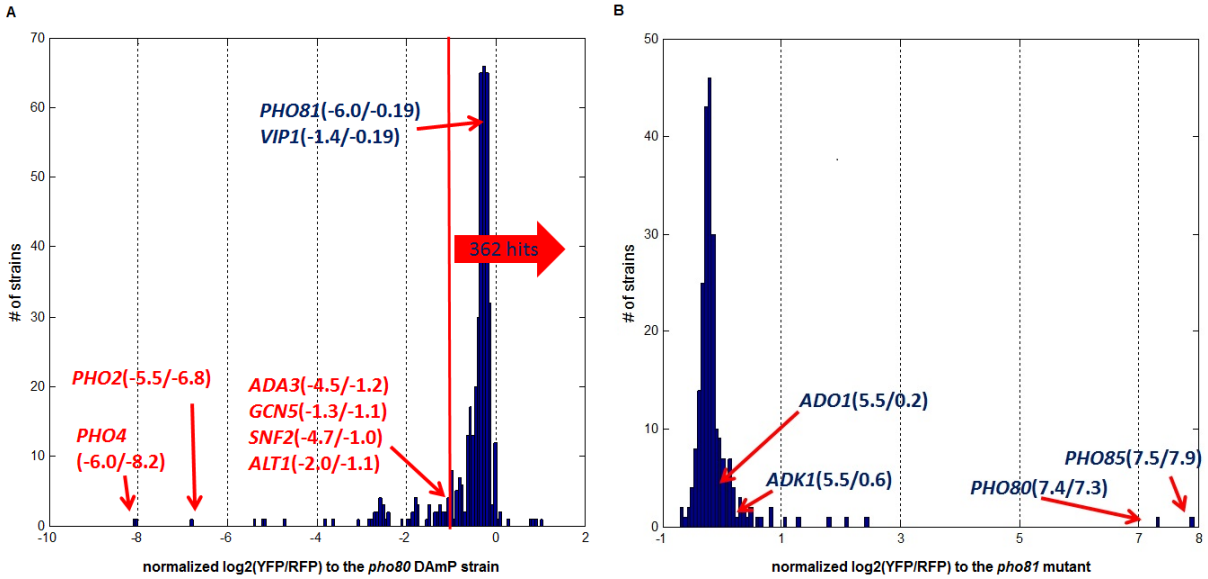

Figure 2. 2. Identification of genes upstream of *PHO80* and *PHO81*. (A) The histogram of normalized reporter levels of double mutants carrying all the weakly inducible hits and the *pho80* DAmP in 50 uM P_i. The first value in the parentheses is the phenotype of a weakly inducible single mutant normalized to wild type in 50 uM P_i. The second value in the parentheses is the phenotype of a double mutant carrying the weakly inducible mutant and the *pho80* DAmP normalized to *pho80* DAmP in 50 uM P_i. (B) The histogram of normalized reporter levels of double mutants carrying all the constitutively induced hits and the *pho81* mutant in 1 mM P_i. The first value in the parentheses is the phenotype of a constitutively induced single mutant normalized to wild type in 1 mM P_i. The second value in the parentheses is the phenotype of a double mutant carrying the constitutively induced mutant and the *pho81*mutant normalized to the pho81 mutant in 1 mM P_i. Genes in blue and red are previously identified as upstream and downstream of *PHO80* or *PHO81*, respectively.

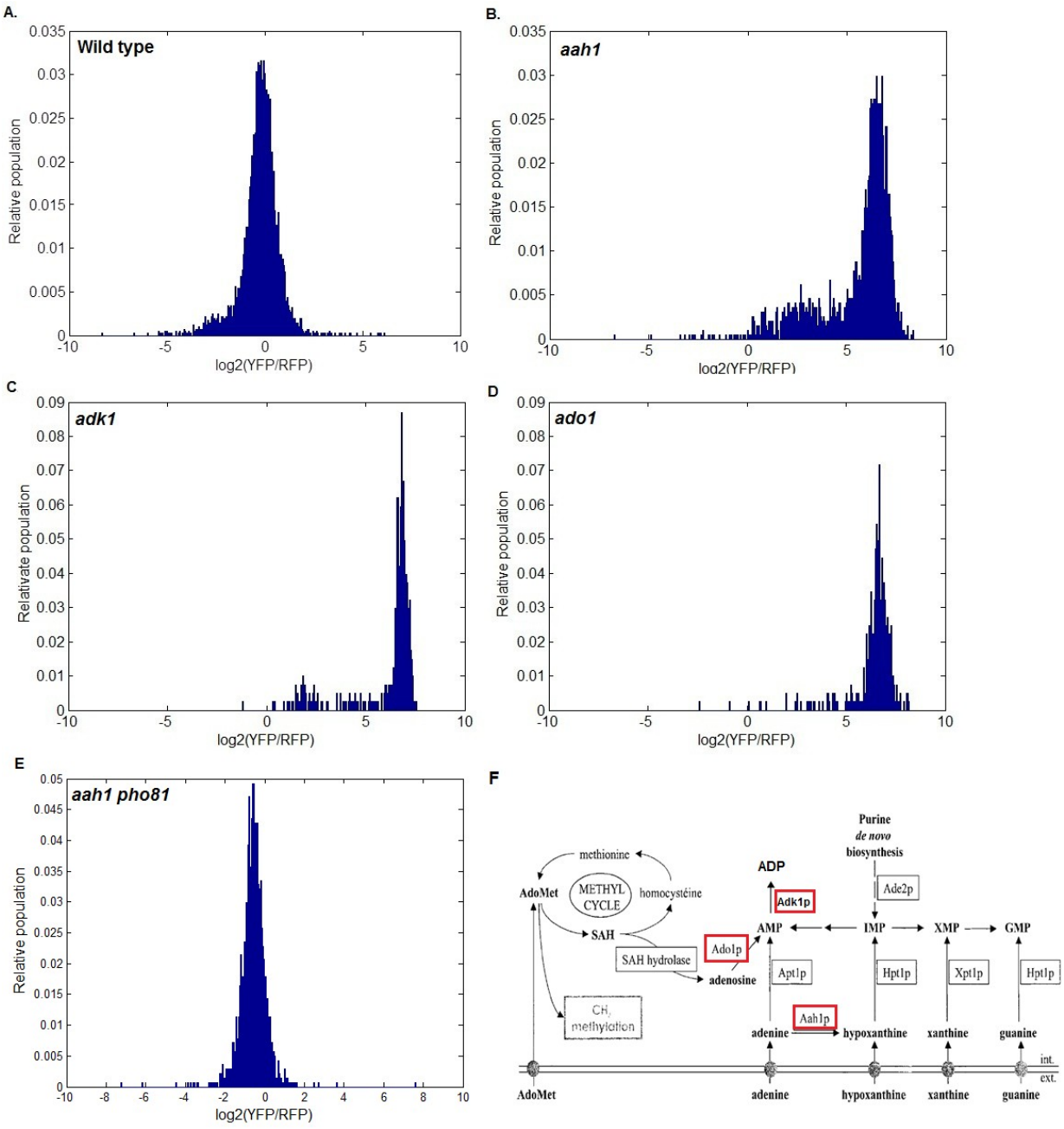

Figure 2.3. The raw *PHO84* expression levels of the purine metabolism mutants and the *aah1 pho81* double mutants in 1 mM P_i. *PHO84* and constitutive *TEF2* promoters drive YFP and RFP expressions, respectively. The *PHO84* expression levels of single cells were quantified as log2 intensity ratios of YFP to RFP. (A) Wild type, (B) the *aah1* mutant, (C) the *adk1* mutant, (D) the *ado1* mutant, and (E) the *aah1 pho81* double mutant in 1 mM P_i, respectively. (F) The adenine nucleotide metabolism pathway. Red rectangles indicate the identified genes in this screen. This diagram is credited with Lecoq et al. (Lecoq et al., 2000).

Novel phenotype of the *vip1* mutant in prolonged P_i starvation

In 2007, Lee et al. showed that deletion of *VIP1* leads to an uninducible phenotype suggesting a role for Vip1- synthesized IP_7 in the P_i starvation response (Lee et al., 2007). In the genome-wide single mutant analysis, I observed that the *vip1* mutant was able to activate the PHO pathway upon prolonged P_i starvation. The *vip1* mutant induced *PHO84* expression 65% less than the wild type when it was grown in low P_i for eight hours (Supplementary table 2.2). At first, this result was surprising because it seemed inconsistent with the study mentioned above (Lee et al., 2007). In the view of the two different P_i starvation durations used in the two studies, one possible explanation is that the induction of the PHO pathway in the *vip1* mutant is slower than in the wild type rather than completely absent. To test this hypothesis, a kinetic assay for *PHO84* expression in the *vip1* mutant was performed. The wild type induced *PHO84* expression in one hour in low P_i, whereas the *vip1* mutant showed *PHO84* expression only after four hours (Figure 2.4). This suggests that the *vip1* mutant is kinetically defective in regulation of the PHO pathway and eventually partially activates the PHO pathway in prolonged P_i starvation.

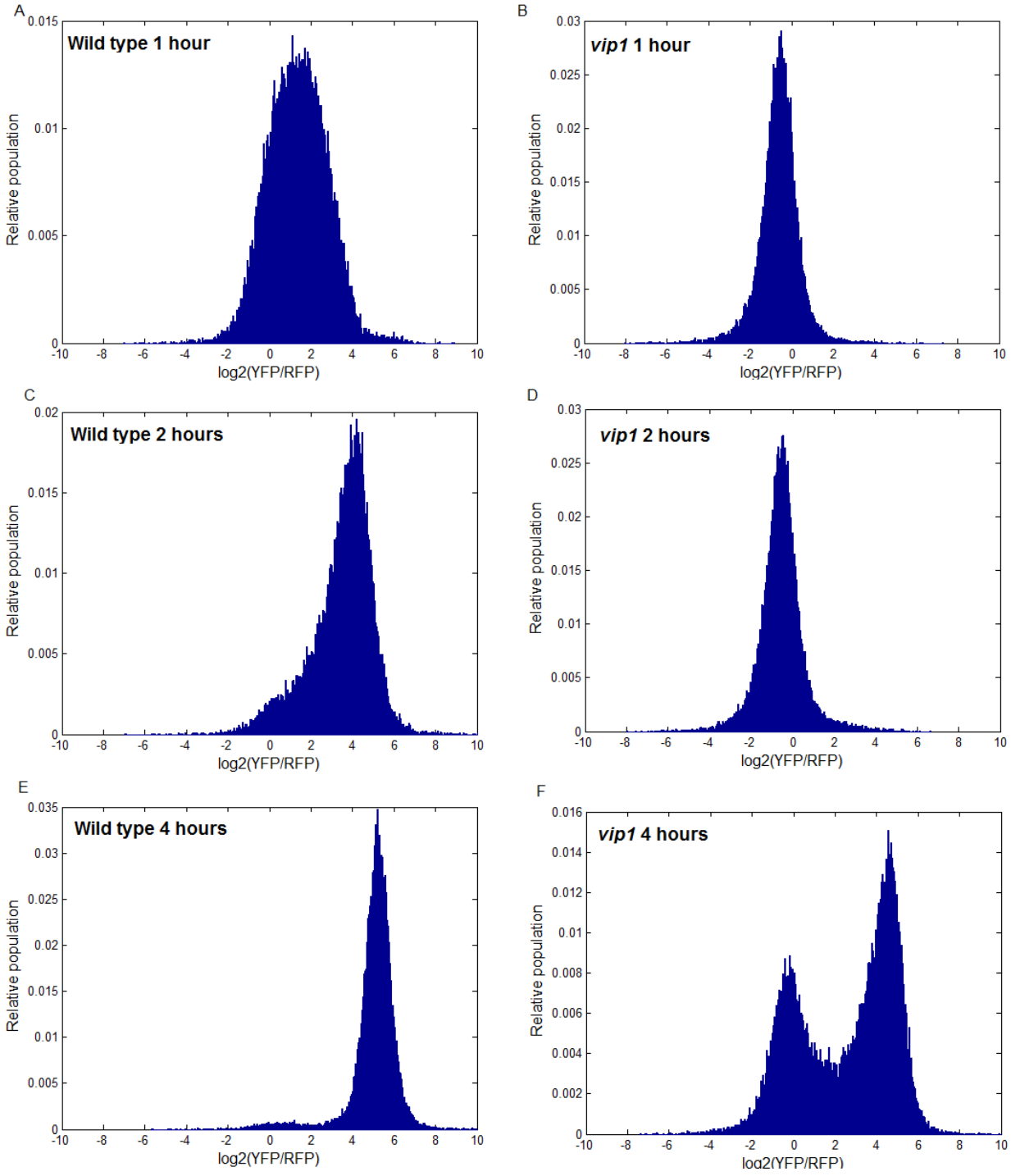

Figure 2. 4. The *PHO84* expression time course measurements of wild type and the *vip1* mutant in 50 uM P_i. (A, C, E) The *PHO84* expression levels of the wild type in 1, 2, and 4 hours, respectively.(B, D, F) The *PHO84* expression levels of the *vip1* mutant in 1, 2, and 4 hours, respectively. Refer Figure 2.3.A to the *PHO84* expression levels of wild type in 1 mM P_i.

Identification of novel genetic interactions with the purine and inositol polyphosphate metabolism pathway components

As shown in a previous section, the genome-wide genetic screen identified 310 weakly inducible mutants and 30 constitutively induced mutants acting upstream of *PHO80* and *PHO81*. Furthermore, it has been shown here and by others that the purine metabolism genes *ADO1*, *AAH1* and *ADK1* and also *VIP1* are involved in signaling in the PHO pathway upstream of Pho80/85/81 (Huang and O'Shea, 2005, Lee et al., 2007). In order to investigate the functional relationship between the 340 genes identified in the screens and the four genes mentioned above, double mutants of the 340 genes with *ADO1*, *AAH1* and *ADK1* and also *VIP1* were constructed and their *PHO84* expression levels were measured in high and low P_i conditions. The goal of this double mutant screen was to identify genes that perturb the constitutively activated phenotype of the three purine metabolism mutants or the weakly inducible phenotype of the *vip1* mutant. For example, if a gene is required for the constitutively induced phenotype of the *ado1* mutant, a double mutant carrying both mutants should be unable to express *PHO84* in high P_i. On the other hand, if two weakly uninducible mutants show similar *PHO84* expression levels to the wild type in low P_i and the double mutant carrying both mutants is uninducible, it shows that one gene can compensate for the loss of the other gene. This relationship indicates that the two genes act in parallel (Tong et al., 2004) in terms of regulation of the PHO pathway.

To identify which genes are required for the constitutive PHO phenotype of the purine metabolism mutants, double mutants of all 340 identified single mutants from the

initial screening with the *ado1* or the *aah1* mutant were generated and their *PHO84* expression levels in high P_i were measured. The double mutants carrying deletion of *ADK1* could not be generated for technical reasons (see “Making double mutants with the array strains”). Among each set of 340 double mutants of the *aah1* and the *ado1* mutants, there were 51 and 18 uninducible double mutants in the *aah1* and *ado1* analysis, respectively. (Figure 2.5.A and B, Supplementary table 2.4, 2.5). Moreover, as seen in Table 2.1., nine genes were shared between the two groups of double mutants indicating that these ten genes are required for the constitutively induced phenotype of both the *ado1* and the *aah1* mutants in high P_i. I investigated common features of the ten genes to find their functional relationships with purine metabolism, but found no obvious common feature among them. The function of three genes *YJL175W*, *OPI11*, *YPR045C* are unknown and four genes (*TMA23*, *TRM9*, *RSA1*, *KTI11*) are related to transcription or translational machinery. It is not clear why these eight genes are required for the constitutively activated phenotype of the *aah1* and *ado1* mutants. Interestingly, however, the *aah1 vip1* and the *ado1 vip1* double mutants repressed the constitutively activated phenotype of the *aah1* and the *ado1* single mutants, indicating that *VIP1* is required for the constitutively activated phenotype of the *ado1* and the *aah1* mutants (Figure 2.5.C.). This is consistent with the observation that IP_7 was upregulated in the *ado1* and the *adk1* mutants in high P_i (10 mM) (Lee and O’Shea, unpublished data). Therefore, it appears that *VIP1* is downstream of *ADO1* and *AAH1* when the two gene products repress the PHO pathway in high P_i.

Table 2.1. List of genes whose double mutants with both *ado1* and *aah1* mutants are uninducible. Reporter levels of all the mutants are normalized to the wild type in 50 uM P_i. The reporter level of wild type in high P_i is -4.5. Uninducible double mutants were chosen as the ones whose reporter level is lower than -4.

Gene	normalized log2(YFP/RFP) to wild type in 50 uM P_i as a single mutant	normalized log2(YFP/RFP) to wild type in 50 uM P_i as a double mutant of *aah1* mutant	normalized log2(YFP/RFP) to wild type in 50 uM Pi as a double mutant of *ado1* mutant
VIP1	-1.66	-6.48	-4.47
YJL175W	-5.14	-5.91	-4.47
PHO81	-5.75	-5.48	-5.16
OPI11	-4.73	-5.45	-5.60
TMA23	-3.91	-5.39	-4.55
TRM9	-4.38	-5.34	-5.37
YPR045C	-2.85	-5.10	-5.79
RSA1	-3.77	-4.89	-5.25
KTI11	-1.58	-4.31	-4.31

To identify genes that can compensate for the absence of Vip1-synthesized IP_7 to activate the PHO pathway in prolonged P_i starvation, double mutants of all 340 mutants identified as acting upstream of *PHO80* or *PHO81* with the *vip1* and the *ipk1* mutants were measured in low P_i (Figure 2.6.A and B.). *IPK1* encodes an inositol pentakisphosphate (IP_5) kinase whose substrate is a precursor of IP_7 synthesis (Ives et al., 2000). Like the *vip1* mutant, the *ipk1* mutant showed no detectable IP_7 levels and did not activate the PHO pathway early in P_i-starvation (Lee et al., 2007). Among each set of 340 double mutants of the *vip1* and the *ip1k* mutants, there were 80 and 40 uninducible double mutants carrying deletion of *VIP1* and *IPK1*, respectively (Figure 2.6.A and B., Supplementary table 2.6 and 2.7). From those uninducible double mutants,

as seen in Table 2.2., there were 11 genes whose single mutants were weakly defective in activation of the PHO pathway but were uninducible as double mutants of both the *vip1* and the *ipk1* mutants. The function of six genes (*YGR160W*, *YLR184W*, *YMR242W-A*, *YGL188C-A*, *FYV1*, *BUD28*) are unknown and two genes (*ARP8* and *MET18*) are related to transcription or translational machinery. Although it is not clear how IP_7 synthesis can be related to the functions of the ten genes, the three genes (*MCT1*, *HTD2*, and *PDB1*) share common defects in converting pyruvate into acetyl-CoA upon their deletion. The relationships between Vip1-synthesized IP_7 and these three genes are presented in the discussion.

Table 2.2. List of genes whose double mutants with *vip1* and *ipk1* mutants are uninducible in 50 uM P_i. Reporter levels of all the mutants are normalized to the wild type in 50 uM P_i .The reporter level of wild type in high Pi is -4.5. Weakly inducible single mutants were chosen as the ones whose reporter level is higher than -2. Uninducible double mutants with the *ipk1* and *vip1* mutant were chosen as the ones whose reporter level is lower than -4.

Gene	normalized log2(YFP/RFP) to wild type in 50 uM P_i as a single mutant	normalized log2(YFP/RFP) to wild type in 50 uM P_i as a double mutant of *vip1* mutant	normalized log2(YFP/RFP) to wild type in 50 uM P_i as a double mutant of *ipk1* mutant
YGR160W	-1.06	-5.74	-5.28
YLR184W	-1.08	-6.25	-5.52
HTD2	-1.16	-4.78	-4.76
PDB1	-1.30	-5.48	-4.27
YMR242W-A	-1.32	-6.23	-5.83
ARP8	-1.54	-5.42	-4.12
YGL188C-A	-1.55	-6.56	-5.37
FYV1	-1.80	-4.42	-4.12
MET18	-1.89	-6.01	-5.17
MCT1	-1.94	-5.24	-5.13
BUD28	-1.99	-6.08	-5.29

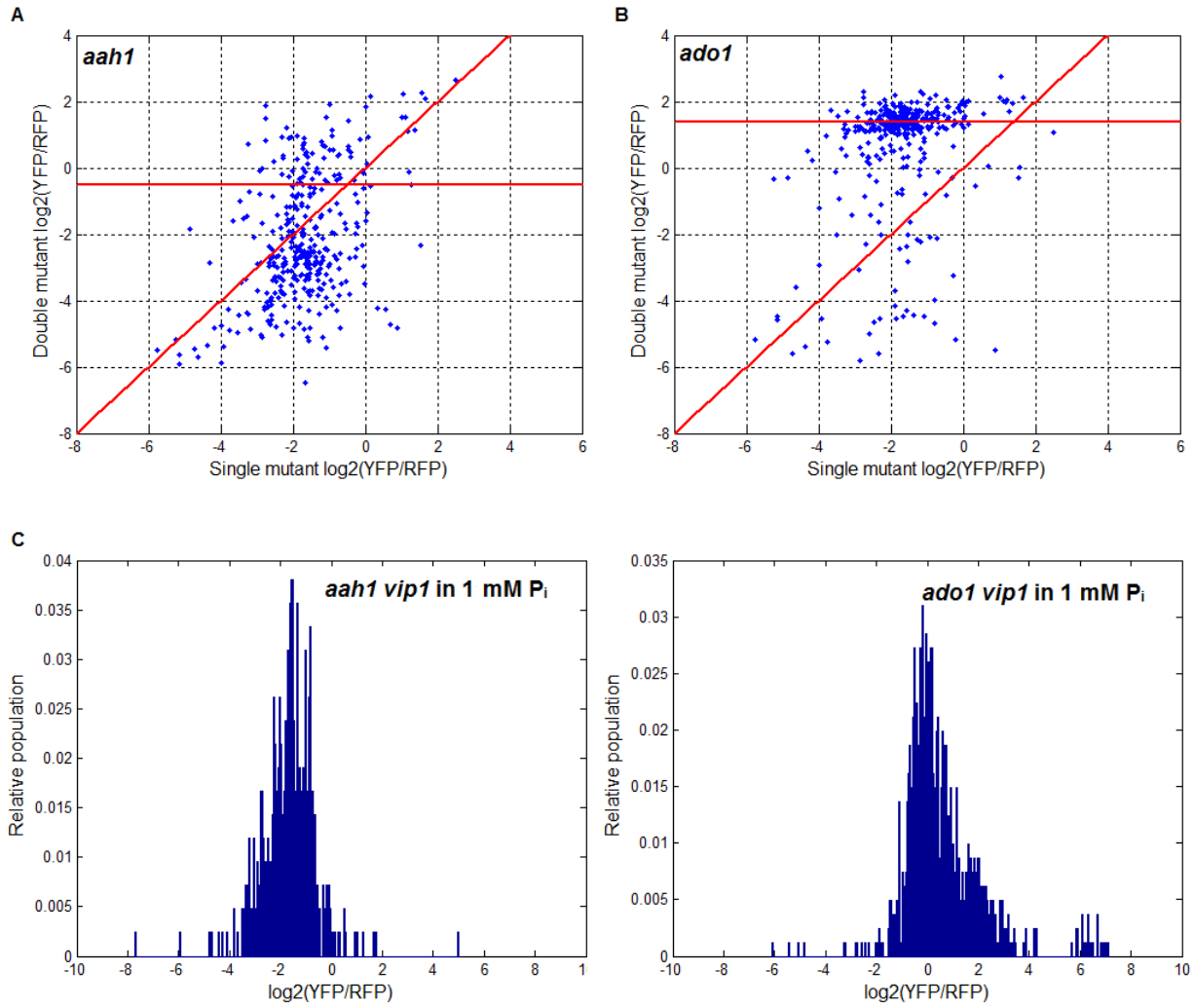

Figure 2.5. Double mutant (DM) plot of (A) the *aah1* and (B) the *ado1* mutant in 1 mM P_i. Each point represents a gene identified as involved in regulation of the PHO pathway upstream of *PHO80* or *PHO81*. X coordinate represents the reporter level of a strain deleted for that gene in the wild-type (WT) background. Y coordinate represents the reporter level in a double mutant lacking the same gene and additionally deleted for *AAH1* and *ADO1*, respectively. All the phenotypes of single and double mutants were normalized to wild type in 50 uM P_i. The normalized phenotype of wild type in 1 mM P_i (no activation of the PHO pathway) is -4.5. The horizontal red line in each diagram indicates the normalized phenotype of the *aah1* and *ado1* single mutant in 1 mM P_i, respectively.(C) The raw *PHO84* expression levels of the *aah1 vip1* (left) and the *ado1 vip1* (right) double mutants in 1 mM P_i. Refer Figure 2.4.A to the *PHO84* expression levels of wild type in 1 mM P_i.

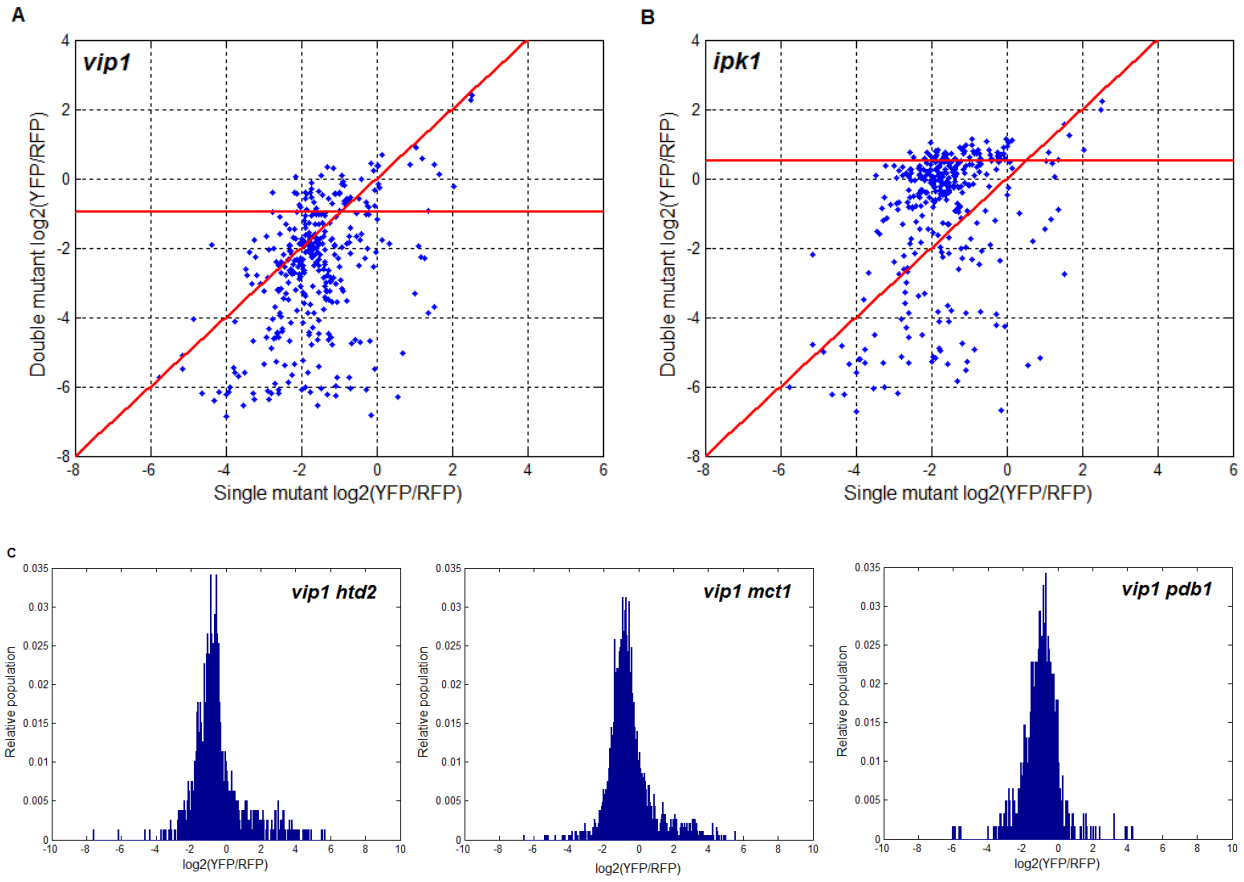

Figure 2.6. DM plot of (A) the *vip1* and (B) the *ipk1* mutant in 50 uM P_i. The horizontal red line in each diagram indicates the normalized phenotype of *vip1* and *ipk1* mutant in 50 uM P_i, respectively. (**C)** Raw *PHO84* expression level of the *vip1 htd2*, *vip1 mct1*, and *vip1 pdb1* double mutants**.** Refer Figure 2.4.A to the *PHO84* expression levels of wild type in 1 mM P_i.

Discussion

In this study, I identified more than 300 novel single mutants that are defective in regulation of the PHO pathway, a much larger number than was identified in the previous genome-wide screening (Huang and O'Shea, 2005). Because the screening was performed under milder conditions than Huang et al (50 uM and 1 mM P_i versus no and 10 mM P_i), genes that are weakly involved in regulation of the PHO pathway - such as those that only shift an activation threshold - could be detected. Synthetic gene array (SGA) (Tong and Boone, 2006) screens made it possible to insert a fluorescence reporter in the entire yeast deletion library and to generate massive numbers of double mutants in order to compare the phenotypes of double mutants to their constituent single mutants.

In this screen, a purine metabolism gene *AAH1* was identified as acting upstream of *PHO81.* Combined with the knowledge that the *ado1* and *adk1* mutants are also involved in the purine metabolism and are constitutively induced mutants acting upstream of *PHO81*, the discovery of the *aah1* mutant phenotype supports the idea that regulation of the PHO pathway could be associated with changes in purine metabolism. Because the role of *ADO1* and *ADK1* in purine metabolism is not clear, measuring the purine metabolism response during a transition from high to low P_i conditions may provide insights into details of the upstream PHO pathway. There is an exciting possibility that purine metabolites could trigger the response of the PHO pathway to changes in P_i concentrations. In chapter 3, I measured the metabolomic response to

changes in P_i concentration and observed variations in purine metabolism in different P_i concentrations.

I showed that the *vip1* mutant activated the PHO pathway slowly compared to the wild type in low P_i conditions. This aspect of the phenotype of the *vip1* mutant could explain why *VIP1* was not identified in the previous screening (Huang and O'Shea, 2005) as being defective in signaling of the PHO pathway. The conditions used by Huang et al. in their screening do not allow the identification of mutants which have a kinetic defect in regulation of the PHO pathway. Therefore, it is likely that the *vip1* mutant did not meet the chosen criteria for uninducible mutants.

To quantify genetic interactions, we should define a neutrality function that predicts the quantitative phenotype of double mutants carrying two non-interacting mutations (Mani et al., 2008). If the phenotype of interest is a growth defect in mutants, it was shown that in the absence of a genetic interaction the growth defect of a double mutant is expected to be the product of the individual growth defects of the constituent single mutants (Boone et al., 2007, Segre et al., 2005) . However, a neutrality function for gene expression levels as a quantitative phenotype is not well defined and it was difficult to find a neutrality function for my data between the phenotype of a double mutant and its non-interacting corresponding single mutants. However, extreme genetic interactions - such as complete repression of a constitutive single mutant phenotype as a double mutant - are easily detectable and their interpretation is straightforward. The 10 genes in Table 2.1 are required for the constitutive phenotype of purine metabolism mutants. One interesting gene required for the constitutive phenotype of *aah1* and *ado1*

mutants is *VIP1*. The *vip1 aah1* and v*ip1 ado1* double mutants do not constitutively activate the PHO pathway (Figure 2.5.C). This implies that purine metabolism and IP_7 synthesis may be interconnected to repress the PHO pathway in high P_i conditions (Figure 2.8). To investigate this relationship, I performed in chapter 3 metabolic profiling of the *aah1, vip1 aah1, ado1, vip1 ado1* mutants in high P_i conditions and compared the adenine nucleotide levels of all mutants.

The delayed activation of the PHO pathway in the *vip1* mutant in prolonged P_i starvation suggests two possible mechanisms: synthesis of IP_7 in the absence of Vip1 or a novel mechanism that regulates Pho81 activity without IP_7. To resolve this conundrum, it is crucial to measure IP_7 levels in the *vip1* mutant in a long period of P_i starvation. If IP_7 is observed in the *vip1* mutant, there must be a novel pathway synthesizing IP_7 without Vip1. In this work, a number of the double mutants carrying the *vip1* mutant that are completely uninducible in low P_i conditions upon prolonged starvation were identified (Table 2.2). If another gene is capable of synthesizing IP_7 in the absence of Vip1, it is expected that a double mutant of both genes should be uninducible. This raises the exciting possibility that one of the 13 genes mentioned in Table 2.2 could be crucial for the synthesis of IP_7 in the absence of Vip1. Among the 13 genes, two genes *HTD2* (mitochondrial 3-hydroxyacyl-thioester dehydratase) and *MCT1* (a component of a type-II mitochondrial fatty acid synthase) are involved in mitochondrial fatty acid biosynthesis (mtFAS) (Figure 2.7.) (Kastaniotis et al., 2004, Schneider et al., 1997). Given that only three mtFAS genes (*MCT1*, *HTD2*, and *CEM1*) are included among the identified single mutants in this screen, it is statistically significant that two genes *MCT1* and *HTD2* interacting with both *VIP1* and *IPK1* are involved in the mtFAS pathway (p-

value =1.81*10^{-9}). Based on the observation that lesions within the mtFAS pathway exhibited low levels of lipoic acid (Brody et al., 1997), it was suggested that the major role of mtFAS is to provide octanoate which serves as a precursor for lipoic acid (Hiltunen et al., 2009, Tehlivets et al., 2007). In the presence of lipoic acid, pyruvate dehydrogenase (PDH) can convert pyruvate into acetyl-CoA. Given that Pdb1 is the E1 beta subunit of PDH and the *vip1 pdb1* and the *ipk1 pdb1* double mutants were uninducible in low P_i (Table 2.3), the uninducible phenotypes of the double mutants carrying the *htd2*, *mct1*, and *pdb1* mutants appear to be associated with defects in acetyl-CoA biosynthesis (Figure 2.7). In chapter 3, I showed that phosphatidylcholine (PC), a major membrane phospholipid, was downregulated in low P_i conditions. Given that phospholipids contain two fatty acid chains and acetyl-CoA is a C2-carbon donor of fatty acid biosynthesis, it is conceivable that activation of the PHO pathway in the *vip1* mutant in prolonged P_i starvation is associated with changes in fatty acid metabolism (Figure 2.8). Interestingly, disruption of the mtFAS pathway in *Trypanosoma brucei* resulted in changes in the composition of cellular phospholipids (Guler et al., 2008). The phospholipid Inositol 1,4,5-trisphosphate (IP_3) is a precursor of IP_7 synthesis (Monserrate and York, 2010) and is generated by hydrolysis of phosphatidylinositol 4,5-bisphosphate (PIP_2), a minor phospholipid component of cell membranes (York, 2006). This relationship between inositol polyphosphate and phospholipid metabolism suggests that activation of the PHO pathway in the *vip1* mutant in low P_i conditions could be coupled with changes in phospholipid metabolism.

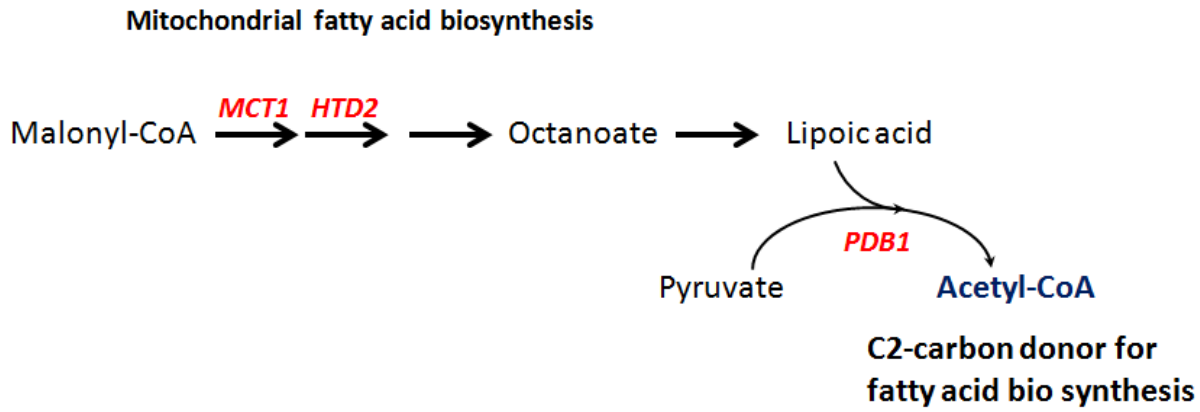

Figure 2.7. *MCT1* and *HTD2* are involved in mitochondrial fatty acid synthesis (p-value = $1.81*10^{-9}$).The major role of this pathway is to provide octanoyl-ACP which serves as a precursor for lipoic acid. Lipoic acid is required for converting pyruvate into acetyl-CoA mediated by pyruvate dehydrogenase (PDH).

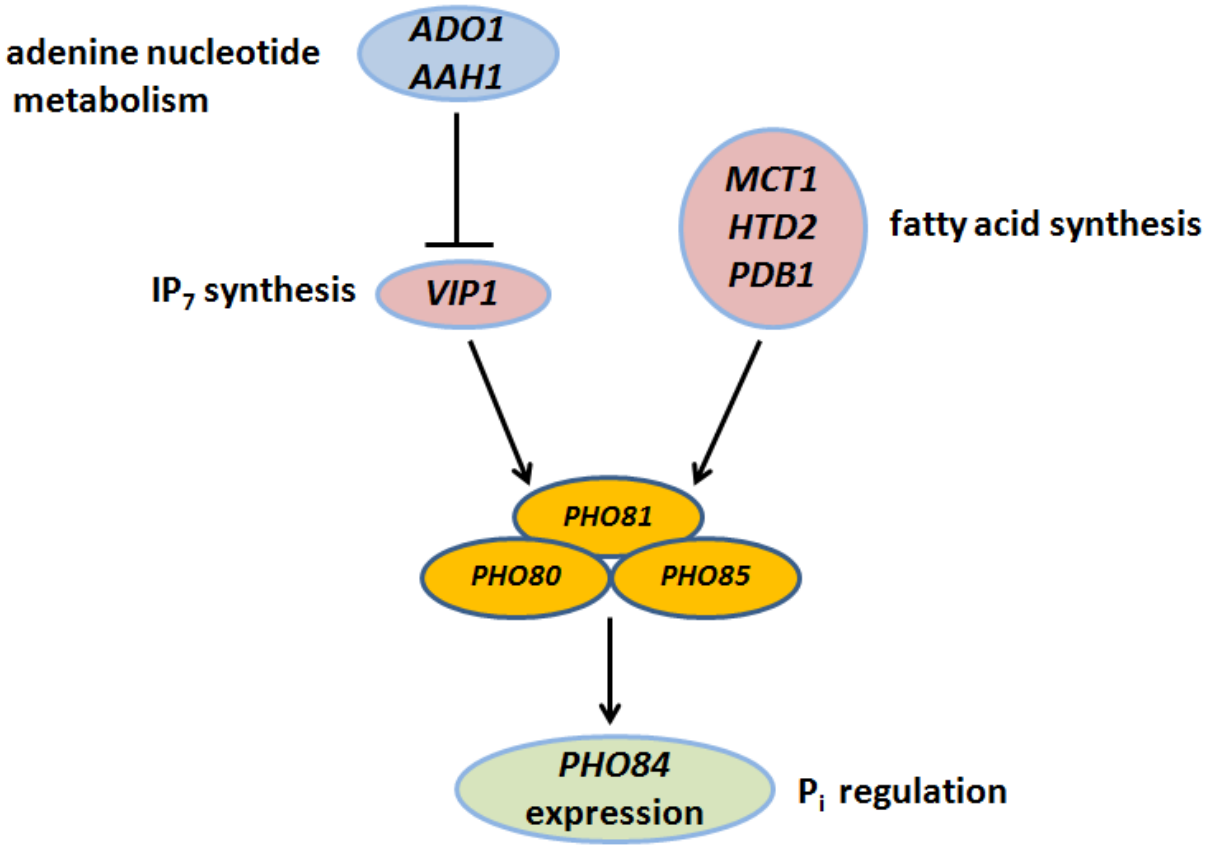

Figure 2.8. Novel genetic interactions among the genes acting upstream of *PHO80* and *PHO81*. The blue ovals indicate the genes whose deletion leads to constitutively activated PHO pathway. The purple ovals indicate the genes whose deletion leads to defective in induction of the PHO pathway in low P_i.

Materials and methods

Strains

All the strains used in this study were in the BY4741 strain background (MATa *his3Δ1 leu2Δ0 met15Δ0 ura3Δ0*) and are listed in Table 2.3. Gene deletions were introduced by transformation of gel-purified PCR products consisting of a nourseothricin marker (Nat^R) flanked at each end by 40 base pair (bp) homologous to the upstream and the downstream region of the targeted open reading frame. The transformation was followed by selection on a YEPD+Nat growth medium. All the mutations shown in this work are ablations of the open reading frame except the pho80 DAmP (Decreased Abundance by mRNA Perturbation) strain. To make the pho80 DAmP strain, a PCR product including a Nat marker was introduced after the stop codon and selected on YEDP+Nat media. The cassette for the *PHO84* reporter strain was generated by a series of fusion PCRs with 1 kb of *PHO84* promoter sequence, Venus fluorescence protein, and the sequence of *TEF2* promoter-RFP-MET15-URA3 from yMJ003.

Table 2.3. Strains used in this study

Strain	Genotype	Reference
BY4741	MATa *his3Δ1 leu2Δ0 met15Δ0 ura3Δ0*	(Brachmann et al., 1998)
yMJ001	MATα *his3Δ1 leu2Δ0 met15Δ0 ura3Δ0 LYS+ Δcan1::STE2*pr-*spHIS5 Δlyp1::STE3*pr-*LEU2 cyh2*	(Jonikas et al., 2009)
yMJ003	MATα *his3Δ1 leu2Δ0 met15Δ0 ura3Δ0 LYS+ Δcan1::STE2*pr-*spHIS5 Δlyp1::STE3*pr-*LEU2 cyh2 Δura3*::UPRE-GFP-*TEF2*pr-RFP-*MET15-URA3*	(Jonikas et al., 2009)
PHO84 reporter	MATα *his3Δ1 leu2Δ0 met15Δ0 ura3Δ0 LYS+ Δcan1::STE2*pr-*spHIS5 Δlyp1::STE3*pr-*LEU2 cyh2 Δura3*::*PHO84*pr-Venus-*TEF2*pr-RFP-*MET15-URA3*	This study
vip1::Nat^R	MATa *his3Δ1 leu2Δ0 met15Δ0 ura3Δ0 Δvip1::Nat^R*	This study
ipk1::Nat^R	MATa *his3Δ1 leu2Δ0 met15Δ0 ura3Δ0 Δipk1::Nat^R*	This study
aah1::Nat^R	MATa *his3Δ1 leu2Δ0 met15Δ0 ura3Δ0 Δaah1::Nat^R*	This study
ado1::Nat^R	MATa *his3Δ1 leu2Δ0 met15Δ0 ura3Δ0 Δado1::Nat^R*	This study
pho81::Nat^R	MATa *his3Δ1 leu2Δ0 met15Δ0 ura3Δ0 Δpho81::Nat^R*	This study
pho80 DAmp	See “Strains”	This study

Insertion of the *PHO84* expression reporter into a yeast library

Using the Synthetic Genetic Array strategy (SGA) (Tong et al., 2001), the *PHO84* reporter strain was mated to approximately 6100 MATa strains in a deletion library (Jonikas et al., 2009) in addition to DAmP strains for essential genes (Breslow et al., 2008). The protocol I used was similar to the one described by (Schuldiner et al., 2005). The major difference between the two protocols is that MATα - not MATa- haploids were selected as final haploid strains having both the *PHO84* expression reporter and deletion of a gene. This allowed subsequent mating of the final haploid strains to another deletion strain of interest in order to generate double mutants. (see “Making double mutants with array strains” below). After haploid selection, strains were grown twice on SD(MSG) –LEU –ARG –LYS +can +S-AEC +G418 –URA plates to select for

MATα strains carrying the *PHO84* reporter and Kan-marked deletions (Tong and Boone, 2006).

P_i concentrations for screening

50 uM and 1 mM P_i were chosen as low and high P_i conditions, respectively. It was known that there are two populations of cells over a range of P_i concentrations from 100 to 200 uM (intermediate P_i): one that expresses little *PHO84* (off-population) and another that highly expresses *PHO84* (on-population) (Wykoff et al., 2007). Because the relative portion of off- and on-population is sensitive to small changes in P_i, intermediate ranges of P_i were avoided. In order to identify mutants showing subtle defects such as different threshold to activate or repress the PHO pathway, mild conditions -50 uM and 1 mM P_i - for inducing and repressing the PHO pathway were chosen.

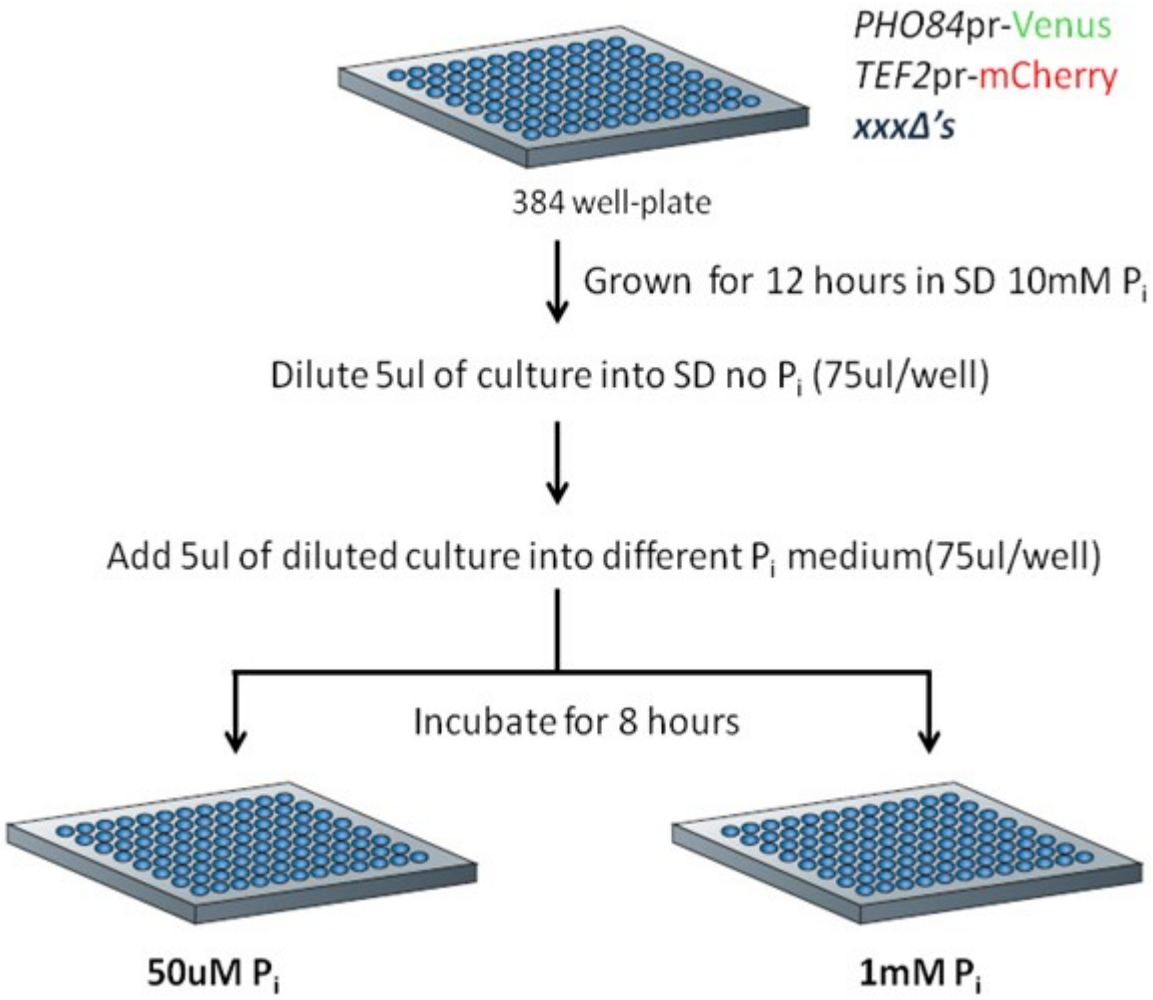

Figure 2.9. Preparation of samples to measure reporter levels in flow cytometry

Measurement of reporter levels

Reporter levels were measured by flow cytometry using YFP and RFP channels. All cell cultures were grown in synthetic complete medium at 30ºC in a 384 well-plate on a plate shaker. Strains were inoculated from the final haploid selection agar plate to 384-well liquid cultures of 80 ul/well SD complete medium with 10 mM P_i concentration

(Figure 2.9). These cultures were grown overnight and back-diluted 16 times using a BioMek FX (Beckman Coulter, Inc.,Fullerton, CA, USA) liquid handling robot in a final volume of 80 ul of SD complete no P_i medium in 384-well plates. Subsequently, the liquid cultures in no Pi medium were diluted 16 fold in a final volume of 80ul of SD complete medium with 1 mM and 50 uM P_i concentration depending on the screening conditions. The strains were grown for additional eight hours before measurements (Figure 2.9).

Plates were then transferred to a Becton Dickinson (BD, Franklin Lakes, NJ USA) High Throughput Sampler (HTS). The HTS injected cells directly from the wells in which they were grown into a LSR Fortessa flow cytometer (BD). The measurement of one 384-well plate required approximately 110 minutes. The detected number of cells was 2,000 ~ 6000 cells. Venus was excited at 488nm and fluorescence was collected through a 505nm long-pass filter and a HQ515/20 band-pass filter (Chroma Technology). mCherry was excited at 532nm and fluorescence was collected through a 600nm long-pass filter and a 610/20 band-pass filter (Chroma Technology). Each plate included two wells containing fluorescent particles (RCP-30-5A, Spherotech) to allow compensation for the eventual variation of laser intensity and at least six wells containing the *PHO84* reporter strain to normalize the fluorescence signals of samples to those of the wild type.

Quantification of *PHO84* expression level of the single mutant

Each cell's intensity in the YFP and RFP channels was used as raw data for further processing. To correct for non-reporter-specific variations in single-cell YFP

abundance - such as altered translation efficiency caused by deletion of some genes - the Venus fluorescence of each cell was normalized to the RFP signal driven by a constitutive *TEF2* promoter. The average of the log2 YFP/RFP ratios across the cells within 30% of the range of top and bottom in a sample was used as the sample's reporter levels in all data shown in this chapter. A customized Matlab code was written to analyze ".fcs" data files from the flow cytometer. Samples with low cell counts (<300/well) were not used. The reporter levels of each sample were normalized by the median of reporter levels of all samples on the same plate to compare the reporter level of each strain regardless of different locations on different plates.

p-value analysis to determine if the deviation of measured phenotypes of single mutants from that of the wild type is statistically significant

The distribution of measurement errors was assumed as the sum of two Gaussian distributions with different standard deviations and an average of zero. The standard deviations were obtained using an iterative fit of the predicted to the actual distribution of the difference between replicate measurements of reporter levels in the deletion library. The error distribution was used to generate the expected distribution of measured values for the wild-type reporter levels. Using this distribution, a p-value lookup table was generated: for each reporter level (R) and the number of measurements (N), the table estimated the probability of obtaining a reporter levels equal to, or more extreme than, R upon the averaging of N independent measurements of a wild-type strain. Because I measured all the library plates three times, the possible values of N for each sample can equal two or three, depending on the strains. The first

weakly inducible candidates were defined as strains with normalized mean intensity ratios to the wild type of < 0 and p-value < 0.001 in 50uM P_i. Similarly, the first constitutively induced candidates were defined as mutants with normalized mean intensity ratios to the wild type of > 0 and a p-value < 0.001 in 1mM P_i.

Making double mutants with the array strains

The protocol used to generate double mutants carrying the array strains and deletion of a gene of interest was exactly the same as described in "Insertion of the *PHO84* expression reporter into yeast library" above except that 100 ug/L nourseothricin was included in haploid selection after sporulation to select for MATα strains carrying the *PHO84* reporter and Kan- and Nat- marked double deletions. The double mutants carrying the *adk1* mutant could not be generated because germination of haploids after sporulation was failed.

Double mutant analysis to identify genes upstream of *PHO80* and *PHO81*

To generate a mutant defective in Pho80, a pho80 DAmP strain was used instead of a *pho80* deletion mutant. It was previously known that the PHO pathway is activated very strongly in the *pho80* deletion mutant, therefore it appeared difficult to detect a decrease in *PHO84* expression levels due to deletion of the weakly inducible genes even if the defect exists. To circumvent that potential problem, I used a *pho80* DAmP strain – instead of the *pho80* mutant - which reduces the stability of *PHO80* transcripts significantly.

The hypothesis regarding epistasis analysis results with the *pho80* mutant was checked by previously known mutants acting upstream and downstream of *PHO80*. The same argument can be applied to constitutively induced mutants. If they act upstream of *PHO81*, double mutants carrying *pho81* deletion and the constitutively induced hits should not be constitutively activated in high P_i conditions.

To validate the hypothesis that double mutants carrying the *pho80* DAmP mutation and weakly inducible genes downstream of *PHO80* show lower reporter levels than the *pho80* DAmP strain, double mutants carrying all the first 445 weakly inducible hits and the *pho80* DAmP mutation were generated through SGA (Tong and Boone, 2006) and their reporter levels were compared to that of the *pho80* DAmP strain (Fig 2.3.A). Double mutants with known downstream gene of *PHO80* - such as *ADA3* and *SNF2* - showed reporter levels of about two times lower than the *pho80* DAmP strain. On the other hand, *pho81 pho80* and *vip1 pho80* double mutants carrying genes upstream of *PHO80* showed very similar reporter levels (-0.19) to the *pho80* DAmP strain. To ensure that no possible hits were lost due to a very stringent threshold to determine the hits, the maximum reporter level among the double mutants carrying the known downstream genes was used to determine if a weakly inducible hit acted upstream of *PHO80*. From this analysis, the first 445 weakly inducible hits were narrowed to 362. On the other hand, the epistasis analysis with the *pho81* mutant for the first constitutively induced hits showed that almost every hit seems to act upstream of *PHO81* (Fig 2.3.B). Through the two steps, I determined 362 weakly inducible hits and 280 constitutively induced hits acting upstream of the core complex.

Chapter 3

Metabolomic Measurements in Response to Changes in P_i Availability

Rationale

Studies have shown that metabolites are involved in regulation of the PHO pathway. Deletion of *ADO1*, *ADK1,* and *AAH1* – genes involved in purine metabolism - constitutively activates the PHO pathway. Furthermore, inositol heptakisphosphate (IP_7) synthesized by Vip1 is required for activating the PHO pathway in P_i starvation conditions. Given these observations, it appears that metabolites relevant to these pathways are key factors in influencing PHO pathway activity. However, little is known about which metabolite is actually responsible for regulation of the PHO pathway. To cover as many metabolites as possible, liquid chromatography/ mass spectrometry was used to measure scores of metabolites simultaneously in response to changes in P_i concentration. Based on dynamic behaviors of metabolites in different P_i conditions, potential regulatory signals for the PHO pathway can be detected.

Results

Measuring variations in the metabolome in response to changes in P_i concentration

To investigate how changes in P_i availability affect a cellular metabolic network, metabolomic variations in the wild type were measured over time upon transferring cells from high to no P_i (P_i-limited condition), and from no to high P_i (P_i-replenished condition) (Figure 3.1, Supplementary table 3.1 and 3.2.). For the measurements in P_i-limited conditions, cells were grown in high P_i first , transferred to no P_i, and taken in 2, 5, 10, 15, 30, 60, and 90 minutes in no P_i. Then, metabolite extractions from the cell cultures were carried out at indicated time points and their abundances were measured with liquid chromatography coupled with mass spectrometry. For the measurements in P_i-replenished conditions, cells starved of P_i for one hour first. Then, P_i was added to the no P_i cell culture to make high P_i (10 mM P_i) and the cell cultures were taken in 0.5, 1.5, 3, 5, 10, 15, 30, and 60 minutes in high P_i. The total number of detected metabolites in both measurements was 85. When the metabolites were clustered depending on the similarity of their dynamic behaviors in different P_i concentrations, two important subgroups were identified. First, some metabolites were downregulated quickly in no P_i but upregulated again in high P_i. Metabolites involved in purine metabolism, glycolysis and the pentose phosphate pathway were included in this subgroup (Figure 3.2.A, B, and C). Secondly, some metabolites behaved in an opposite direction from the first group: upregulated in no P_i but downregulated in high P_i. S-adenosyl-L-homocysteine (SAH), for example, responded the most quickly and significantly to changes in P_i

concentration among all the detected metabolites (Figure 3.5.A). When cells were transferred from high to no P_i, SAH in no P_i was upregulated about 20 times more than in high P_i within two minutes. When P_i was replenished again, however, it was downregulated to the similar level to high P_i within one minute. Because metabolites involved in regulating the PHO pathway are expected to show a strong correlation between their abundance changes with P_i availability, these two groups were investigated in detail.

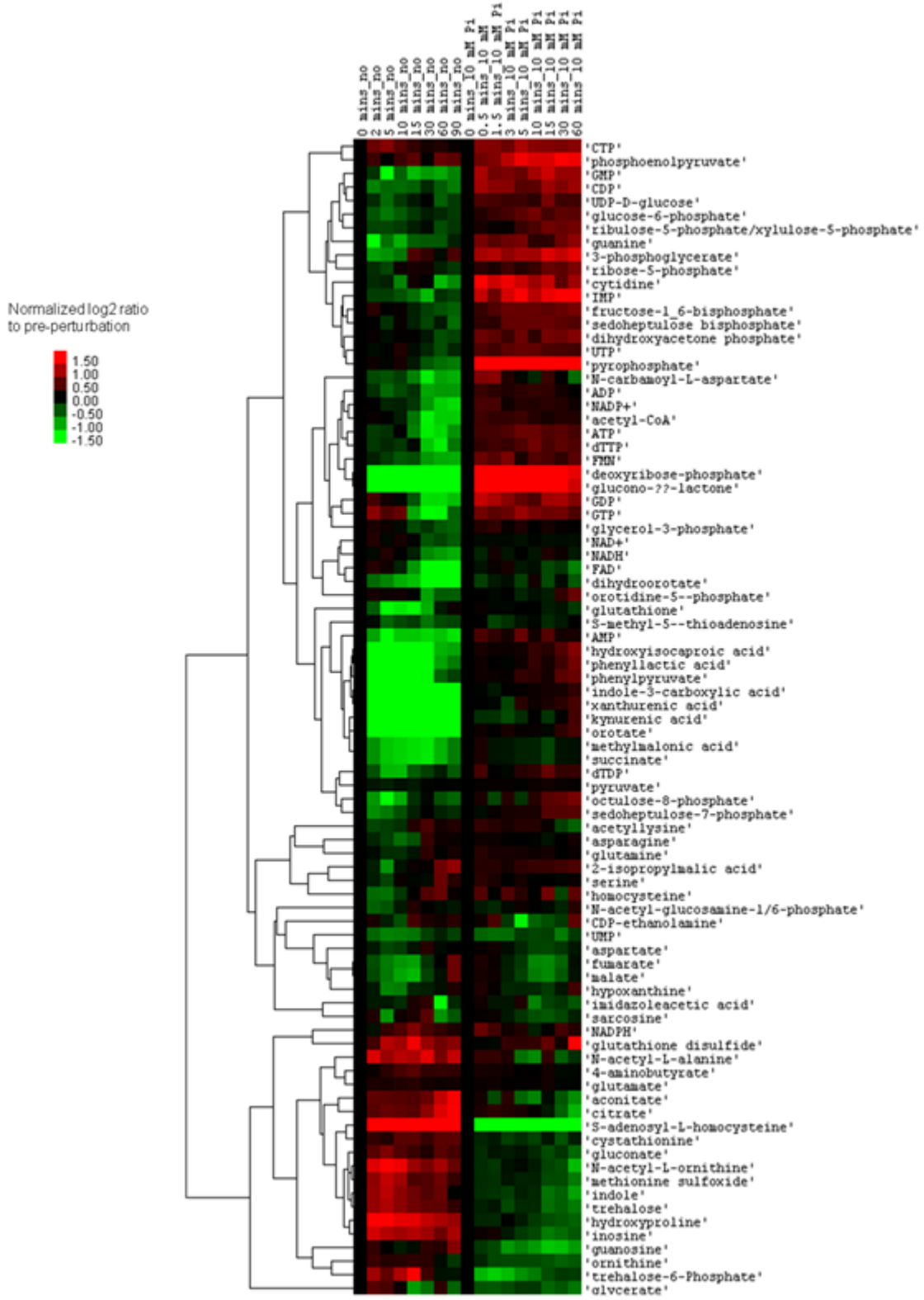

Figure 3.1. A heat map display representing yeast metabolome in response to changes in P_i concentration.

Purine metabolism

As described in Chapter 2, deletion of the purine metabolism genes *ADO1*, *ADK1*, and A*AH1* leads to constitutive activation of the PHO pathway, which suggests that metabolites relevant to purine metabolism may influence PHO pathway activity. The purine metabolism response of the wild type to changes in P_i concentration was consistent with this hypothesis; most of the detected purine metabolites were downregulated in no P_i and were upregulated in high P_i. To test this hypothesis further, variations in the metabolome of the wild type upon transferring it from high to no P_i were compared to those of all the three purine metabolism mutants in high P_i. The abundance of the metabolites regulating the PHO pathway are expected to change in no P_i and the same behavior should be observed in all the *ado1*, *adk1*, and *aah1* mutants in high P_i. As shown in Figure 3.2.A, all the adenine nucleotides were downregulated in both the wild type in no P_i, and all three purine metabolism mutants in high P_i. The nucleotide responses of the wild type occurred within two minutes in no P_i, which meets the criteria of fast response time as a signaling molecule. Interestingly, the responses of nucleosides such as inosine and guanosine in wild type are opposite to the purine nucleotides; they were upregulated in no P_i and were downregulated in high P_i. On the contrary, there were no consistent behaviors among the mutants; the *ado1* mutant showed downregulation of both inosine and guanosine, whereas the *aah1* and *adk1* mutants showed upregulation of inosine and almost no change in guanosine. Putting these observations together, it is conceivable that purine nucleotides could be a regulating signal of the PHO pathway reflecting changes in P_i availability.

Figure 3. 2. Metabolites that were rapidly downregulated in no P_i and were upregulated when P_i is replenished (A) Relative abundance of metabolites in purine metabolism. The first three columns represent the data of the constitutively induced mutants involved in purine metabolism in 10 mM P_i. The rest of the columns represent the data of the wild type in response to changes in P_i concentration. Each time point of the wild type data is the same as Figure 3.1. (B and C) Relative abundance of metabolites in the pentose phosphate pathway and glycolysis, respectively. The different colors of ovals and rectangles in (B) and (C) indicate detected metabolites corresponding to each color in this measurement. Xylulose-5-phosphate and sedoheptulose-7-phosphate are isomers and were not distinguishable in this measurement. (n.d.) stands for “not detected”. (D) Inhibition of hexokinase by trehalose-6-phosphate. (E and F) The variations in trehalose, trehalose-6-phosphate (T6P), and glucose-6-phosphate (G6P) in no and10 mM P_i, respectively.

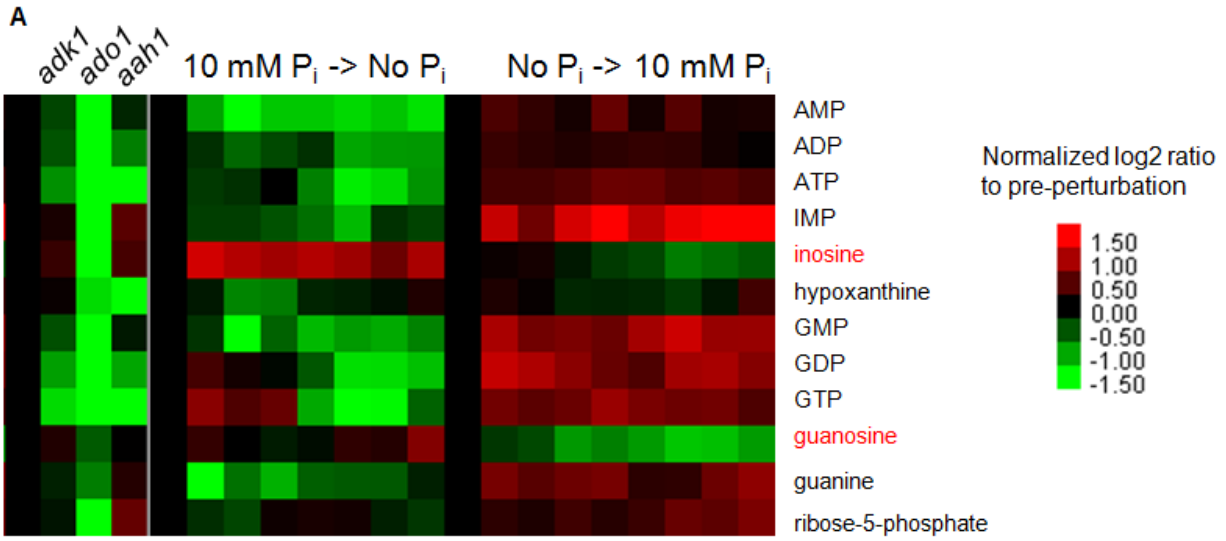

Figure 3. 2. (Continued)

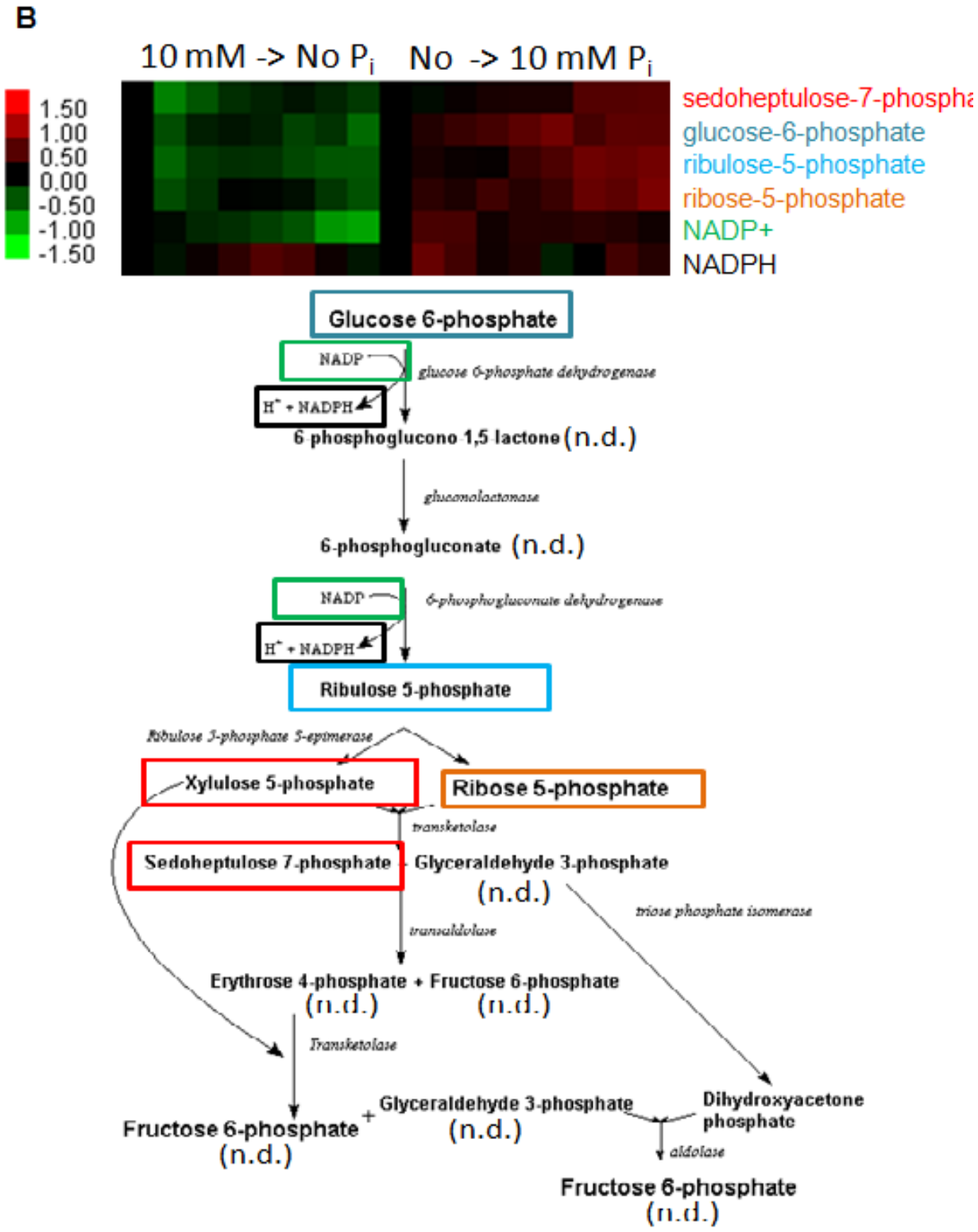

Figure 3. 2. (Continued)

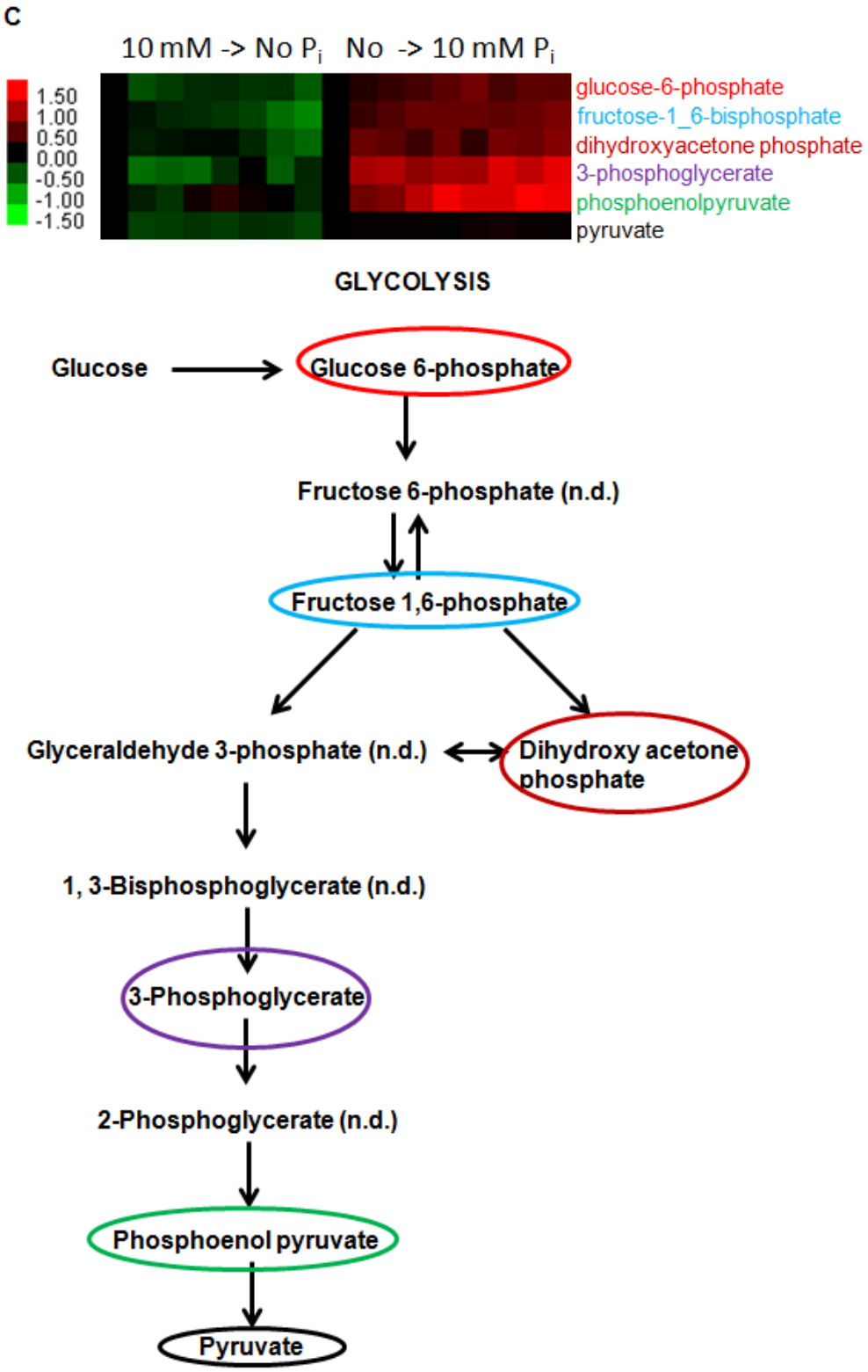

Figure 3. 2. (Continued)

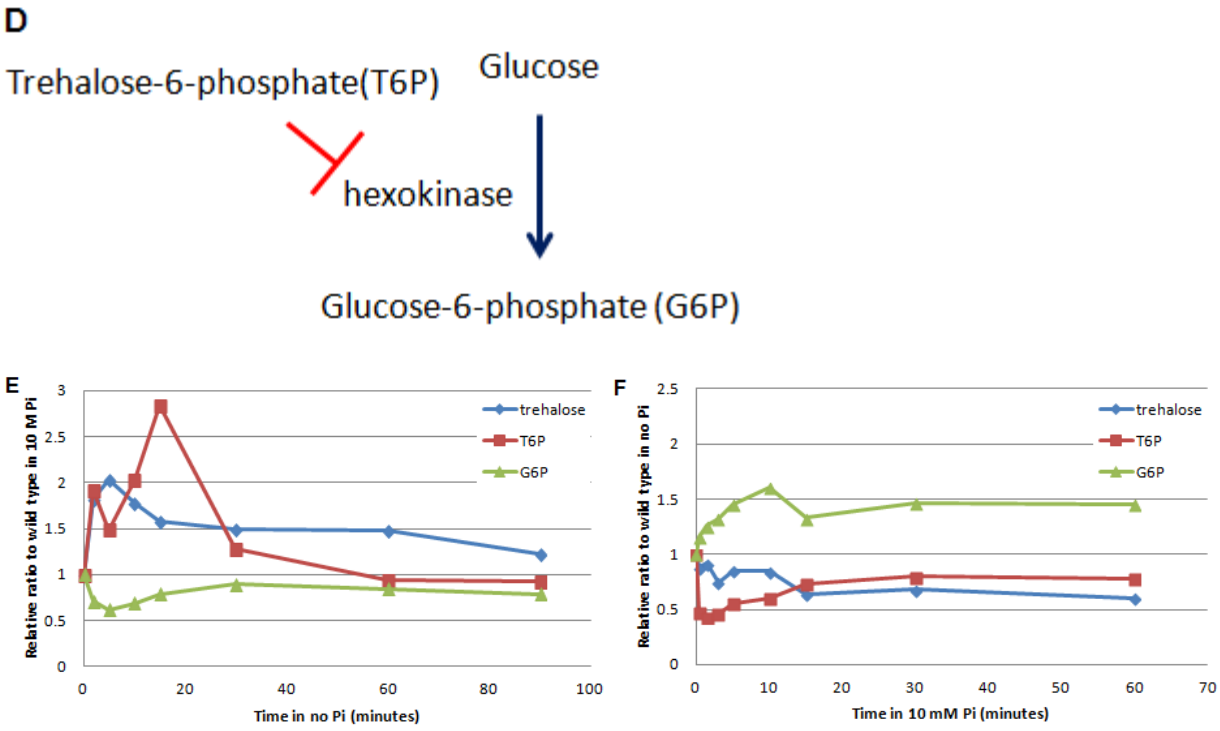

Figure 3. 2. (Continued)

This hypothesis is also consistent with previously reported chemostat data. Boer et al. measured the metabolome of *Saccharomyces cerevisiae* in steady-state cultures in three different limiting nutrients (glucose, ammonium, and P_i) (Boer et al., 2010). In their measurement, ATP was strongly decreased, ADP fell only slightly and AMP accumulated slightly during phosphorus limitation. Moreover, a low adenylate energy charge (AEC) was found selectively in phosphorus limitation. AEC is mainly defined as a ratio of ATP to ADP and represents the amount of metabolically available energy stored in the adenine nucleotide pool. The strong correlation of ATP concentration and AEC with P_i availability in chemostat data suggests that ATP and AEC are reliable indicators for phosphorus availability. Given that the PHO pathway is activated in low P_i conditions, I hypothesized that variations in ATP levels and/or AEC may be P_i-dependent regulatory signals for the PHO pathway.

To test if AEC can reflect the activation of the PHO pathway in low P_i, the AECs of the wild type in no P_i were calculated over time (Figure 3.3.A). When extracellular P_i concentrations change very rapidly from high to no P_i, there was an initial small rise in the AEC for a short period of time; eventually it reached to a similar level to high P_i and was steady until 60 minutes. Given that the PHO pathway is already activated in no P_i in ten minutes (Zhou and O'Shea, unpublished data), AEC does not appear to be P_i-dependent regulatory signals for the PHO pathway.

On the other hand, the AEC correctly predicted the PHO phenotype of single and double mutants carrying deletions of *ADO1* and *AAH1*. As described in Chapter 2, the *aah1* and *ado1* single mutants constitutively activate the PHO pathway (Figure 2.3.B

and C). However, the *aah1 vip1* and *ado1 vip1* double mutants repressed the constitutively activated phenotype of the *aah1* and *ado1* mutants, respectively (Figure 2.5.C). The AECs for the *ado1* and *aah1* mutants were lower than the wild type in P_i starvation for an hour, whereas the *ado1 vip1* and the *aah1 vip1* double mutants had even higher AECs than the wild type in high P_i (Figure 3.3.B). As seen in Figure 3.3.C, deletion of *VIP1* in the *ado1* and *aah1* mutants upregulated ATP the most among adenine nucleotides and led to an increase in AECs in the double mutants. Combined with variations in AECs over time in no P_i, low AEC is sufficient, but not necessary, for activation of the PHO pathway.

Upon P_i limitation, ATP concentration decreased rapidly and the PHO pathway was activated. However, it is not clear whether a decrease in ATP level is a causal factor activating the PHO pathway or a consequence of cellular adaptation to a P_i-limited condition. If a decrease in ATP is an activation signal for the PHO pathway, the PHO pathway should be activated regardless of P_i concentration when ATP is downregulated. This condition can be mimicked by inhibiting glycolysis in high P_i because yeast prefers fermentation to respiration for generating ATP in the presence of glucose in the growth medium. As phosphorylation of glucose mediated by hexokinase is the first step of glycolysis, inhibiting hexokinase activity is expected to lead to a decrease in ATP regardless of P_i concentration. An inhibitor of hexokinase, 3-bromopyruvic acid (3-BrPA) (Pelicano et al., 2006), was introduced in high P_i growth medium to reduce ATP concentrations. As a proxy for the activity of the PHO pathway, Pho4 nuclear localization and *PHO84* expression levels were measured with different concentrations of 3-BrPA (see “Measurement of Pho4 nuclear localization” in Methods).

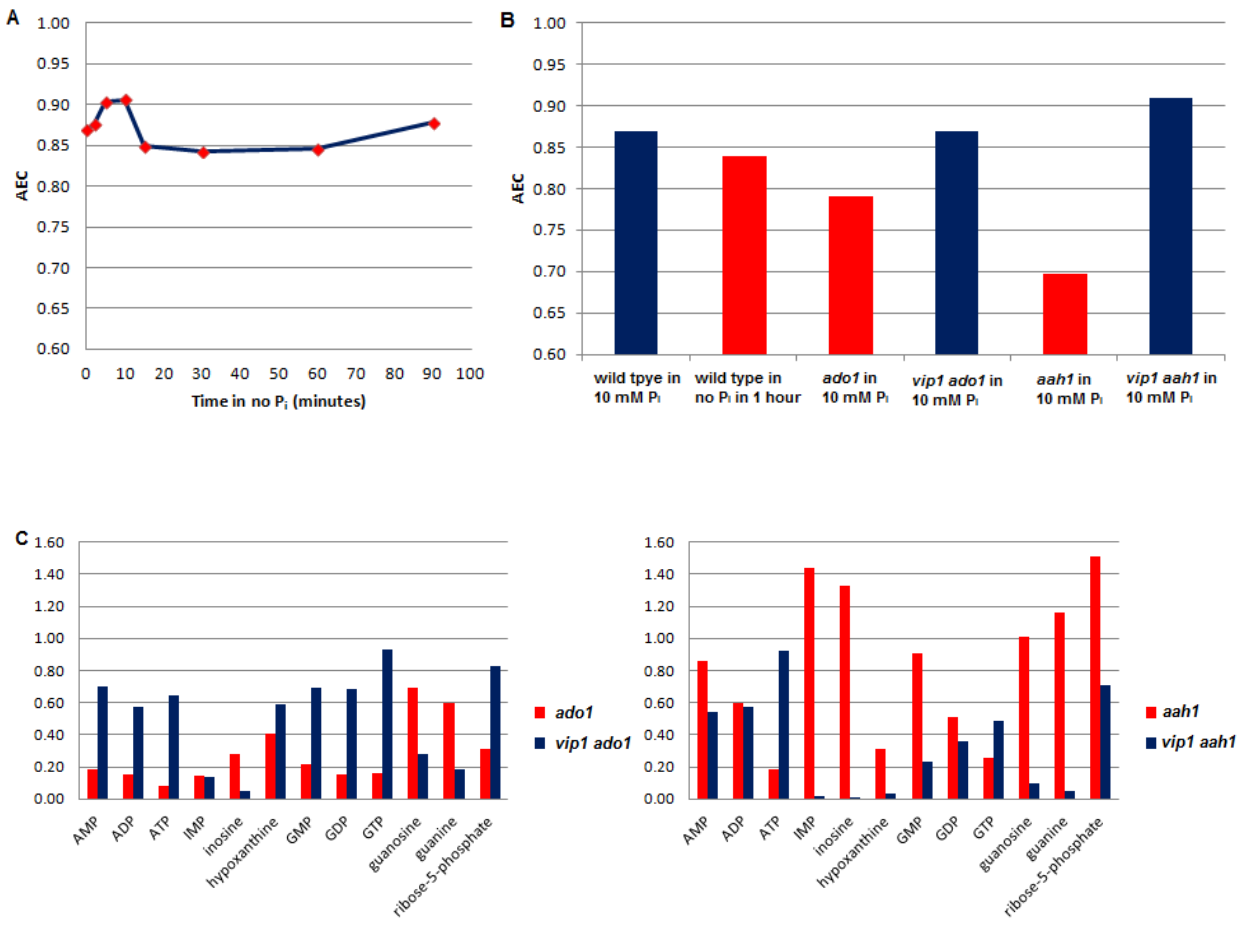

Figure 3. 3. Adenylate energy charges (AEC) in response to changes in P_i concentration and comparison of AEC among the purine metabolism mutants. (A) AECs over time when cells were transferred from 10 mM to no P_i (B) AECs of wild type and purine metabolism mutants. The red and blue bars indicate the activated and repressed state of the PHO pathway, respectively. (C) The relative abundance of purine metabolites in the *aah1,* the *ado1,* the *aah1 vip1* and the *ado1 vip1* mutants in 10 mM P_i. Each metabolite is normalized to the corresponding one in the wild type in 10 mM P_i.

In the presence of 3 and 5 mM 3-BrPA in high P_i, cellular ATP levels decreased by 50% and 90%, respectively, within 30 minutes (Figure 3.4.A). However, no *PHO84* expression and no discernible nuclear Pho4 and were observed even when 90% of ATP was depleted (Figure 3.4.B and C). Given that the extent of decrease in ATP levels in

this condition is below the lowest ATP level observed in no P_i, a decrease in ATP levels alone does not seem to be a regulatory signal for the PHO pathway. Then, is a decrease in ATP levels a consequence of cellular adaptation to P_i starvation? As seen in Figure 3.2. B and C, many intermediates in glycolysis and the pentose phosphate pathway were downregulated in no P_i. Glycolysis and the pentose phosphate pathway are related to purine nucleotide metabolism given that glycolysis is a main route to generate ATPs in budding yeast in the presence of glucose in the environment and one of the major products of the pentose phosphate pathway is ribose-5-phosphate that is required for converting adenine to adenine nucleotide. Therefore, it appears that a decrease in ATP levels in no P_i results from downregulation of glycolysis and the pentose phosphate pathway.

The molecular mechanism by which glycolysis and the pentose phosphate pathway are downregulated in low P_i conditions appears to be associated with downregulation of Glucose-6-phosphate (G6P). Given that G6P lies at the start of glycolysis and the pentose phosphate pathway (Figure 3.2.B. and C.), downregulation of glucose-6-phosphate seems the most efficient way to downregulate both of the metabolic pathways. As seen in Figure 3.2.E and F, trehalose-6-phosphate (T6P), a potent hexokinase inhibitor (Figure 3.2.D) (Blazquez et al., 1993), was upregulated in no P_i and G6P was downregulated almost at the same time. In P_i-replenished conditions, however, T6P was downregulated and G6P was upregulated at the same time. Therefore, an increase in T6P in low P_i conditions appears to cause G6P to be downregulated, resulting in downregulation of glycolysis and the pentose phosphate pathway from their beginning step.

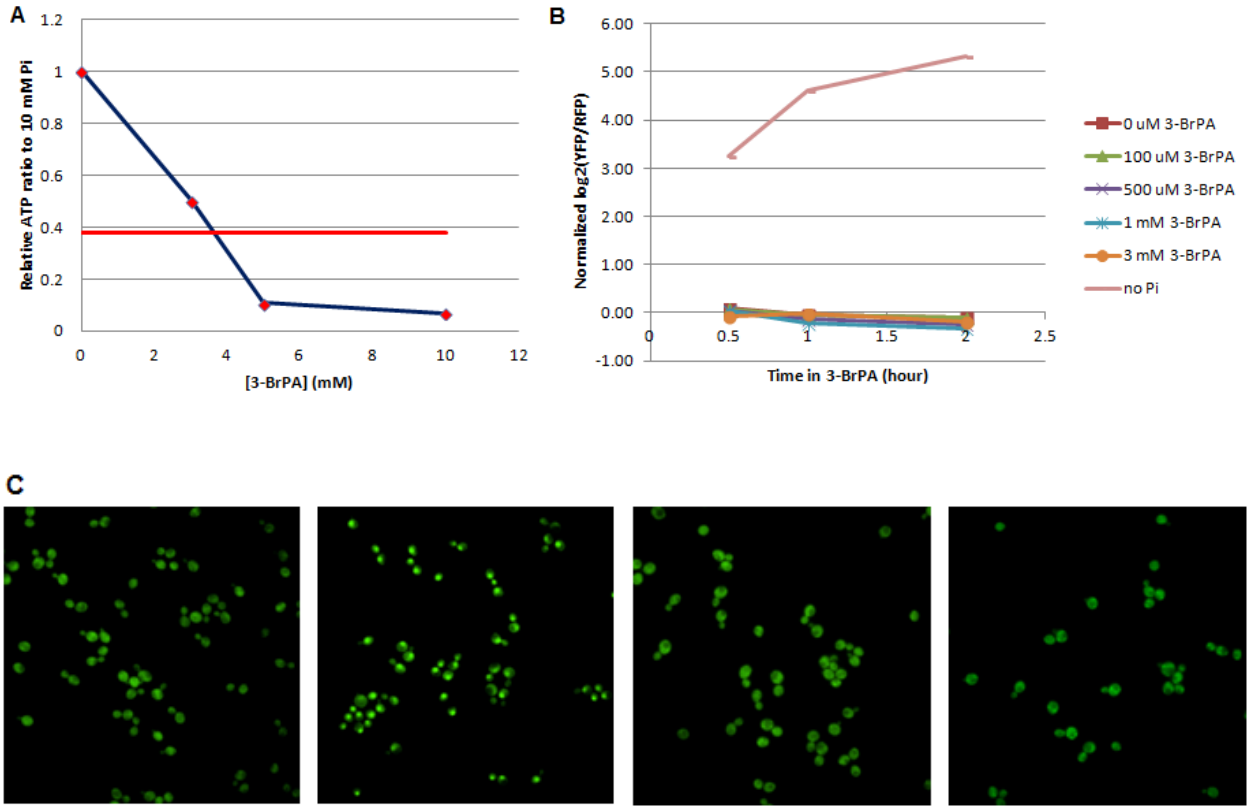

Figure 3. 4. The effect of decreases in ATP levels on activation of the PHO pathway. (A) Depletion of ATP with 3-bromopyruvic acid (3-BrPA) within 30 minutes. The red horizontal line indicates the lowest ATP level measured in no P_i. (B) *PHO84* expression levels as a function of 3-BrPA concentrations over time. *PHO84* expression levels were normalized to wild type in 10 mM P_i. (C) No Pho4 nuclear localization was observed in the presence of 3-BrPA in 10 mM P_i. (From the left) Pho4 localization in the nucleus in 10 mM P_i, no P_i, 10 mM P_i with 3 mM 3-BrPA, and 10 mM P_i with 5 mM 3-BrPA.

Changes in the de *novo* phosphatidylcholine (PC) biosynthesis in response to changes in P_i concentration

In contrast to purine metabolism, glycolysis and the pentose phosphate pathway, some metabolites were upregulated quickly in no P_i but downregulated again in high P_i, S-adenosyl-L-homocysteine (SAH) was included in this group and responded the most

quickly and significantly to changes in P_i concentration among the detected metabolites. Upon changing P_i concentration from high to no P_i, SAH was upregulated to a level about 20 times more than in high P_i within two minutes. However, SAH was downregulated to a level similar to that in high P_i within one minute of P_i replenishment (Figure 3.5.A).

Given the fast time scale and large amplitude variations in response to changes in P_i concentration, SAH appears to have an important physiological role associated with P_i availability. One possibility is that SAH is a regulatory signal for the PHO pathway. To test this hypothesis, Pho4 nuclear localization and *PHO84* expression levels were measured as a function of SAH concentration in high P_i. Christopher et al. showed that simply adding exogenous SAH into the growth medium can lead to an increase in intracellular SAH concentrations without changing P_i concentration (Christopher et al., 2002). If SAH regulates the activity of the PHO pathway, changes in the SAH concentration in the growth medium should activate the PHO pathway independent of the actual P_i concentrations. As seen in Figure 3.5.B, C, and D, both nuclear Pho4 localization and *PHO84* expression levels increased as SAH concentration increases, suggesting that the PHO pathway can be activated in a SAH-dependent manner without changing P_i concentration. However, the extent of activation of the PHO pathway with SAH in high P_i was less than that without SAH in no P_i. Averaged nuclear Pho4 levels were already saturated in 500 uM SAH but lower than those in no P_i (Figure 3.5.C).

Figure 3. 5. S-adenosyl-L-homocysteine (SAH) and the activity of the PHO pathway (A) SAH response to changes in P_i concentration. (B) The histograms of Pho4 nuclear localization intensities in 10 mM Pi with different SAH concentrations. From the left, SAH concentrations were 0, 10, 50, 100, 300, 500 uM, respectively. (C) Averaged Pho4 nuclear localization as a function of SAH concentration. Pho4 intensity is arbitrary unit and the error bar is standard deviation of each SAH concentration. (D) *PHO84* expression levels as a function of SAH concentration in 10 mM P_i.

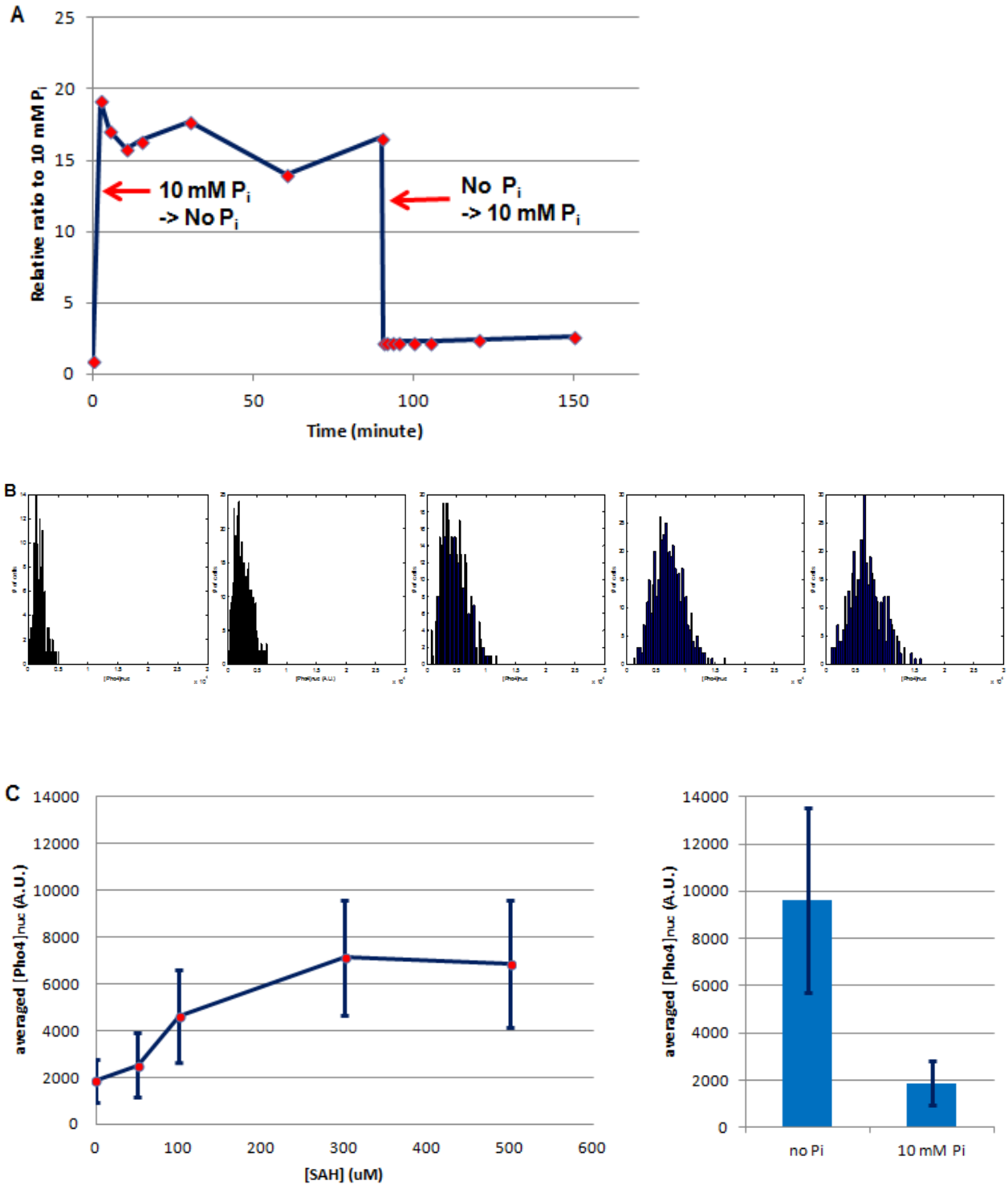

Figure 3. 5. (Continued)

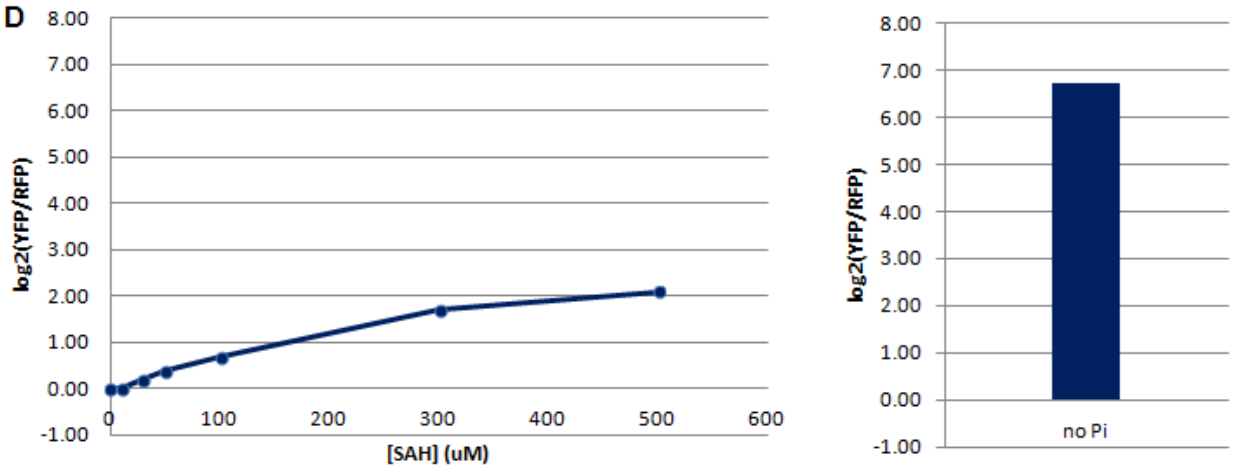

Figure 3. 5. (Continued)

Accordingly, *PHO84* expression levels increased just four times compared to 1 mM P_i as opposed to ~80 times in no P_i (Figure 3.5.D). Presumably, the uptake capacity of exogenous SAH from the medium was already saturated in 300 uM SAH such that the increased intracellular SAH concentration was still lower than that in no P_i. These preliminary data are consistent with the hypothesis that an increase in SAH could be an activation signal of the PHO pathway.

Another possible physiological role for SAH is serving as a signal for regulating other cellular reactions utilizing P_i as a substrate. It was previously shown that SAH is a potent inhibitor of S-adenosyl-L-methionine-dependent methyltransferases, two of which are responsible for *de novo* synthesis of phosphatidylcholine (PC) (Figure 3.6.A) (Wolfe and Borchardt, 1991, Lee et al., 1998). In the absence of choline, sequential methylation of phosphatidylethanolamine (PE) is a dominant pathway for PC synthesis (Choi et al., 2005, Malanovic et al., 2008). Given that the growth medium in this study did not contain choline, a possible working model is that SAH acts as an antagonist of *de novo* synthesis of PC in P_i starvation. To test this model, PC levels in no P_i were quantified over time and were shown to be downregulated by 40% within an hour (Figure 3.6.B, see “PC quantification”).

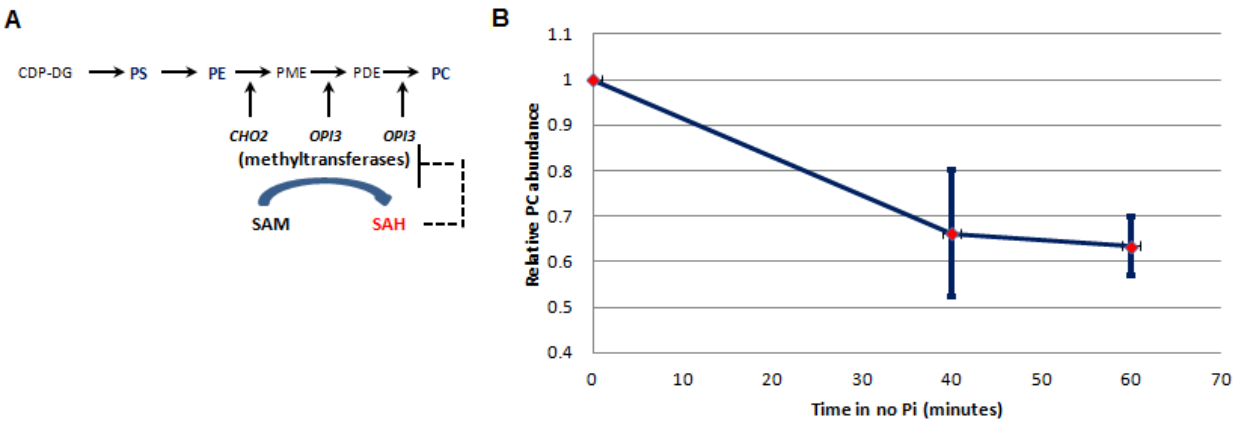

Figure 3. 6. S-adenosyl-L-homocysteine (SAH) as an inhibitor of *de novo* phosphatidylcholine (PC) biosynthesis (A) *de novo* PC synthesis via sequential methylation of PE; CDP-DG, CDP-diacylglycerol; PS, phosphatidylserine; PE, phosphatidylethanolamine; PME, phsosphatidylmonomethylamine; PDE, phsosphatidyldimethylamine (B) Relative PC abundance in no P_i over time.

Discussion

Given that the *ado1*, *adk1*, and *aah1* mutants constitutively activate the PHO pathway and they are involved in purine metabolism, measuring changes in purine metabolites in different P_i concentrations is of high interest. The metabolomic measurements in this study revealed the common features between wild type in no P_i and all the three purine metabolism *ado1*, *adk1* and *aah1* mutants in high P_i; all adenine nucleotides were downregulated. This purine metabolism response is consistent with the idea that changes in adenine nucleotides could regulate the PHO pathway. From previously reported chemostat experiments during P_i limitation (Boer et al., 2010), it was suggested that ATP levels and/or adenylate energy charge (AEC) signals P_i availability. Given that the PHO pathway is activated in low P_i, low ATP levels and/or low AEC may be initiating a signal of activation of the PHO pathway. However, I showed that a decrease in ATP levels alone does not appear to activate the PHO pathway and AEC does not change from high to low P_i conditions, implying that those two factors alone cannot be triggering signals to activate the PHO pathway. Rather, low levels of all nucleotides appear to be the consequence of the downregulation of glycolysis and the pentose phosphate pathway in a P_i-limited condition as glycolysis is a major source of ATP generation and the pentose phosphate pathway produces ribose-5-phosphate that is required for nucleotide synthesis.

Like purine metabolism, glycolysis and the pentose phosphate pathway were downregulated in no P_i. The reason why glycolysis is downregulated in P_i starvation may be associated with the mechanism by which glycolysis generates ATPs. The initial two steps in glycolysis consume ATP to activate glucose and a surplus of ATP is

generated further down the pathway. The first substrate for energy-yielding steps is glyceraldehyde-3-phosphate, which reacts with NAD+ and P_i. When P_i starvation makes intracellular P_i levels at least transiently low, this reaction may be less favorable due to low level of intracellular P_i. In this case, cells may not go through glycolysis to the end and just consume ATPs in vain. In order not to waste ATPs in a P_i-limited condition, glycolysis may be inhibited from its beginning step, phosphorylation of glucose. Given that gluocose-6-phosphate is also the first substrate entering the pentose phosphate pathway, the pentose phosphate pathway is also inhibited from the first step during P_i starvation. Therefore, it appears that downregulation of glycolysis and the pentose phosphate pathway in response to P_i starvation is the consequence of the metabolomic rearrangements in order to optimize the usage of cellular resources.

Among detected metabolites, SAH showed the largest variations in response to change in P_i concentrations. Given that a metabolite involved in regulation of the PHO pathway is expected to show a strong correlation between its abundance and changes in P_i availability, I tested the hypothesis that SAH could be a regulatory signal of the PHO pathway. As exogenous SAH levels increased in the medium, the PHO pathway was activated even in high P_i presumably by increasing cellular SAH levels. This preliminary data is consistent with the hypothesis, although it remains uncertain that the SAH-dependent activation is relevant to a P_i starvation signal. Given that the *pho81* mutant is uninducible in low P_i, the *pho81* mutant is expected to be uninducible with SAH if SAH-induced activation is relevant to P_i limitation signal. As a proxy for activity of the PHO pathway, Pho4 nuclear localization and *PHO84* expression will be measured as a function of SAH concentration in the *pho81* mutant.

Another issue with the SAH-induced activation of the PHO pathway was that the extent of the activation induced by exogenous SAH is still lower than that in no P_i. One possible explanation is that the increased intracellular SAH concentration by exogenous SAH is still lower than the level increased by P_i starvation conditions. Given that the SAH hydrolase Sah1 is the only enzyme responsible for degrading SAH in yeast (Malanovic et al., 2008), downregulation of Sah1 could increase intracellular SAH concentration higher than the maximum level achieved by exogenous SAH. With a strain expressing *SAH1* under control of the doxycycline-repressible tetO7 promoter, the Sah1 level can be titrated as a function of doxycycline. Therefore, the activity of the PHO pathway in this strain will be measured as a function of doxycycline concentration in high P_i to address this issue.

In addition to being a possible signaling molecule of the PHO pathway, SAH was previously known to inhibit Cho2 and Opi2 which are responsible for *de novo* synthesis of PC (Malanovic et al., 2008). Given that PC biosynthesis is one of the major anabolic pathways consuming P_i, it may need to be inhibited to maintain intracellular P_i concentration in a low P_i environment. I showed that PC levels decreased in no P_i condition, suggesting that PC biosynthesis is regulated by P_i concentration. Given that SAH levels were downregulated in P_i replenishment (Figure 3.5.A), PC levels are expected to recover in 10 mM P_i. Combined with the changes in PC abundance observed in no P_i, the recovery of PC levels in high P_i would be strong evidence that PC abundance is regulated by P_i concentration through SAH. For this purpose, experiments focused on measuring PC in both 0 and 10 mM P_i are ongoing. Furthermore, as other kinds of phospholipids such as phosphatidylserine and phosphatidylethanolamine are

precursors of PC biosynthesis (Carman and Han, 2009), it is possible that downregulation of PC in low P_i can affect the composition of phospholipids. To investigate how cells rearrange the distribution of phospholipids in response to changes in P_i concentration, I am working on a global profiling of the lipidome in different P_i concentrations.

Materials and methods

Strains

All the strains used in Chapter 3 were generated by the same method described in Chapter 2. These are the strains used in Chapter 3.

Table 3.1. Strains used in this study

Strain	Genotype	Reference
ado1 vip1	MATa *his3Δ1 leu2Δ0 met15Δ0 ura3Δ0 Δvip1::Kan^R ado1::Nat^R*	This study
aah1 vip1	MATa *his3Δ1 leu2Δ0 met15Δ0 ura3Δ0 Δvip1::Kan^R aah1::Nat^R*	This study
Pho4-GFP	K699 ade2-1 trp1-1 can 1-100 leu2-3,112 his3-11,15 ura3 GAL+, PHO4::PHO4-GFP, NHP6a::NHP6a-mRFP	EY2516
pho81 mutant in EY2516	*Δpho81::CgHis* in EY2516	This study
pho81 mutant in PHO84 reporter	*Δpho81::Nat^R* in PHO84 reporter	This study

Metabolic profiling

The metabolome of *Saccharomyces cerevisiae* was characterized as previously described (Xu et al., 2012). Briefly, O.D. of 0.3 overnight cultures were diluted 1:70 and grown in 10 mM P_i synthetic complete medium in a shaking flask to A600 of ~ 0.2 over 12 hours. For experiments in no P_i, cells were filtered onto a nylon membrane filter, washed with no P_i medium, and transferred into pre-warmed no P_i medium. For experiments in P_i replenished conditions, cells starved of P_i for one hour first and 1M

KH_2PO_4 were directly added to the shaker such that the final concentration was 10 mM P_i. A portion of the cells (5 mL) were filtered onto the nylon filter, which was immediately transferred into - 20°C extraction solvent (40:40:20 acetonitrile/methanol/water). Serial extraction was then carried out at indicated time points after cells were transferred to different P_i media. Cell extracts were analyzed by reversed phase ion-pairing liquid chromatography (LC) coupled with electrospray ionization (ESI) (negative mode) to a high-resolution, high-accuracy mass spectrometer (Exactive; Thermo Fisher Scientific) operated in full scan mode at 1 s scan time, 10^5 resolution, with compound identities verified by mass and retention time matched to authenticated standard (Lu et al., 2010). Isomers are reported separately only where they are fully chromatographically resolved.

Quantification of relative abundance of metabolites and clustering

To convert raw LC-MS/MS ion counts to relative cellular concentration data, ion counts were first normalized by the total number of cells. The typical cell density was ~ 0.2 and 5 ml of cell culture was used. After normalization, absent values (where no peak was detected) and normalized ion counts below 300 were set to 300 to remove variations in compounds that were near the limit of detection. The selection of 300 normalized ion counts as a floor value is based on the lower limit of quantitation typically being ~100 ion counts and the smallest normalization factor being around 0.30. Normalized ion counts for each metabolite in every sample are provided in Supplementary Data 1. Normalized ion counts were then converted to relative concentrations by dividing the value for the experimental samples by the corresponding

value from 10 mM P_i. All time-point data were sampled twice and each experiment was replicated at least once. The average of two time-point data was used to represent each time point for one experiment and averaged relative abundance of each experiment was used for further analysis. To display the clustered heat map in Figure 3.1., each relative concentration was log2 transformed first and hierarchically clustered by metabolite using Pearson correlation (Eisen et al., 1998).

Calculation of adenylate energy charge

Adenylate energy charge (AEC) is defined as follows:

$$AEC = ([ATP]+0.5*[ADP])/([ATP]+[ADP]+[AMP]) \quad (1)$$

The absolute concentrations of adenine nucleotides in high P_i were known; [ATP] = 1.93 mM, [ADP] = 0.491 mM, and [AMP] = 0.0835 mM (Xu and Rabinowitz, unpublished data). Using the relative abundance of each purine nucleotide to the wild type in 10 mM P_i, AEC was calculated with the equation (1).

Measurement of relative intracellular ATP concentration with 3-BrPA.

O.D. 600 of 0.2 of cells grown in 10 mM P_i were transferred into fresh 10 mM P_i with 0, 3, 5, 10 mM 3-BrPA and incubated for 30 minutes. Cells were lysed with an ATP assay kit (BacTiter-Glo Microbial Cell Viability Assay, Promega) and luminescence was measured with Beckman Top counter for one second. The raw intensity was divided by

the one with no 3-BrPA and the ratio was reported as ATP relative abundance to 10 mM P_i.

Measurement of Pho4 nuclear localization

Nuclear Pho4 was observed with an inverted fluorescence microscope. The nucleus and cytoplasm portion of each cell was segmented with my customized Matlab code. The Pho4 nuclear localization signal was defined as a difference in GFP intensities between in the nucleus and in the cytoplasm.

PC quantification

The protocol to measure PC levels was the same as described in "Metabolite measurement" above except for an additional lipid extraction. To extract lipids from cell pellets, each was resuspended in 1 mL PBS and transferred into a douncer. 1 ml of MeOH and 2 ml of $CHCl_3$ was added and dounced 40 times. In this step, the internal standard for PC was added in order to correct for different extraction efficiencies between the samples. The suspension was transferred into an 8 ml glass vial. The used douncer was washed with 2 ml of $CHCl_3$ and dounced 10 more times to take the residual amount of lipids on the surface of the douncer. The lysed cell suspension was spun down at the maximum speed for 8 minutes. The bottom organic phase was taken and blown with N_2 to distill $CHCl_3$. When no liquid was observed, the extracted lipids were resuspended in 200 ul of $CHCl_3$.

The majority of detected PCs were the ones with C32:1, C34:1 and C34:2 of lipid class; a raw PC signal in each time-point was the sum of the raw intensities of the three members. Then, the raw PC signals were normalized by the used number of cells and the detected internal standard signal.

Chapter 4

Conclusion

The metabolism in living organisms is highly adaptive in response to changes in nutrient availability because a quick adaptation to nutrient-limited environment is essential for cell survival. P_i is an essential nutrient and cells should be able to rectify a decrease in intracellular P_i concentration resulting from a P_i-limited condition. In *Saccharomyces cerevisiae*, the PHO pathway allows a coordinated cellular response and adaptation to changes in external P_i availability. The cellular response to P_i limitation and surplus conditions requires the ability of sensing P_i availability. Although the molecular mechanism of how the transcription of the PHO regulon responds to changes in P_i availability is well understood, little was known about how cells sense the P_i availability.

Given that signaling factors for the PHO pathway should be identified in order to understand the molecular mechanism by which cells sense P_i availability, I exploited two orthogonal experimental approaches; genetic screening is to identify protein components in the signaling network of the PHO pathway and metabolic profiling is to identify small molecules conveying information of P_i availability. From genetic screening, I found novel genes involved in upstream signaling of the PHO pathway and functional relationships among the identified genes. Metabolic profiling showed how the metabolome of *Saccharomyces cerevisiae* responded to changes in P_i availability.

These two experimental approaches addressed different aspects of the signaling of the PHO pathway, whereas the outcome of these two experiments converged to a particular metabolism: a connection between methyl cycle and purine metabolism (Figure 4.1). In addition to the purine metabolism genes *ADK1* and *ADO1* whose deletion lead to strong activation of the PHO pathway constitutively, my genetic

screening showed that another purine metabolism gene *AAH1* also acts upstream of *PHO81* and represses the PHO pathway in high P_i. This suggests that purine metabolism is relevant to sensing P_i availability. Moreover, SAH abundance was upregulated in P_i-limited conditions in my metabolic profiling and exogenous SAH in the growth medium could induce activation of the PHO pathway regardless of P_i availability. Given that SAH is connected to purine metabolism via adenosine, a byproduct of SAH hydrolysis and a substrate for Ado1, variations in SAH abundance in response to changes in P_i availability implicates that SAH is a potential activation signal of the PHO pathway.

However, it still remains unclear that SAH is a P_i-dependent signaling factor for the PHO pathway. To address this issue, it will be necessary to confirm that the extent to which the PHO pathway is activated by an increase in SAH levels in the cells can be similar to the level induced by P_i starvation. In addition, measuring the PHO phenotype in the *pho81* mutant in the presence of SAH will be crucial in order to determine that SAH activates the PHO pathway through the same route as P_i-limited conditions.

I believe that my work will be useful resource for the future research on understanding the sensing mechanism of P_i availability. It will be interesting to explore more genetic interactions between the genes involved in upstream signaling of the PHO pathway shown in Supplementary table 2.1 and 2.2 in order to generate a more comprehensive map for the metabolic network relevant to the P_i sensing mechanism. And the further characterization of metabolic profiling data shown in Supplementary table 3.1 and 3.2 might be fruitful for continuing research on identifying small molecules like SAH that could be involved in sensing P_i availability.

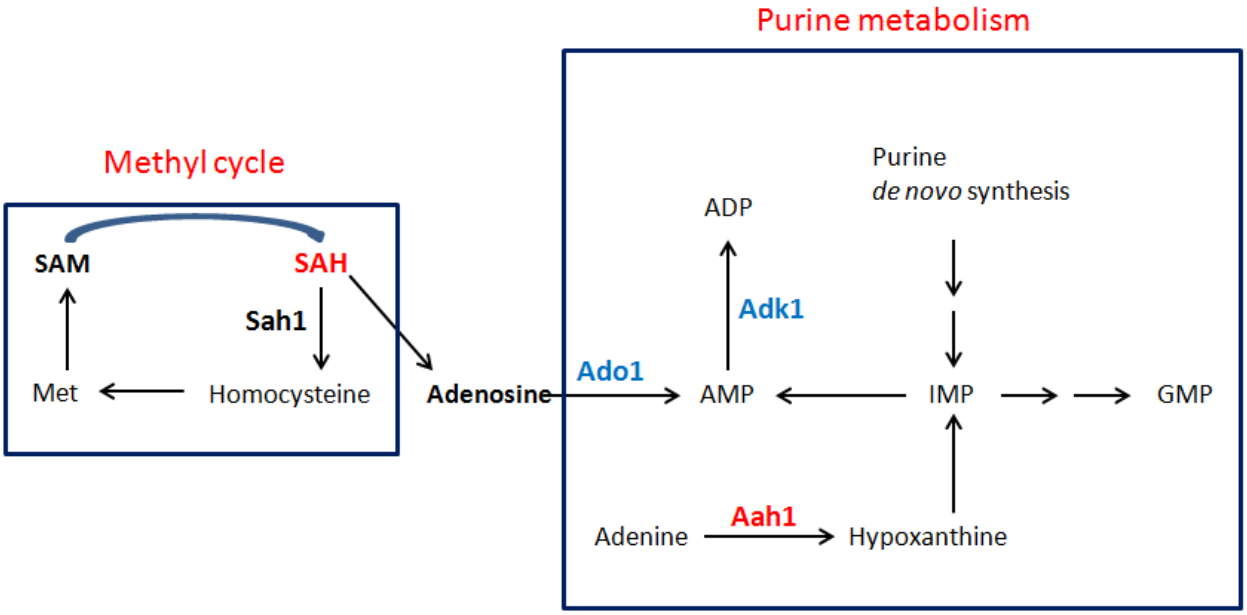

Figure 4.1. S-adenosyl-L-homocysteine (SAH) as a potential activation signal for the PHO pathway. Enzymes in blue were known as the ones involved in upstream signaling of the PHO pathway. SAH and Aah1 in red were identified in this study; Met, methionine; SAM, S-adenosyl-L-methionine; AMP, adenosine monophosphate; ADP, adenosine diphosphate; IMP, inosine monophosphate; GMP, guanosine monophosphate.

Appendix 1. Supplementary Tables

Supplementary table 2.1. List of constitutively induced mutants identified from the single mutant screening. The normalized log2 (YFP/RFP) ratio of the wild type in 50 uM P_i is 4.5.

Gene	averaged log2 (YFP/RFP) ratio normalized to WT in 1mM P_i	standard deviation	p-value	# of experiments
PHO85	7.46	0.22	<1.0E-247	3
PHO80	7.44	0.39	<1.0E-247	2
ADK1	6.22	0.70	<1.0E-247	3
ADO1	5.50	0.60	<1.0E-247	3
REC8	4.47	3.96	2.7E-247	2
AAH1	3.92	0.25	3.5E-191	3
PHO90	3.83	0.81	1.1E-182	3
SAM37	2.66	1.74	2.47E-90	3
TUF1	2.54	0.20	9.7E-83	3
HBS1	2.51	0.11	6.11E-55	2
YOR200W	2.42	0.15	1.21E-75	3
RPL2B	2.27	0.97	6.26E-67	3
LDB7	1.97	0.95	5.81E-35	2
SLM5	1.84	0.64	2.12E-45	3
YER087W	1.81	0.64	3.56E-44	3
PHO87	1.65	0.94	1.29E-37	3
EAP1	1.37	0.02	1.14E-18	2
SAC3	1.34	0.05	3.09E-26	3
EOS1	1.23	0.05	9.96E-16	2
OPI1	1.23	0.19	1.32E-22	3
THP1	1.22	0.33	1.87E-22	3
CTK3	1.10	0.10	2.85E-13	2
PEX5	1.10	0.07	2.85E-13	2
PPQ1	1.10	0.04	3.51E-13	2
MFT1	1.09	0.04	9.54E-19	3
HIS6	1.07	0.03	1.34E-12	2
ECM30	1.04	0.03	4.04E-12	2
RPA43	1.04	0.06	3.09E-17	3

Supplementary table 2.2. List of weakly inducible mutants acting upstream of *PHO80* identified from the single mutant screening. The normalized log2 (YFP/RFP) ratio of the wild type in 1 mM P_i is -4.5

Gene	averaged log2 ratio normalized to WT in 50 uM P_i	standard deviation	p-value	Averaged log2 ratio normalized ratio to the *pho80* mutant	number of measurements
PHO81	-5.86	0.79	5.79E-31	-0.19	3
PHO4	-5.23	0.34	4.23E-28	-8.19	3
PHO2	-5.05	0.21	3.53E-24	-6.82	2
YJL175W	-4.87	1.33	1.66E-12	-0.29	2
NSR1	-4.11	1.01	2.23E-18	-0.13	3
TRM9	-4.10	1.33	1.81E-08	-0.55	3
RPL36B	-4.04	0.91	1.37E-15	-1.00	3
YGL188C-A	-3.86	1.14	1.08E-09	-0.80	2
OPI11	-3.77	1.34	1.25E-12	-0.30	2
DLT1	-3.48	1.68	1.64E-09	-0.37	3
RPL20A	-3.47	1.16	7.54E-08	-0.49	3
LDB16	-3.42	1.50	1.44E-06	-0.55	2
RSA1	-3.40	1.29	1.46E-05	-0.45	2
SIM1	-3.37	1.65	7.49E-06	-0.24	3
YBR196C-A	-3.32	1.88	3.51E-10	-0.42	3
RPL19B	-3.30	2.83	3.10E-12	-0.34	3
SHR3	-3.29	1.91	7.48E-10	-0.74	2
EFG1	-3.22	1.17	2.80E-05	-0.29	3
YOR309C	-3.20	1.24	3.78E-12	-0.01	3
SAK1	-3.03	2.09	2.74E-07	-0.59	3
SPA2	-2.98	1.86	1.41E-10	-0.38	3
SPT4	-2.97	0.94	4.24E-08	0.80	3
YOR309C	-2.94	1.59	3.78E-12	-0.08	3
SSF1	-2.93	1.65	1.41E-05	-0.31	3
SNF11	-2.90	1.83	1.91E-08	-0.65	3
YPL225W	-2.88	1.82	9.92E-04	-0.37	3
APM3	-2.88	1.99	1.20E-11	-0.65	3
YOR338W	-2.85	1.77	3.31E-04	-0.27	3
YPR197C	-2.81	1.68	2.74E-07	-0.51	3
YNL010W	-2.78	2.03	2.07E-10	-0.32	3
WHI2	-2.76	1.64	7.67E-06	-0.22	3
CSM1	-2.73	1.83	2.61E-06	-0.30	3

Supplementary table 2.2. (Continued)					
EAF6	-2.73	1.86	5.38E-05	-0.52	3
MTC6	-2.73	1.81	7.07E-09	-0.17	3
STV1	-2.71	2.01	3.19E-09	-0.24	3
YOL162W	-2.68	1.60	6.57E-05	-0.46	3
ATG27	-2.67	1.81	2.62E-05	-0.64	3
RIT1	-2.67	1.72	8.92E-04	-0.35	3
HSC82	-2.61	1.53	5.10E-04	-0.55	3
RSA3	-2.59	1.75	1.10E-06	-0.18	2
TMA23	-2.59	1.62	2.45E-13	-0.41	3
RPL22A	-2.58	1.68	2.90E-11	-0.92	3
SCW10	-2.57	1.82	8.01E-05	-0.18	3
YPR045C	-2.56	1.44	1.28E-16	-0.15	3
YNL320W	-2.54	1.82	8.73E-04	-0.31	3
RPL16A	-2.54	1.71	3.33E-05	-0.36	2
MNI1	-2.51	1.66	2.13E-05	-0.29	3
AZF1	-2.50	1.81	3.83E-10	-0.22	3
YJR011C	-2.50	2.01	2.20E-06	0.28	3
SKI3	-2.46	1.77	6.67E-07	-0.73	3
YDR056C	-2.46	1.77	5.68E-04	-0.32	3
YPL077C	-2.45	2.97	5.80E-04	-0.56	3
MTC4	-2.41	1.84	1.90E-06	-0.22	3
DAT1	-2.41	2.05	1.73E-07	-0.12	3
THO2	-2.40	1.80	3.16E-06	-0.39	3
STB2	-2.39	1.74	4.75E-11	-0.23	3
FKH2	-2.39	1.80	1.20E-07	-0.20	3
SPL2	-2.37	1.45	2.50E-04	0.00	3
YPR050C	-2.36	1.86	4.21E-05	-0.82	3
YIL152W	-2.35	1.89	1.12E-05	-0.24	3
YKL075C	-2.33	1.77	8.21E-11	-0.29	3
RPS10A	-2.32	0.97	2.74E-05	-0.65	3
MTC2	-2.32	2.22	3.40E-06	-0.25	3
RPL6B	-2.32	1.61	1.45E-06	-0.66	3
YNR025C	-2.30	1.95	1.38E-05	-0.24	3
BUD23	-2.30	1.62	3.33E-04	-0.20	2
GAP1	-2.28	2.20	4.11E-04	-0.23	3
RPS17A	-2.27	1.08	4.68E-04	-0.56	3
SGN1	-2.26	1.77	1.27E-04	-0.21	3
APS3	-2.25	1.96	5.41E-10	-0.65	3
NDJ1	-2.23	1.54	8.37E-05	-0.15	3

Supplementary table 2.2. (Continued)					
PAD1	-2.22	1.80	1.84E-04	-0.27	3
MCT1	-2.22	0.93	3.77E-09	0.09	3
DAL80	-2.22	2.02	4.99E-04	-0.19	3
TMT1	-2.21	1.92	2.25E-06	-0.21	3
RCE1	-2.20	2.13	1.02E-05	-0.37	3
RHO2	-2.20	1.88	6.67E-07	-0.20	3
TMA108	-2.20	1.83	3.22E-04	-0.13	2
ARO1	-2.20	1.75	5.75E-05	-0.37	3
SOL4	-2.20	1.95	7.51E-04	-0.33	3
SLM6	-2.20	1.81	1.10E-09	-0.42	3
MAG2	-2.18	1.81	1.20E-05	-0.30	3
ARP8	-2.18	1.15	4.07E-11	-0.22	3
YBR197C	-2.13	2.11	9.31E-04	-0.30	3
RGP1	-2.12	2.16	2.45E-05	-0.24	3
BUL2	-2.12	2.17	3.07E-05	-0.18	3
TPN1	-2.10	2.17	1.42E-04	-0.32	3
HOM6	-2.10	2.14	8.36E-04	-0.76	3
YML007C-A	-2.05	2.14	1.82E-05	-0.23	3
PIH1	-2.05	1.67	1.99E-09	-0.24	3
BRX1	-2.04	1.94	6.32E-04	-0.31	3
CEM1	-2.04	0.95	4.02E-08	-0.08	3
FYV7	-2.03	1.84	1.09E-08	-0.57	3
LAG1	-2.02	1.76	3.77E-04	-0.22	3
YDL114W	-1.97	1.80	2.97E-04	-0.42	3
STM1	-1.97	2.05	1.35E-05	-0.36	3
HUL5	-1.96	1.83	1.97E-04	-0.23	3
YOR325W	-1.96	2.15	3.28E-05	-0.41	3
CSM2	-1.96	1.88	2.61E-04	-0.16	3
ECM32	-1.94	1.95	7.19E-07	-0.21	3
YEL007W	-1.94	2.71	5.32E-04	-0.22	3
VHS2	-1.94	1.75	1.72E-04	-0.23	2
YOL097W-A	-1.94	1.97	2.25E-06	-0.18	3
SEC20	-1.93	1.96	1.70E-05	-0.19	3
SWD1	-1.93	1.92	1.68E-07	-0.55	3
CYK3	-1.93	2.10	5.00E-06	-0.84	3
ARO9	-1.93	2.08	3.59E-05	-0.23	3
RPS4B	-1.93	2.21	4.69E-09	-0.34	3
RAD16	-1.92	1.88	4.20E-04	-0.16	3
BUD28	-1.91	1.73	2.33E-11	-0.89	3

Supplementary table 2.2. (Continued)					
YKL162C	-1.91	1.75	5.88E-07	-0.16	3
HIS2	-1.90	1.98	4.70E-05	-0.18	3
MRT4	-1.90	1.41	2.42E-06	-0.58	3
CGR1	-1.89	2.01	3.44E-05	-0.43	3
YNL108C	-1.89	1.88	1.14E-05	-0.28	3
YLR428C	-1.89	1.88	2.70E-08	-0.31	3
ATG11	-1.88	1.70	4.85E-04	-0.30	2
PXL1	-1.88	1.85	3.53E-04	-0.30	3
ARO2	-1.87	1.90	1.61E-06	-0.30	2
COG6	-1.87	2.00	1.92E-04	-0.29	3
YJL120W	-1.87	1.94	1.22E-06	-0.42	3
GET3	-1.86	1.98	1.80E-06	-0.46	3
FMP27	-1.85	1.74	4.68E-04	-0.40	3
YGL261C	-1.84	1.72	2.84E-04	-0.29	3
RPL18B	-1.84	1.84	2.24E-07	-0.38	3
RPL9B	-1.83	1.93	1.07E-06	-0.64	3
ARO7	-1.83	1.78	2.34E-05	-0.28	3
BUD7	-1.82	1.80	1.17E-05	-0.31	3
YDR203W	-1.81	2.70	3.45E-04	-0.38	3
PCD1	-1.80	1.90	1.34E-06	-0.23	3
SIP18	-1.79	1.80	4.40E-05	-0.37	3
YMR242W-A	-1.79	1.26	5.25E-06	-0.30	3
YBR174C	-1.79	2.11	4.68E-04	-0.63	3
TRM10	-1.77	1.83	1.12E-10	-0.24	2
RGD1	-1.77	1.76	3.69E-04	-0.36	3
SEH1	-1.77	2.14	8.01E-05	-0.12	3
MCH4	-1.77	1.89	1.19E-04	-0.37	3
CSN12	-1.76	1.94	4.48E-04	-0.42	3
YPR153W	-1.76	2.15	1.97E-07	-0.26	3
MRPL50	-1.76	2.01	1.48E-04	-0.27	3
YPR114W	-1.76	1.80	4.13E-06	-0.30	3
FRE6	-1.75	1.79	8.92E-04	-0.24	3
ITR2	-1.75	1.82	1.07E-04	-0.18	3
CTK2	-1.75	1.53	1.65E-04	-0.34	3
TIF6	-1.74	1.12	8.23E-06	-0.28	3
YOR072W	-1.73	1.80	3.61E-04	-0.33	3
OXR1	-1.73	2.06	2.54E-06	-0.30	3
SEO1	-1.72	1.84	5.32E-04	-0.35	3
DDR2	-1.72	1.92	3.00E-05	-0.20	3

Supplementary table 2.2. (Continued)					
KSS1	-1.72	1.98	1.58E-04	-0.30	3
SAL1	-1.70	1.94	9.31E-04	-0.24	3
RPL41A	-1.70	1.92	6.89E-04	-0.27	3
PEA2	-1.70	2.12	8.18E-04	-0.15	3
KTR7	-1.70	1.91	1.48E-05	-0.19	3
ARO3	-1.69	1.62	4.20E-04	-0.27	3
YAL037C-A	-1.69	1.94	3.68E-05	-0.18	3
HFD1	-1.69	1.85	3.31E-04	-0.50	3
POR2	-1.69	1.86	8.01E-04	-0.24	3
AST2	-1.67	1.96	3.02E-04	-0.14	2
RPL16B	-1.67	1.78	4.80E-07	-0.33	3
YNL190W	-1.67	1.81	3.76E-05	-0.12	3
FBP26	-1.66	2.10	5.38E-05	-0.25	3
YLR363W-A	-1.65	2.10	1.27E-07	-0.19	3
GAL83	-1.64	1.92	8.18E-04	-0.25	3
YIL102C	-1.64	1.88	2.31E-06	-0.15	3
ECM30	-1.63	2.03	8.64E-05	-0.68	2
YDL133W	-1.63	2.11	5.88E-07	-0.30	3
YPR123C	-1.63	2.17	1.92E-07	-0.22	3
YOL046C	-1.62	2.04	4.40E-05	-0.30	3
YKL199C	-1.62	1.83	7.21E-05	-0.18	2
YNL120C	-1.62	2.66	9.78E-08	-0.19	3
YHR199C	-1.61	1.87	8.01E-04	-0.26	3
RPL4A	-1.61	1.75	8.29E-04	-0.27	2
YNR004W	-1.60	1.89	4.50E-05	-0.45	3
PTM1	-1.59	2.08	7.84E-05	-0.31	3
DMC1	-1.59	1.73	1.48E-06	-0.23	3
YKL071W	-1.59	1.61	4.12E-04	-0.24	2
YMC1	-1.59	2.14	5.80E-04	-0.22	3
YGR107W	-1.59	1.66	5.38E-05	-0.25	3
PDB1	-1.58	1.20	5.53E-04	-0.23	2
SWD3	-1.57	2.07	9.15E-05	-0.65	3
YML108W	-1.57	2.06	9.92E-04	-0.53	3
PNP1	-1.56	1.75	3.92E-04	-0.30	2
RPL43B	-1.56	2.03	1.24E-04	-0.46	3
YPR172W	-1.55	1.79	9.51E-04	-0.31	3
YDR095C	-1.55	2.12	1.82E-05	-0.33	3
STE23	-1.55	1.96	3.84E-06	-0.26	3
PSK2	-1.53	2.05	5.32E-04	-0.30	3

Supplementary table 2.2. (Continued)					
YGR035W-A	-1.53	1.89	1.84E-04	-0.17	3
HEF3	-1.52	1.75	1.24E-04	-0.17	3
ARO8	-1.51	2.10	1.07E-05	-0.27	3
MAL32	-1.51	2.03	3.93E-04	-0.19	3
PEP5	-1.50	1.85	1.30E-04	-0.44	3
YOR283W	-1.50	1.84	1.19E-06	-0.19	3
YER108C	-1.48	1.88	2.24E-04	-0.14	3
NMD4	-1.47	1.75	1.48E-04	-0.37	3
YNL067W-B	-1.46	2.03	1.14E-04	-0.97	3
YKL077W	-1.44	1.63	3.66E-06	-0.24	3
EAR1	-1.43	1.91	3.32E-06	-0.37	3
ARL1	-1.42	2.04	9.59E-04	-0.49	2
TOF2	-1.41	1.84	1.12E-05	-0.22	3
CRN1	-1.40	1.91	7.84E-05	-0.26	3
NQM1	-1.39	1.74	1.35E-04	-0.23	2
MET10	-1.38	1.79	1.56E-07	-0.41	3
IPT1	-1.38	1.76	8.73E-04	-0.30	3
YJL213W	-1.38	1.98	8.75E-05	-0.27	3
YHR033W	-1.38	1.91	1.02E-05	-0.26	3
FYV1	-1.36	1.56	9.35E-05	-0.98	3
STI1	-1.35	2.01	7.84E-05	-0.33	3
YKL063C	-1.35	1.88	4.13E-08	-0.26	3
EGD1	-1.35	1.92	2.39E-05	-0.52	3
PDR16	-1.35	2.14	2.19E-04	-0.12	3
PMD1	-1.35	1.81	1.88E-04	-0.23	3
YJR107W	-1.33	1.76	1.99E-05	-0.45	3
YIL158W	-1.32	1.89	2.14E-04	-0.17	3
YMR272W-B	-1.32	1.91	1.84E-04	-0.15	3
BUD31	-1.31	0.80	7.50E-05	-0.34	3
YER135C	-1.30	1.91	1.55E-05	-0.24	3
SNT309	-1.29	1.09	3.28E-04	-0.76	2
SEY1	-1.29	1.61	1.00E-04	-0.23	2
MNN9	-1.28	1.88	4.02E-07	-0.22	3
RPC25	-1.28	0.90	8.78E-09	-0.78	3
YGL140C	-1.28	1.89	5.21E-04	-0.24	3
YLL047W	-1.27	1.70	3.10E-04	-0.21	3
BRE1	-1.25	2.07	6.89E-04	-0.97	3
YLR225C	-1.25	1.78	2.14E-04	-0.21	2
LRP1	-1.22	1.51	6.89E-04	-0.24	3

Supplementary table 2.2. (Continued)					
NAB6	-1.21	1.90	3.03E-04	-0.62	3
YJR146W	-1.20	1.87	1.22E-04	-0.38	3
LYS14	-1.19	1.14	8.04E-06	-0.75	3
THI12	-1.19	1.86	2.08E-05	-0.10	3
PAI3	-1.18	1.88	5.80E-04	-0.26	3
DBP3	-1.17	1.76	9.77E-05	-0.37	3
TIF6	-1.16	1.44	8.23E-06	-0.38	3
TKL1	-1.16	1.83	1.09E-04	-0.36	3
YGR054W	-1.15	2.01	2.19E-04	-0.17	3
RPN14	-1.14	1.78	2.97E-04	-0.15	3
RPL19A	-1.14	1.67	3.20E-07	-0.83	3
YGR160W	-1.13	1.21	2.54E-07	-0.89	3
YPS3	-1.12	1.93	5.10E-04	-0.30	3
RAV2	-1.12	1.80	9.05E-06	-0.87	3
MCK1	-1.11	1.80	2.39E-04	-0.62	3
NCS2	-1.11	1.83	6.79E-08	-0.25	3
ERG28	-1.11	1.86	2.78E-04	-0.25	3
MMS2	-1.11	1.97	8.01E-04	-0.34	3
YJL064W	-1.10	1.97	5.75E-05	-0.34	3
IMH1	-1.09	1.99	5.80E-04	-0.19	3
RCK1	-1.09	1.84	1.13E-06	-0.22	3
YGR122W	-1.08	2.02	2.72E-04	-0.49	3
YDL157C	-1.07	1.89	8.18E-04	-0.23	3
RRS1	-1.07	1.75	4.65E-06	-0.29	3
KTI11	-1.07	1.46	1.60E-06	-0.22	3
UBP13	-1.07	2.08	5.25E-06	-0.24	3
MYO3	-1.04	1.77	1.84E-05	-0.21	2
YMR209C	-1.02	1.77	6.74E-04	-0.27	3
CTK3	-1.02	1.87	8.73E-04	1.06	3

Supplementary table 2.3. List of array strains used in the double mutant analysis. For constitutively induced mutants, normalized log2 ratios to the *pho80* DAmP strain are not available. Some genes do not have normalized log2 ratios to the *pho80* DAmP strain because I added them regardless of the screening data due to its interest.

Gene	normalized log2(YFP/RFP) to wild type in 50 uM P_i as a single mutant	Averaged log2 ratio normalized ratio to the *pho80* mutant
THP1	-3.95	Constitutively induced mutants
PHO80	2.51	Constitutively induced mutants
YOR200W	-2.21	Constitutively induced mutants
PHO90	-2.44	Constitutively induced mutants
SAC3	-3.47	Constitutively induced mutants
ADK1	1.53	Constitutively induced mutants
PHO87	-3.24	Constitutively induced mutants
KCS1	0.57	Constitutively induced mutants
EAP1	-3.07	Constitutively induced mutants
AAH1	0.56	Constitutively induced mutants
UGO1	-2.01	Constitutively induced mutants
PHO85	2.55	Constitutively induced mutants
RPL2B	-3.18	
YER087W	-3.26	Constitutively induced mutants
MSN5	1.72	
ADO1	1.55	Constitutively induced mutants
SEO1	-1.70	-0.35
PEX22	-1.79	-0.43
YPS3	-1.49	-0.30
CHA4	-2.77	-0.54
FYV7	-2.67	-0.57
BUD28	-3.54	-0.89
RPL22A	-3.84	-0.92
HSC82	-2.56	-0.55
RPS17A	-2.46	-0.56
SWD1	-2.32	-0.55
TRM9	-3.42	-0.55
IRC25	-2.53	-0.81
YMR010W	-2.30	-0.44

Supplementary table 2.3. (Continued)		
SOK2	-1.81	-0.41
PEP5	-1.86	-0.44
SPA2	-3.00	-0.38
FRE6	-1.74	-0.24
YLL047W	-1.53	-0.21
RPL20A	-4.25	-0.49
RCE1	-2.32	-0.37
RPS10A	-2.18	-0.65
BUD7	-1.87	-0.31
PSK2	-1.95	-0.30
YOL046C	-2.31	-0.30
RIT1	-1.91	-0.35
TIR2	-2.16	
HST3	-2.03	
STI1	-1.83	-0.33
SCW10	-1.52	-0.18
YOR338W	-1.77	-0.27
THI12	-1.55	-0.10
WHI2	-1.85	-0.22
YNL320W	-1.78	-0.31
RPL18B	-1.76	-0.38
RIM21	-1.67	-0.33
YOR072W	-1.45	-0.33
WHI5	-3.04	
YPL225W	-1.71	-0.37
YBR174C	-2.09	-0.63
SWD3	-2.09	-0.65
DOA4	-4.10	
RPP2B	-4.03	
IPT1	-1.24	-0.30
SNF11	-3.26	-0.65
OXR1	-2.49	-0.30
YDR095C	-2.28	-0.33
RSA1	-4.50	-0.45
YBR197C	-1.39	-0.30
PDB1	-1.34	-0.23
YEL007W	-1.17	-0.22
ARO1	-2.50	-0.37
GCN4	-2.45	

Supplementary table 2.3. (Continued)		
RGP1	-2.10	-0.24
MTC4	-2.61	-0.22
RGD1	-0.96	-0.36
SLM6	-3.27	-0.42
MAK10	-1.93	-0.39
YDR056C	-1.56	-0.32
NSR1	-4.73	-0.13
YGR160W	-2.09	-0.89
PIH1	-3.05	-0.24
YHR199C	-1.38	-0.26
RPS4B	-2.43	-0.34
LDB16	-3.69	-0.55
SGF29	-1.07	-0.33
SSF1	-2.54	-0.31
ELP2	-1.62	-0.30
LRP1	-1.90	-0.24
CEM1	-2.06	-0.08
UBA4	-2.66	-1.01
SER3	-0.91	-0.11
SPL2	-1.79	0.00
ARO9	-2.19	-0.23
MTC6	-2.99	-0.17
LAG1	-2.24	-0.22
YKL063C	-1.39	-0.26
STM1	-2.12	-0.36
PCD1	-0.66	-0.23
YKL071W	-1.94	-0.24
RUP1	-1.07	-0.31
ARP8	-2.36	-0.22
RPL26B	-1.94	
YKL075C	-1.92	-0.29
YKL077W	-1.04	-0.24
YLR184W	-2.00	-0.57
NQM1	-1.45	-0.23
SEY1	-1.06	-0.23
YGR054W	-1.67	-0.17
MTC2	-2.64	-0.25
PNP1	-1.17	-0.30
APN1	-1.33	-0.15

Supplementary table 2.3. (Continued)		
RPL11B	-1.66	
RSA3	-2.27	-0.18
YLR225C	-1.09	-0.21
MYO3	-1.64	-0.21
YGR107W	-1.02	-0.25
MCT1	-2.77	0.09
MRT4	-2.77	-0.58
YGR122W	-1.87	-0.49
PTM1	-1.92	-0.31
YKL162C	-1.34	-0.16
AZF1	-1.98	-0.22
STE3	-1.42	
HNT3	-1.56	
YOR283W	-1.62	-0.19
NMD4	-1.35	-0.37
ARO8	-2.39	-0.27
ACO2	-1.86	
IMH1	-1.57	-0.19
BUD19	-5.99	
ATG27	-2.49	-0.64
FBP26	-1.90	-0.25
YGL261C	-1.20	-0.29
YDR203W	-2.59	-0.38
RPS6A	-2.24	-0.35
BRO1	-4.23	
YLR345W	-1.35	-0.33
YPL077C	-2.72	-0.56
YPR172W	-1.28	-0.31
ATG13	-1.26	-0.16
MLC2	-1.38	-0.14
SKI3	-2.09	-0.73
HPA2	-1.31	-0.16
YPR197C	-2.13	-0.51
EGD1	-1.81	-0.52
RIM8	-1.80	-0.59
RPL19B	-3.53	-0.34
DBP3	-1.68	-0.37
PAD1	-1.32	-0.27
FMP37	-1.61	

Supplementary table 2.3. (Continued)		
MMS2	-1.60	-0.34
YPR114W	-1.33	-0.30
UBP13	-1.63	-0.24
RPS8A	-1.41	-0.58
PDR16	-2.07	-0.12
YPR123C	-2.15	-0.22
PHO81	-5.99	-0.19
RPN14	-1.17	-0.15
YPR153W	-2.13	-0.26
YNL190W	-1.48	-0.12
YKL199C	-1.19	-0.18
YVH1	-0.96	-0.44
RTT103	-2.86	0.91
YDR290W	-2.99	0.82
BUD27	-3.02	-0.40
HUA1	-1.11	-0.21
TRM10	-1.27	-0.24
ITR2	-1.10	-0.18
NDJ1	-1.42	-0.15
OPI11	-4.41	-0.30
YPR045C	-3.09	-0.15
AIM22	-0.62	-0.21
ATG11	-1.30	-0.30
RPS7A	-1.35	0.05
ODC1	-0.68	-0.19
MCH4	-1.24	-0.37
MAK3	-2.67	
YMC1	-1.67	-0.22
ARO7	-2.60	-0.28
TKL1	-1.93	-0.36
YML108W	-1.87	-0.53
DAT1	-3.00	-0.12
SPO14	-2.38	-0.23
ECM40	-3.76	
VIP1	-1.45	-0.19
NAB6	-1.73	-0.62
HTD2	-1.68	-0.94
RIM13	-2.09	-0.60
PHO84	-3.91	-0.44

Supplementary table 2.3. (Continued)		
SNF6	-4.42	-0.74
SNT309	-1.30	-0.76
YOL162W	-1.45	-0.46
YJL120W	-1.68	-0.42
EAF6	-1.80	-0.52
HFD1	-1.40	-0.50
DLT1	-2.74	-0.37
YJR146W	-1.17	-0.38
ICS3	-1.30	-0.36
PXL1	-1.21	-0.30
EAR1	-2.26	-0.37
YMR209C	-0.91	-0.27
ELP6	-1.16	-0.30
YJL064W	-1.35	-0.34
YJR107W	-0.97	-0.45
MAG2	-1.16	-0.30
YLR428C	-1.52	-0.31
CRN1	-1.32	-0.26
LYS14	-1.65	
ARO3	-0.95	-0.27
ECM30	-1.49	-0.68
HOM6	-1.74	-0.76
YLR446W	-1.06	-0.15
RPL6B	-2.59	-0.66
FPR4	-1.67	-0.80
HIT1	-4.28	-0.48
SCS22	-1.24	-0.35
APS2	-1.18	-0.29
FMP27	-0.87	-0.40
UNG1	-1.38	-0.27
GET3	-1.62	-0.46
YDL114W	-1.39	-0.42
CYK3	-2.37	-0.84
YOR309C	-3.24	-0.01
PAI3	-1.09	-0.26
SIP18	-1.18	-0.37
YDL133W	-2.16	-0.30
YDL157C	-0.84	-0.23
CSM1	-1.88	-0.30

Supplementary table 2.3. (Continued)		
YGL214W	-5.61	
APS3	-2.67	-0.65
CSN12	-1.51	-0.42
RPL43B	-1.13	-0.46
FYV1	-1.25	-0.98
RPL41A	-1.34	-0.27
YJR011C	-0.84	0.28
YOR309C	-1.75	-0.08
YOR325W	-2.20	-0.41
YNL010W	-3.22	-0.32
POR2	-1.14	-0.24
RAV2	-1.52	-0.87
SIM1	-2.08	-0.24
MET18	-1.03	-0.17
YBR028C	-1.15	-0.30
RPL4A	-1.29	-0.27
CSM2	-1.30	-0.16
RPL16A	-1.14	-0.36
VHS2	-1.50	-0.23
KSS1	-1.61	-0.30
TMA108	-1.92	-0.13
SPT4	-2.82	0.80
COG6	-1.27	-0.29
YIL152W	-1.23	-0.24
SOL4	-1.07	-0.33
ATO2	-1.06	-0.24
YNR004W	-0.76	-0.45
SGN1	-1.45	-0.21
YJL175W	-4.23	-0.29
RPL39	-3.89	-0.16
YBR074W	-1.00	-0.19
MRPL50	-1.55	-0.27
YNR025C	-1.23	-0.24
ACO2	-1.28	0.13
YJL213W	-1.13	-0.27
THO2	-1.49	-0.39
TOF2	-1.56	-0.22
RPL9B	-1.41	-0.64
FKH2	-2.18	-0.20

Supplementary table 2.3. (Continued)		
DAL80	-1.84	-0.19
GAP1	-1.40	-0.23
YNL108C	-1.42	-0.28
SAL1	-0.94	-0.24
RPL19A	-2.14	-0.83
MNI1	-1.34	-0.29
NCS2	-1.28	-0.25
YNL120C	-1.42	-0.19
APM3	-2.93	-0.65
SNF5	-4.11	
BUD23	-1.94	-0.20
VMA2	-1.99	-0.31
TUP1	-2.42	
ADA2	-2.31	
HIS2	-1.28	-0.18
GAL83	-2.02	-0.25
MET10	-1.50	-0.41
ARL1	-2.04	-0.49
YPR050C	-2.14	-0.82
HIT1	-4.49	-0.24
RAD16	-1.11	-0.16
TMT1	-1.16	-0.21
ECM32	-1.10	-0.21
DMC1	-1.06	-0.23
YGL140C	-1.01	-0.24
HUL5	-1.21	-0.23
STE23	-1.17	-0.26
RPC25	-1.35	-0.78
ARO2	-1.64	-0.30
STB2	-2.43	-0.23
STV1	-1.98	-0.24
RCK1	-1.08	-0.22
MNN9	-0.45	-0.22
YIL102C	-0.90	-0.15
YIL158W	-0.76	-0.17
DJP1	-0.95	
KTR7	-1.06	-0.19
BRE1	-1.40	-0.97
AST2	-1.03	-0.14

Supplementary table 2.3. (Continued)		
YER108C	-1.00	-0.14
LPD1	-1.49	
BUL2	-2.07	-0.18
CTK3	-1.20	1.06
ERG28	-0.52	-0.25
YHR033W	-1.07	-0.26
BUD31	-1.40	-0.34
MAL32	-0.13	-0.19
SAK1	-2.77	-0.59
PMD1	-0.68	-0.23
YER135C	-1.30	-0.24
CTK2	-1.84	-0.34
PEA2	-1.09	-0.15
HEF3	-0.74	-0.17
PDX3	-2.55	
YAL037C-A	-1.12	-0.18
KTI11	-1.70	-0.22
SEH1	-1.24	-0.12
YBR196C-A	-3.34	-0.42
TPN1	-1.59	-0.32
MDJ1	-1.87	
YLR363W-A	-1.12	-0.19
YML007C-A	-2.40	-0.23
YMR242W-A	-1.63	-0.30
YGL188C-A	0.00	-0.80
YGR035W-A	-0.85	-0.17
YMR272W-B	-0.92	-0.15
YNL067W-B	-1.46	-0.97
CGR1	-1.68	-0.43
EFG1	-3.70	-0.29
DDR2	-0.65	-0.20
YOL097W-A	-0.78	-0.18
TMA23	-2.99	-0.41
RHO2	-1.24	-0.20
BRX1	-1.01	-0.31
YPL038W-A	-1.06	-0.20
RPB4	-4.16	
YJR151W-A	-3.24	-0.20
RPL16B	-1.67	-0.33

Supplementary table 2.3. (Continued)		
MCK1	-0.92	-0.62
RPL36B	-4.30	-1.00
GPI11	-0.89	-0.46
SEC20	-1.18	-0.19
SPB4	-1.41	
SHR3	-3.55	-0.74
TIM50	-1.85	-0.26
RET1	-0.96	-0.29
TIF6	-1.30	-0.38
TIF6	-1.05	-0.28
RRS1	-1.62	-0.29
LYS14	-1.42	-0.75
PTC4	-1.90	-0.53

Supplementary table 2.4. List of genes whose double mutant with the *aah1* mutant is uninducible. Uninducible double mutants were chosen as the ones whose normalized log2 ratio to the wild type in 50 uM P_i is lower than -4. The reporter level of the wild type when the PHO pathway is repressed is -4.5.

Gene	normalized log2(YFP/RFP) to wild type in 50 uM P_i as a single mutant	normalized log2(YFP/RFP) to wild type in 50 uM P_i as a double mutant of the *aah1* mutant	normalized log2(YFP/RFP) to wild type in 50 uM P_i as a double mutant of the *ado1* mutant
VIP1	-1.66	-6.48	-4.47
YJL175W	-5.14	-5.91	-4.47
RPL39	-3.98	-5.89	-2.93
RPL36B	-4.64	-5.71	-3.58
PHO81	-5.75	-5.48	-5.16
OPI11	-4.73	-5.45	-5.60
BUD31	-1.06	-5.42	0.28
TMA23	-3.91	-5.39	-4.55
TRM9	-4.38	-5.34	-5.37
YGL188C-A	-1.55	-5.20	-2.39
ACO2	-5.25	-5.17	-0.33
IPT1	-1.59	-5.12	0.98
RPS17A	-1.17	-5.12	0.19
YPR045C	-2.85	-5.10	-5.79
TUP1	-2.88	-5.03	-3.07
PIH1	-2.31	-5.02	0.25
RPP2B	-3.52	-4.95	-0.12
RSA1	-3.77	-4.89	-5.25
RPS10A	-1.69	-4.87	-0.79
RPL19B	-3.19	-4.85	1.14
ARP8	-1.54	-4.83	-2.83
EFG1	-4.17	-4.83	0.22
BUD28	-1.99	-4.82	0.52
MRT4	-0.68	-4.81	-0.13
ADA2	-2.47	-4.80	-4.64
NSR1	-3.97	-4.75	-1.19
RPS6A	-2.62	-4.73	0.74
RPS8A	0.69	-4.71	0.05
ARO2	-1.83	-4.70	1.00
ELP6	-2.17	-4.65	1.12
RPS4B	-2.70	-4.61	-2.29

Supplementary table 2.4. (Continued)			
SSF1	-2.60	-4.56	0.12
ECM40	-3.49	-4.44	-2.02
ARO1	-2.61	-4.43	-0.22
RPL20A	-3.24	-4.42	0.35
RPC25	-1.28	-4.39	-2.17
RPL22A	-3.27	-4.39	0.91
TKL1	-0.79	-4.31	-3.99
KTI11	-1.58	-4.31	-4.31
RPL6B	-2.79	-4.25	0.39
WHI5	-3.79	-4.25	0.98
RPS7A	0.58	-4.25	1.61
LDB16	0.34	-4.24	-0.56
YLR184W	-1.08	-4.19	0.88
BUD27	-1.82	-4.19	-0.74
HSC82	-2.68	-4.18	1.12
UBA4	-2.80	-4.18	1.18
BUD23	-2.23	-4.16	1.43
TIF6	-0.90	-4.13	-2.10
SLM6	-2.60	-4.12	1.09
SKI3	-2.72	-4.05	-0.85

Supplementary table 2.5. List of genes whose double mutant with the *ado1* mutant is uninducible. Uninducible double mutants were chosen as the ones whose normalized log2 ratio to wild type in 50 uM P_i is lower than -4. The reporter level of the wild type when the PHO pathway is repressed is -4.5.

Gene	normalized log2(YFP/RFP) to wild type in 50 uM P_i as a single mutant	normalized log2(YFP/RFP) to wild type in 50 uM P_i as a double mutant of the *aah1* mutant	normalized log2(YFP/RFP) to wild type in 50 uM P_i as a double mutant of the *ado1* mutant
YPR045C	-2.85	-5.10	-5.79
OPI11	-4.73	-5.45	-5.60
CTK2	-2.33	-3.30	-5.59
TRM9	-4.38	-5.34	-5.37
RSA1	-3.77	-4.89	-5.25
SSM4	-0.22	-1.02	-5.18
PHO81	-5.75	-5.48	-5.16
ATG11	-2.61	-2.73	-5.01
MMS2	-0.80	-1.06	-4.67
ADA2	-2.47	-4.80	-4.64
YEL007W	-2.30	-0.20	-4.56
TMA23	-3.91	-5.39	-4.55
YML108W	-1.85	-0.79	-4.53
YJL175W	-5.14	-5.91	-4.47
RIM8	-1.07	1.53	-4.47
VIP1	-1.66	-6.48	-4.47
MAG2	-1.38	-1.79	-4.44
KTI11	-1.58	-4.31	-4.31

Supplementary table 2.6. List of genes whose double mutant with the *vip1* mutant is uninducible. Uninducible double mutants were chosen as the ones whose normalized log2 ratio to wild type in 50 uM P_i is lower than -4. The reporter level of the wild type when the PHO pathway is repressed is -4.5.

Gene	normalized log2(YFP/RFP) to wild type in 50 uM P_i as a single mutant	normalized log2(YFP/RFP) to wild type in 50 uM P_i as a double mutant of the *vip1* mutant	normalized log2(YFP/RFP) to wild type in 50 uM P_i as a double mutant of the *ipk1* mutant
RPL39	-3.98	-6.86	-6.72
BUD19	-0.15	-6.83	-6.69
RPP2B	-3.52	-6.56	-6.06
YGL188C-A	-1.55	-6.56	-5.37
FYV7	-4.30	-6.40	-6.21
YPR045C	-2.85	-6.38	0.23
RPL20A	-3.24	-6.35	-6.02
RPS7A	0.58	-6.29	-5.38
YLR184W	-1.08	-6.25	-5.52
YMR242W-A	-1.32	-6.23	-5.83
NSR1	-3.97	-6.21	-5.60
RPL36B	-4.64	-6.20	-6.24
RPL6B	-2.79	-6.19	-5.13
SLM6	-2.60	-6.18	-5.32
RPL22A	-3.27	-6.18	-5.32
RPL11B	-1.75	-6.17	-4.97
TMA23	-3.91	-6.15	-5.22
EFG1	-4.17	-6.15	-5.35
TUP1	-2.88	-6.13	-6.20
SSF1	-2.60	-6.09	-3.86
BUD28	-1.99	-6.08	-5.29
LRP1	-0.27	-6.08	-3.91
MRT4	-0.68	-6.07	-3.85
RPL16B	-1.47	-6.04	-3.82
DOA4	-3.88	-6.02	-5.19
MET18	-1.89	-6.01	-5.17
RRS1	-1.09	-5.99	-3.86
RPS4B	-2.70	-5.91	-3.60
CTK2	-2.33	-5.88	-3.40
YGR160W	-1.06	-5.74	-5.28
PHO81	-5.75	-5.73	-6.02

Supplementary table 2.6. (Continued)			
SPB4	-0.72	-5.73	-2.46
BRX1	-3.66	-5.71	-2.72
BUD23	-2.23	-5.66	-4.51
RSA1	-3.77	-5.61	-4.94
BUD27	-1.82	-5.61	-3.83
SNF6	-5.14	-5.50	-2.21
PDB1	-0.05	-5.48	-4.27
WHI5	-3.79	-5.45	-3.48
ARP8	-1.54	-5.42	-4.12
MNI1	-2.44	-5.39	-2.14
ELP6	-2.17	-5.37	-3.32
RPL16A	-2.98	-5.35	-2.42
NPR2	-2.65	-5.27	-4.28
MCT1	-1.94	-5.24	-5.13
YJL175W	-5.14	-5.10	-4.79
RPS8A	0.69	-5.05	-1.80
UBA4	-2.80	-4.91	-4.04
RPL19A	-1.73	-4.80	-2.12
HTD2	-1.16	-4.78	-4.76
UBP15	-0.65	-4.74	-2.09
TIF6	-0.43	-4.72	-1.90
SHR3	-3.28	-4.70	-1.23
PIH1	-2.31	-4.69	-1.46
HNT3	-0.17	-4.68	-2.37
ELP2	-0.57	-4.66	-0.92
RPC25	-1.28	-4.65	-2.62
RSA3	-1.57	-4.65	-1.33
CHA4	-2.73	-4.62	-2.24
ARO1	-2.61	-4.59	-4.58
CTK3	-1.20	-4.58	-1.13
HST3	-2.66	-4.57	-2.98
YKL075C	-2.93	-4.57	-0.70
GCN4	-1.78	-4.51	-4.90
THP1	-2.63	-4.46	-2.68
YNL120C	-1.26	-4.46	-0.97
PEP5	-1.55	-4.46	-0.33
RPS6A	-2.62	-4.43	-2.58
FYV1	-1.80	-4.42	-4.12
SEO1	-2.49	-4.40	-0.82

Supplementary table 2.6. (Continued)			
SPA2	-2.49	-4.34	-0.86
APM3	-2.84	-4.34	-2.75
DBP3	-1.69	-4.31	-1.29
YDR290W	-2.28	-4.17	-1.85
RPL26B	-1.94	-4.15	-0.16
SNF5	-3.77	-4.14	-5.30
YDR203W	-1.54	-4.08	-1.69
TCO89	-4.84	-4.06	-5.02
RTT103	-2.75	-4.05	-1.32

Supplementary table 2.7. List of genes whose double mutant with the *ipk1* mutant is uninducible. Uninducible double mutants were chosen as the ones whose normalized log2 ratio to wild type in 50 uM P_i is lower than -4. The reporter level of the wild type when the PHO pathway is repressed is -4.5.

Gene	normalized log2(YFP/RFP) to wild type in 50 uM P_i as a single mutant	normalized log2(YFP/RFP) to wild type in 50 uM P_i as a double mutant of the *vip1* mutant	normalized log2(YFP/RFP) to wild type in 50 uM P_i as a double mutant of the *ipk1* mutant
RPL39	-3.98	-6.86	-6.72
BUD19	-0.15	-6.83	-6.69
RPL36B	-4.64	-6.20	-6.24
FYV7	-4.30	-6.40	-6.21
TUP1	-2.88	-6.13	-6.20
RPP2B	-3.52	-6.56	-6.06
PHO81	-5.75	-5.73	-6.02
RPL20A	-3.24	-6.35	-6.02
YMR242W-A	-1.32	-6.23	-5.83
NSR1	-3.97	-6.21	-5.60
YLR184W	-1.08	-6.25	-5.52
RPS7A	0.58	-6.29	-5.38
YGL188C-A	-1.55	-6.56	-5.37
EFG1	-4.17	-6.15	-5.35
RPL22A	-3.27	-6.18	-5.32
SLM6	-2.60	-6.18	-5.32
SNF5	-3.77	-4.14	-5.30
BUD28	-1.99	-6.08	-5.29
YGR160W	-1.06	-5.74	-5.28
TMA23	-3.91	-6.15	-5.22
DOA4	-3.88	-6.02	-5.19
MET18	-1.89	-6.01	-5.17
RPL6B	-2.79	-6.19	-5.13
MCT1	-1.94	-5.24	-5.13
TCO89	-4.84	-4.06	-5.02
RPL11B	-1.75	-6.17	-4.97
CEM1	-0.85	-0.66	-4.95
RSA1	-3.77	-5.61	-4.94
GCN4	-1.78	-4.51	-4.90
TRM9	-4.38	-1.92	-4.81
YJL175W	-5.14	-5.10	-4.79

Supplementary table 2.7. (Continued)			
HTD2	-1.16	-4.78	-4.76
ARO1	-2.61	-4.59	-4.58
BUD23	-2.23	-5.66	-4.51
NPR2	-2.65	-5.27	-4.28
PDB1	-0.05	-5.48	-4.27
AIM22	-0.28	-1.03	-4.25
FYV1	-1.80	-4.42	-4.12
ARP8	-1.54	-5.42	-4.12
UBA4	-2.80	-4.91	-4.04

Supplementary table 3.1. Relative abundance of metabolites to 10 mM P_i condition. Time course data obtained in no P_i were normalized to the values in 10 mM P_i. This table was used to generate Figure 3.1.

	Time (minutes)							
Metabolites	0	2	5	10	15	30	60	90
CTP	1.00	1.55	1.73	1.41	1.23	1.10	1.15	1.05
phosphoenolpyruvate	1.00	1.28	1.00	1.27	1.44	1.00	1.53	1.44
GMP	1.00	0.81	0.32	0.67	0.47	0.53	0.50	0.59
CDP	1.00	0.59	0.66	0.64	0.67	0.84	0.68	0.60
UDP-D-glucose	1.00	0.84	0.65	0.79	0.90	1.01	0.67	0.79
glucose-6-phosphate	1.00	0.71	0.61	0.69	0.79	0.89	0.84	0.79
ribulose-5-phosphate/xylulose-5-phosphate	1.00	0.75	0.75	0.78	0.88	0.95	0.73	0.80
guanine	1.00	0.33	0.63	0.48	0.68	0.69	0.70	0.88
3-phosphoglycerate	1.00	0.52	0.55	0.62	1.37	1.22	0.96	1.34
ribose-5-phosphate	1.00	0.83	0.75	1.06	1.11	1.08	0.88	0.80
cytidine	1.00	0.84	0.87	0.58	1.09	0.99	0.47	0.57
IMP	1.00	0.77	0.77	0.71	0.63	0.47	0.82	0.76
fructose-1_6-bisphosphate	1.00	1.18	0.99	1.03	0.87	0.77	0.72	0.67
sedoheptulose bisphosphate	1.00	0.99	0.82	1.04	0.87	0.76	0.90	0.64
dihydroxyacetone phosphate	1.00	1.04	0.95	1.02	1.02	0.91	0.72	0.76
UTP	1.00	0.96	0.98	1.14	0.95	0.85	0.73	0.86
pyrophosphate	1.00	1.06	0.98	1.10	0.90	0.70	0.64	0.61
N-carbamoyl-L-aspartate	1.00	0.74	0.71	0.77	0.59	0.38	0.51	0.49
ADP	1.00	0.82	0.65	0.74	0.82	0.51	0.53	0.54
NADP+	1.00	1.00	0.87	0.88	0.80	0.53	0.43	0.40
acetyl-CoA	1.00	1.04	0.99	0.89	0.62	0.37	0.43	0.43
ATP	1.00	0.79	0.82	1.00	0.59	0.38	0.41	0.55
dTTP	1.00	0.80	0.85	0.80	0.97	0.44	0.37	0.62
FMN	1.00	0.87	0.78	0.70	0.73	0.53	0.49	0.49
deoxyribose-phosphate	1.00	0.23	0.27	0.23	0.18	0.17	0.22	0.15
glucono-delta-lactone	1.00	0.24	0.28	0.26	0.18	0.17	0.20	0.16
GDP	1.00	1.33	1.09	0.97	0.70	0.40	0.41	0.45
GTP	1.00	1.76	1.38	1.52	0.50	0.35	0.36	0.67
glycerol-3-phosphate	1.00	1.12	1.06	0.95	0.73	0.81	0.69	0.66
NAD+	1.00	1.15	0.97	1.10	0.98	0.70	0.76	0.69
NADH	1.00	0.97	1.14	1.00	0.88	0.57	0.53	0.49
FAD	1.00	1.16	1.07	0.87	0.53	0.16	0.24	0.24
dihydroorotate	1.00	0.65	0.58	0.49	0.45	0.13	0.30	0.28

Supplementary table 3.1. (Continued)								
orotidine-5--phosphate	1.00	1.09	1.06	1.07	0.99	0.51	0.69	0.68
glutathione	1.00	0.69	0.18	0.39	0.03	0.49	0.90	1.06
S-methyl-5--thioadenosine	1.00	0.96	0.66	0.73	0.78	0.62	0.73	0.76
AMP	1.00	0.51	0.31	0.44	0.44	0.41	0.45	0.39
hydroxyisocaproic acid	1.00	0.18	0.15	0.21	0.22	0.23	0.48	0.51
phenyllactic acid	1.00	0.14	0.16	0.19	0.22	0.27	0.51	0.61
phenylpyruvate	1.00	0.19	0.17	0.20	0.24	0.36	0.66	0.77
indole-3-carboxylic acid	1.00	0.03	0.05	0.03	0.07	0.08	0.17	0.19
xanthurenic acid	1.00	0.02	0.02	0.03	0.04	0.06	0.12	0.20
kynurenic acid	1.00	0.30	0.32	0.22	0.22	0.21	0.19	0.23
orotate	1.00	0.24	0.27	0.26	0.20	0.14	0.28	0.33
methylmalonic acid	1.00	0.55	0.44	0.42	0.40	0.38	0.47	0.60
succinate	1.00	0.55	0.44	0.42	0.40	0.38	0.47	0.60
dTDP	1.00	0.72	0.47	0.46	0.68	0.77	0.89	0.69
pyruvate	1.00	0.91	0.87	0.93	0.90	0.98	1.00	0.98
octulose-8-phosphate	1.00	0.54	0.32	0.49	0.82	0.97	0.72	0.66
sedoheptulose-7-phosphate	1.00	0.56	0.61	0.72	0.88	0.99	0.87	0.83
acetyllysine	1.00	0.75	0.78	0.82	1.15	1.36	1.09	1.15
asparagine	1.00	0.86	0.77	0.64	0.72	1.25	1.06	1.05
glutamine	1.00	0.96	0.83	0.83	0.93	1.20	0.99	1.10
2-isopropylmalic acid	1.00	0.89	0.54	0.93	1.05	1.03	1.56	1.82
serine	1.00	0.89	0.75	1.04	0.98	0.96	1.53	1.17
homocysteine	1.00	0.65	0.63	0.80	1.02	1.39	1.51	1.04
N-acetyl-glucosamine-1/6-phosphate	1.00	0.67	0.71	0.90	1.15	1.02	0.95	0.91
CDP-ethanolamine	1.00	1.11	0.88	0.72	1.32	1.13	1.07	1.17
UMP	1.00	0.66	0.59	0.60	0.62	0.77	0.88	0.77
aspartate	1.00	0.90	0.74	0.78	0.92	1.18	0.96	1.01
fumarate	1.00	0.73	0.60	0.54	0.52	0.81	0.99	1.55
malate	1.00	0.74	0.61	0.51	0.47	0.76	0.94	1.55
hypoxanthine	1.00	0.90	0.58	0.60	0.86	0.88	0.94	1.14
imidazoleacetic acid	1.00	0.91	0.91	0.84	1.12	1.22	0.36	0.85
sarcosine	1.00	1.14	0.54	1.07	1.12	1.44	0.55	0.70
NADPH	1.00	0.94	1.23	1.37	1.68	1.34	1.23	1.12
glutathione disulfide	1.00	1.30	2.11	1.94	2.70	1.86	1.58	1.74
N-acetyl-L-alanine	1.00	2.44	1.87	2.13	2.04	2.55	1.63	2.23
4-aminobutyrate	1.00	1.05	1.19	1.34	1.42	1.23	1.23	1.21
glutamate	1.00	1.12	1.11	1.14	1.17	1.09	1.07	1.07
aconitate	1.00	1.47	1.44	1.41	1.38	1.51	2.20	2.78
citrate	1.00	1.41	1.53	1.48	1.43	1.79	2.49	3.20

Supplementary table 3.1. (Continued)								
S-adenosyl-L-homocysteine	1.00	19.2	17.1	15.2	16.4	17.7	14.0	16.6
cystathionine	1.00	1.23	1.15	1.44	1.44	1.26	1.44	1.45
gluconate	1.00	1.43	1.67	1.38	1.26	1.13	1.44	1.32
N-acetyl-L-ornithine	1.00	2.49	3.22	2.65	1.89	1.62	1.96	1.51
methionine sulfoxide	1.00	1.79	2.22	1.93	1.36	1.39	1.56	1.23
indole	1.00	1.83	2.14	1.77	1.56	1.39	1.52	0.99
trehalose	1.00	1.82	2.03	1.77	1.58	1.49	1.48	1.22
hydroxyproline	1.00	2.91	3.02	2.56	2.56	2.22	2.02	1.85
inosine	1.00	2.35	2.08	1.93	2.08	1.91	1.55	2.00
guanosine	1.00	1.24	1.00	0.89	0.95	1.22	1.16	1.71
ornithine	1.00	1.27	1.17	1.17	1.22	1.19	0.96	0.80
trehalose-6-Phosphate	1.00	1.92	1.49	2.03	2.84	1.29	0.94	0.93
glycerate	1.00	1.42	1.35	1.05	0.53	0.63	1.21	0.67

Supplementary table 3.2. Relative abundance of metabolites to no P_i condition. Time course data obtained in 10 mM P_i were normalized to the values in no P_i. This table was used to generate Figure 3.1.

	Time (minutes)								
Metabolites	0	0.5	1.5	3	5	10	15	30	60
CTP	1.00	1.73	1.70	1.55	2.00	1.76	1.72	1.65	1.77
phosphoenolpyruvate	1.00	1.58	1.69	2.15	2.70	2.46	2.45	2.94	2.68
GMP	1.00	2.00	1.59	1.66	1.54	1.95	2.31	1.86	1.86
CDP	1.00	1.94	1.75	1.74	1.43	1.45	1.91	1.68	1.91
UDP-D-glucose	1.00	1.38	1.34	1.27	1.29	1.20	1.63	1.29	1.31
glucose-6-phosphate	1.00	1.15	1.26	1.32	1.45	1.60	1.33	1.46	1.45
ribulose-5-phosphate/xylulose-5-phosphate	1.00	1.10	1.05	1.03	1.26	1.37	1.57	1.52	1.60
guanine	1.00	1.63	1.43	1.56	1.62	1.20	1.21	1.55	1.79
3-phosphoglycerate	1.00	1.97	2.09	1.78	1.96	1.93	2.46	2.21	2.57
ribose-5-phosphate	1.00	1.20	1.13	1.30	1.17	1.26	1.53	1.46	1.66
cytidine	1.00	6.06	2.32	2.68	2.32	1.90	2.25	1.46	1.93
IMP	1.00	2.24	1.57	2.38	3.13	2.13	2.65	3.18	3.30
fructose-1_6-bisphosphate	1.00	1.26	1.39	1.54	1.52	1.53	1.47	1.53	1.64
sedoheptulose bisphosphate	1.00	1.22	1.20	1.50	1.51	1.51	1.54	1.46	1.41
dihydroxyacetone phosphate	1.00	1.55	1.47	1.29	1.56	1.22	1.61	1.56	1.72
UTP	1.00	1.39	1.31	1.46	1.51	1.50	1.37	1.34	1.31
pyrophosphate	1.00	42.8	42.5	45.1	44.2	43.0	38.4	37.1	30.7
N-carbamoyl-L-aspartate	1.00	1.70	1.75	1.16	0.97	0.85	1.27	0.99	0.65
ADP	1.00	1.26	1.19	1.14	1.20	1.24	1.21	1.09	1.02
NADP+	1.00	1.35	1.34	1.07	1.17	1.16	1.20	1.15	1.07
acetyl-CoA	1.00	1.30	1.24	1.24	1.28	1.16	1.10	1.15	1.15
ATP	1.00	1.32	1.32	1.38	1.54	1.53	1.39	1.44	1.34
dTTP	1.00	1.23	1.30	1.26	1.38	1.58	1.35	1.46	1.39
FMN	1.00	1.55	1.41	1.66	1.13	1.41	1.35	1.22	1.44
deoxyribose-phosphate	1.00	3.19	3.23	3.87	3.86	3.79	2.89	3.58	2.60
glucono-delta-lactone	1.00	3.34	3.38	3.78	3.73	3.41	3.15	3.21	2.34
GDP	1.00	2.24	2.03	1.77	1.52	1.38	1.93	1.99	1.72
GTP	1.00	1.59	1.45	1.54	1.88	1.64	1.56	1.59	1.37
glycerol-3-phosphate	1.00	1.16	1.23	1.04	1.15	1.00	1.10	1.04	1.01
NAD+	1.00	0.96	0.97	0.97	0.93	0.98	0.94	0.96	0.94
NADH	1.00	0.86	1.08	0.92	1.00	0.92	1.14	1.06	0.90

Supplementary table 3.2. (Continued)									
FAD	1.00	0.93	1.04	1.11	0.91	0.94	0.74	0.80	0.59
dihydroorotate	1.00	0.77	0.90	0.94	0.78	1.08	0.74	0.95	0.70
orotidine-5--phosphate	1.00	1.00	0.98	1.00	0.86	0.94	0.89	1.22	1.52
glutathione	1.00	1.04	0.98	0.97	1.00	0.99	0.89	0.93	0.79
S-methyl-5--thioadenosine	1.00	1.01	0.77	0.82	0.92	0.98	0.84	0.91	1.00
AMP	1.00	1.36	1.23	1.09	1.52	1.09	1.42	1.09	1.12
hydroxyisocaproic acid	1.00	1.11	1.05	1.06	1.08	1.24	1.17	1.39	1.71
phenyllactic acid	1.00	1.07	1.01	0.98	1.07	1.24	1.10	1.30	1.60
phenylpyruvate	1.00	1.06	1.04	1.04	1.23	1.20	1.09	1.44	1.53
indole-3-carboxylic acid	1.00	0.98	0.91	1.01	1.03	1.06	1.09	1.10	1.22
xanthurenic acid	1.00	1.00	0.97	0.76	1.18	1.05	1.11	1.18	1.33
kynurenic acid	1.00	0.83	0.82	0.73	0.83	1.01	0.81	0.98	1.32
orotate	1.00	1.06	1.01	1.11	1.03	1.03	0.97	1.19	1.35
methylmalonic acid	1.00	1.12	0.93	0.91	0.87	0.87	0.76	0.93	0.93
succinate	1.00	1.12	0.93	0.91	0.87	0.87	0.76	0.93	0.93
dTDP	1.00	1.33	1.00	0.97	1.16	1.21	1.51	1.24	1.26
pyruvate	1.00	1.03	1.03	1.03	0.98	1.05	1.08	1.04	1.03
octulose-8-phosphate	1.00	1.12	0.75	1.16	0.81	1.18	1.42	1.49	1.64
sedoheptulose-7-phosphate	1.00	0.95	1.04	1.10	1.11	1.11	1.41	1.41	1.43
acetyllysine	1.00	1.24	1.17	1.10	1.17	1.17	1.05	0.77	0.67
asparagine	1.00	1.06	1.05	1.01	1.00	0.98	0.93	1.00	1.09
glutamine	1.00	1.18	1.10	1.10	1.08	1.06	1.09	1.00	1.05
2-isopropylmalic acid	1.00	1.17	1.17	1.10	1.20	1.25	1.26	1.30	1.37
serine	1.00	1.19	1.12	1.00	1.09	0.99	1.00	0.98	1.04
homocysteine	1.00	1.41	0.99	1.39	1.17	1.00	1.58	0.76	1.46
N-acetyl-glucosamine-1/6-phosphate	1.00	0.90	0.85	0.96	1.07	0.99	0.96	0.87	1.18
CDP-ethanolamine	1.00	1.05	1.35	0.80	0.37	0.66	0.73	0.79	1.48
UMP	1.00	0.67	0.64	0.64	0.78	0.75	0.77	0.60	0.79
aspartate	1.00	1.04	1.07	0.95	0.85	0.76	0.75	0.80	0.91
fumarate	1.00	1.13	1.04	0.89	0.79	0.58	0.57	0.66	0.94
malate	1.00	1.10	1.06	0.88	0.77	0.60	0.57	0.70	0.93
hypoxanthine	1.00	1.13	1.03	0.85	0.86	0.85	0.78	0.91	1.31
imidazoleacetic acid	1.00	1.07	0.92	0.92	1.13	0.59	0.76	0.81	0.71
sarcosine	1.00	1.03	1.04	0.91	0.81	0.72	0.70	0.75	0.87
NADPH	1.00	1.52	1.31	1.07	1.15	0.88	1.00	1.31	1.17
glutathione disulfide	1.00	0.99	0.98	1.23	1.21	1.23	1.50	1.08	4.35
N-acetyl-L-alanine	1.00	1.23	1.23	1.14	0.63	0.57	1.23	0.68	0.83

Supplementary table 3.2. (Continued)									
4-aminobutyrate	1.00	1.10	1.08	1.06	1.01	1.01	1.09	0.97	0.97
glutamate	1.00	1.04	1.06	1.01	1.02	1.02	1.08	0.98	0.98
aconitate	1.00	1.08	0.74	1.18	0.66	0.58	0.96	0.70	0.56
citrate	1.00	1.12	1.21	1.15	1.12	1.03	0.90	0.68	0.47
S-adenosyl-L-homocysteine	1.00	0.14	0.13	0.11	0.10	0.13	0.11	0.15	0.17
cystathionine	1.00	0.86	0.90	0.77	0.83	0.76	0.91	0.71	0.89
gluconate	1.00	0.84	0.92	0.89	0.93	0.85	0.74	0.81	0.66
N-acetyl-L-ornithine	1.00	0.84	0.80	0.93	0.97	0.90	0.76	0.72	0.47
methionine sulfoxide	1.00	0.84	0.82	0.91	0.87	0.87	0.74	0.74	0.61
indole	1.00	0.83	0.82	0.78	0.88	0.85	0.63	0.68	0.51
trehalose	1.00	0.88	0.92	0.75	0.85	0.84	0.63	0.68	0.60
hydroxyproline	1.00	0.86	0.85	0.99	0.90	0.79	0.73	0.70	0.67
inosine	1.00	1.05	1.09	0.90	0.79	0.75	0.60	0.64	0.69
guanosine	1.00	0.80	0.74	0.54	0.59	0.53	0.44	0.46	0.53
ornithine	1.00	0.86	0.75	0.74	0.74	0.74	0.72	0.67	0.70
trehalose-6-Phosphate	1.00	0.48	0.43	0.46	0.55	0.61	0.73	0.80	0.78
glycerate	1.00	0.71	0.69	0.73	0.80	0.80	0.66	0.70	0.62

References

BLAZQUEZ, M. A., LAGUNAS, R., GANCEDO, C. & GANCEDO, J. M. 1993. Trehalose-6-phosphate, a new regulator of yeast glycolysis that inhibits hexokinases. *FEBS Lett,* 329**,** 51-4.

BOER, V. M., CRUTCHFIELD, C. A., BRADLEY, P. H., BOTSTEIN, D. & RABINOWITZ, J. D. 2010. Growth-limiting intracellular metabolites in yeast growing under diverse nutrient limitations. *Mol Biol Cell,* 21**,** 198-211.

BOONE, C., BUSSEY, H. & ANDREWS, B. J. 2007. Exploring genetic interactions and networks with yeast. *Nat Rev Genet,* 8**,** 437-49.

BRACHMANN, C. B., DAVIES, A., COST, G. J., CAPUTO, E., LI, J., HIETER, P. & BOEKE, J. D. 1998. Designer deletion strains derived from Saccharomyces cerevisiae S288C: a useful set of strains and plasmids for PCR-mediated gene disruption and other applications. *Yeast,* 14**,** 115-32.

BRAUER, M. J., YUAN, J., BENNETT, B. D., LU, W., KIMBALL, E., BOTSTEIN, D. & RABINOWITZ, J. D. 2006. Conservation of the metabolomic response to starvation across two divergent microbes. *Proc Natl Acad Sci U S A,* 103**,** 19302-7.

BRESLOW, D. K., CAMERON, D. M., COLLINS, S. R., SCHULDINER, M., STEWART-ORNSTEIN, J., NEWMAN, H. W., BRAUN, S., MADHANI, H. D., KROGAN, N. J. & WEISSMAN, J. S. 2008. A comprehensive strategy enabling high-resolution functional analysis of the yeast genome. *Nat Methods,* 5**,** 711-8.

BRODY, S., OH, C., HOJA, U. & SCHWEIZER, E. 1997. Mitochondrial acyl carrier protein is involved in lipoic acid synthesis in Saccharomyces cerevisiae. *FEBS Lett,* 408**,** 217-20.

BUN-YA, M., NISHIMURA, M., HARASHIMA, S. & OSHIMA, Y. 1991. The PHO84 gene of Saccharomyces cerevisiae encodes an inorganic phosphate transporter. *Mol Cell Biol,* 11**,** 3229-38.

CHOI, M. G., KURNOV, V., KERSTING, M. C., SREENIVAS, A. & CARMAN, G. M. 2005. Phosphorylation of the yeast choline kinase by protein kinase C. Identification of Ser25 and Ser30 as major sites of phosphorylation. *J Biol Chem,* 280**,** 26105-12.

CHRISTOPHER, S. A., MELNYK, S., JAMES, S. J. & KRUGER, W. D. 2002. S-adenosylhomocysteine, but not homocysteine, is toxic to yeast lacking cystathionine beta-synthase. *Mol Genet Metab,* 75**,** 335-43.

COLLINS, S. R., MILLER, K. M., MAAS, N. L., ROGUEV, A., FILLINGHAM, J., CHU, C. S., SCHULDINER, M., GEBBIA, M., RECHT, J., SHALES, M., DING, H., XU, H., HAN, J., INGVARSDOTTIR, K., CHENG, B., ANDREWS, B., BOONE, C., BERGER, S. L., HIETER, P., ZHANG, Z., BROWN, G. W., INGLES, C. J., EMILI, A., ALLIS, C. D., TOCZYSKI, D. P., WEISSMAN, J. S., GREENBLATT, J. F. & KROGAN, N. J. 2007. Functional dissection of protein complexes involved in yeast chromosome biology using a genetic interaction map. *Nature,* 446**,** 806-10.

EISEN, M. B., SPELLMAN, P. T., BROWN, P. O. & BOTSTEIN, D. 1998. Cluster analysis and display of genome-wide expression patterns. *Proc Natl Acad Sci U S A,* 95**,** 14863-8.

EJSING, C. S., SAMPAIO, J. L., SURENDRANATH, V., DUCHOSLAV, E., EKROOS, K., KLEMM, R. W., SIMONS, K. & SHEVCHENKO, A. 2009. Global analysis of the yeast lipidome by quantitative shotgun mass spectrometry. *Proc Natl Acad Sci U S A,* 106**,** 2136-41.

FIEHN, O., KOPKA, J., DORMANN, P., ALTMANN, T., TRETHEWEY, R. N. & WILLMITZER, L. 2000. Metabolite profiling for plant functional genomics. *Nat Biotechnol,* 18**,** 1157-61.

GULER, J. L., KRIEGOVA, E., SMITH, T. K., LUKES, J. & ENGLUND, P. T. 2008. Mitochondrial fatty acid synthesis is required for normal mitochondrial morphology and function in Trypanosoma brucei. *Mol Microbiol,* 67**,** 1125-42.

HILTUNEN, J. K., SCHONAUER, M. S., AUTIO, K. J., MITTELMEIER, T. M., KASTANIOTIS, A. J. & DIECKMANN, C. L. 2009. Mitochondrial fatty acid synthesis type II: more than just fatty acids. *J Biol Chem,* 284**,** 9011-5.

HUANG, S. & O'SHEA, E. K. 2005. A systematic high-throughput screen of a yeast deletion collection for mutants defective in PHO5 regulation. *Genetics,* 169**,** 1859-71.

IVES, E. B., NICHOLS, J., WENTE, S. R. & YORK, J. D. 2000. Biochemical and functional characterization of inositol 1,3,4,5, 6-pentakisphosphate 2-kinases. *J Biol Chem,* 275**,** 36575-83.

JONIKAS, M. C., COLLINS, S. R., DENIC, V., OH, E., QUAN, E. M., SCHMID, V., WEIBEZAHN, J., SCHWAPPACH, B., WALTER, P., WEISSMAN, J. S. & SCHULDINER, M. 2009. Comprehensive characterization of genes required for protein folding in the endoplasmic reticulum. *Science,* 323**,** 1693-7.

KAFFMAN, A., HERSKOWITZ, I., TJIAN, R. & O'SHEA, E. K. 1994. Phosphorylation of the transcription factor PHO4 by a cyclin-CDK complex, PHO80-PHO85. *Science,* 263**,** 1153-6.

KAFFMAN, A., RANK, N. M., O'NEILL, E. M., HUANG, L. S. & O'SHEA, E. K. 1998a. The receptor Msn5 exports the phosphorylated transcription factor Pho4 out of the nucleus. *Nature,* 396**,** 482-6.

KAFFMAN, A., RANK, N. M. & O'SHEA, E. K. 1998b. Phosphorylation regulates association of the transcription factor Pho4 with its import receptor Pse1/Kap121. *Genes Dev,* 12**,** 2673-2683.

KASTANIOTIS, A. J., AUTIO, K. J., SORMUNEN, R. T. & HILTUNEN, J. K. 2004. Htd2p/Yhr067p is a yeast 3-hydroxyacyl-ACP dehydratase essential for mitochondrial function and morphology. *Mol Microbiol,* 53**,** 1407-21.

KONRAD, M. 1988. Analysis and in vivo disruption of the gene coding for adenylate kinase (ADK1) in the yeast Saccharomyces cerevisiae. *Journal of Biological Chemistry,* 263**,** 19468-19474.

LECOQ, K., BELLOC, I., DESGRANGES, C. & DAIGNAN-FORNIER, B. 2001. Role of adenosine kinase in Saccharomyces cerevisiae: identification of the ADO1 gene and study of the mutant phenotypes. *Yeast,* 18**,** 335-42.

LEE, H., KIM, J. H., CHAE, Y. J., OGAWA, H., LEE, M. H. & GERTON, G. L. 1998. Creatine synthesis and transport systems in the male rat reproductive tract. *Biol Reprod,* 58**,** 1437-44.

LEE, Y. S., HUANG, K., QUIOCHO, F. A. & O'SHEA, E. K. 2008. Molecular basis of cyclin-CDK-CKI regulation by reversible binding of an inositol pyrophosphate. *Nat Chem Biol,* 4**,** 25-32.

LEE, Y. S., MULUGU, S., YORK, J. D. & O'SHEA, E. K. 2007. Regulation of a cyclin-CDK-CDK inhibitor complex by inositol pyrophosphates. *Science,* 316**,** 109-12.

LU, W., CLASQUIN, M. F., MELAMUD, E., AMADOR-NOGUEZ, D., CAUDY, A. A. & RABINOWITZ, J. D. 2010. Metabolomic analysis via reversed-phase ion-pairing liquid chromatography coupled to a stand alone orbitrap mass spectrometer. *Anal Chem,* 82**,** 3212-21.

MALANOVIC, N., STREITH, I., WOLINSKI, H., RECHBERGER, G., KOHLWEIN, S. D. & TEHLIVETS, O. 2008. S-adenosyl-L-homocysteine hydrolase, key enzyme of methylation metabolism, regulates phosphatidylcholine synthesis and triacylglycerol homeostasis in yeast: implications for homocysteine as a risk factor of atherosclerosis. *J Biol Chem,* 283**,** 23989-99.

MANI, R., ST ONGE, R. P., HARTMAN, J. L. T., GIAEVER, G. & ROTH, F. P. 2008. Defining genetic interaction. *Proc Natl Acad Sci U S A,* 105**,** 3461-6.

MONSERRATE, J. P. & YORK, J. D. 2010. Inositol phosphate synthesis and the nuclear processes they affect. *Curr Opin Cell Biol,* 22**,** 365-73.

NEEF, D. W. & KLADDE, M. P. 2003. Polyphosphate Loss Promotes SNF/SWI- and Gcn5-Dependent Mitotic Induction of PHO5. *Molecular and Cellular Biology,* 23**,** 3788-3797.

O'NEILL, E. M., KAFFMAN, A., JOLLY, E. R. & O'SHEA, E. K. 1996. Regulation of PHO4 nuclear localization by the PHO80-PHO85 cyclin-CDK complex. *Science,* 271**,** 209-12.

OGAWA, N., DERISI, J. & BROWN, P. O. 2000. New components of a system for phosphate accumulation and polyphosphate metabolism in Saccharomyces cerevisiae revealed by genomic expression analysis. *Mol Biol Cell,* 11**,** 4309-21.

OSHIMA, Y. 1997. The phosphatase system in Saccharomyces cerevisiae. *Genes Genet Syst,* 72**,** 323-34.

OZCAN, S., DOVER, J. & JOHNSTON, M. 1998. Glucose sensing and signaling by two glucose receptors in the yeast Saccharomyces cerevisiae. *EMBO J,* 17**,** 2566-73.

OZCAN, S., DOVER, J., ROSENWALD, A. G., WOLFL, S. & JOHNSTON, M. 1996a. Two glucose transporters in Saccharomyces cerevisiae are glucose sensors that generate a signal for induction of gene expression. *Proc Natl Acad Sci U S A,* 93**,** 12428-32.

OZCAN, S., LEONG, T. & JOHNSTON, M. 1996b. Rgt1p of Saccharomyces cerevisiae, a key regulator of glucose-induced genes, is both an activator and a repressor of transcription. *Mol Cell Biol,* 16**,** 6419-26.

PELICANO, H., MARTIN, D. S., XU, R. H. & HUANG, P. 2006. Glycolysis inhibition for anticancer treatment. *Oncogene,* 25**,** 4633-46.

RAAMSDONK, L. M., TEUSINK, B., BROADHURST, D., ZHANG, N., HAYES, A., WALSH, M. C., BERDEN, J. A., BRINDLE, K. M., KELL, D. B., ROWLAND, J. J., WESTERHOFF, H. V., VAN DAM, K. & OLIVER, S. G. 2001. A functional genomics strategy that uses metabolome data to reveal the phenotype of silent mutations. *Nat Biotechnol,* 19**,** 45-50.

SCHNEIDER, K. R., SMITH, R. L. & O'SHEA, E. K. 1994. Phosphate-regulated inactivation of the kinase PHO80-PHO85 by the CDK inhibitor PHO81. *Science,* 266**,** 122-6.

SCHNEIDER, R., BRORS, B., BURGER, F., CAMRATH, S. & WEISS, H. 1997. Two genes of the putative mitochondrial fatty acid synthase in the genome of Saccharomyces cerevisiae. *Curr Genet,* 32**,** 384-8.

SCHULDINER, M., COLLINS, S. R., THOMPSON, N. J., DENIC, V., BHAMIDIPATI, A., PUNNA, T., IHMELS, J., ANDREWS, B., BOONE, C., GREENBLATT, J. F., WEISSMAN, J. S. & KROGAN, N. J. 2005.

Exploration of the function and organization of the yeast early secretory pathway through an epistatic miniarray profile. *Cell,* 123**,** 507-19.

SEGRE, D., DELUNA, A., CHURCH, G. M. & KISHONY, R. 2005. Modular epistasis in yeast metabolism. *Nat Genet,* 37**,** 77-83.

TEHLIVETS, O., SCHEURINGER, K. & KOHLWEIN, S. D. 2007. Fatty acid synthesis and elongation in yeast. *Biochim Biophys Acta,* 1771**,** 255-70.

THOMAS, M. R. & O'SHEA, E. K. 2005. An intracellular phosphate buffer filters transient fluctuations in extracellular phosphate levels. *Proc Natl Acad Sci U S A,* 102**,** 9565-70.

TO, E. A., UEDA, Y., KAKIMOTO, S. I. & OSHIMA, Y. 1973. Isolation and characterization of acid phosphatase mutants in Saccharomyces cerevisiae. *J Bacteriol,* 113**,** 727-38.

TONG, A. H. & BOONE, C. 2006. Synthetic genetic array analysis in Saccharomyces cerevisiae. *Methods Mol Biol,* 313**,** 171-92.

TONG, A. H., EVANGELISTA, M., PARSONS, A. B., XU, H., BADER, G. D., PAGE, N., ROBINSON, M., RAGHIBIZADEH, S., HOGUE, C. W., BUSSEY, H., ANDREWS, B., TYERS, M. & BOONE, C. 2001. Systematic genetic analysis with ordered arrays of yeast deletion mutants. *Science,* 294**,** 2364-8.

TONG, A. H., LESAGE, G., BADER, G. D., DING, H., XU, H., XIN, X., YOUNG, J., BERRIZ, G. F., BROST, R. L., CHANG, M., CHEN, Y., CHENG, X., CHUA, G., FRIESEN, H., GOLDBERG, D. S., HAYNES, J., HUMPHRIES, C., HE, G., HUSSEIN, S., KE, L., KROGAN, N., LI, Z., LEVINSON, J. N., LU, H., MENARD, P., MUNYANA, C., PARSONS, A. B., RYAN, O., TONIKIAN, R., ROBERTS, T., SDICU, A. M., SHAPIRO, J., SHEIKH, B., SUTER, B., WONG, S. L., ZHANG, L. V., ZHU, H., BURD, C. G., MUNRO, S., SANDER, C., RINE, J., GREENBLATT, J., PETER, M., BRETSCHER, A., BELL, G., ROTH, F. P., BROWN, G. W., ANDREWS, B., BUSSEY, H. & BOONE, C. 2004. Global mapping of the yeast genetic interaction network. *Science,* 303**,** 808-13.

VOGEL, K., HORZ, W. & HINNEN, A. 1989. The two positively acting regulatory proteins PHO2 and PHO4 physically interact with PHO5 upstream activation regions. *Mol Cell Biol,* 9**,** 2050-7.

WINZELER, E. A., SHOEMAKER, D. D., ASTROMOFF, A., LIANG, H., ANDERSON, K., ANDRE, B., BANGHAM, R., BENITO, R., BOEKE, J. D., BUSSEY, H., CHU, A. M., CONNELLY, C., DAVIS, K., DIETRICH, F., DOW, S. W., EL BAKKOURY, M., FOURY, F., FRIEND, S. H., GENTALEN, E., GIAEVER, G., HEGEMANN, J. H., JONES, T., LAUB, M., LIAO, H., LIEBUNDGUTH, N., LOCKHART, D. J., LUCAU-DANILA, A., LUSSIER, M., M'RABET, N., MENARD, P., MITTMANN, M., PAI, C., REBISCHUNG, C., REVUELTA, J. L., RILES, L., ROBERTS, C. J., ROSS-MACDONALD, P., SCHERENS, B., SNYDER, M., SOOKHAI-MAHADEO, S., STORMS, R. K., VERONNEAU, S., VOET, M., VOLCKAERT, G., WARD, T. R., WYSOCKI, R., YEN, G. S., YU, K., ZIMMERMANN, K., PHILIPPSEN, P., JOHNSTON, M. & DAVIS, R. W. 1999. Functional characterization of the S. cerevisiae genome by gene deletion and parallel analysis. *Science,* 285**,** 901-6.
WOLFE, M. S. & BORCHARDT, R. T. 1991. S-adenosyl-L-homocysteine hydrolase as a target for antiviral chemotherapy. *J Med Chem,* 34**,** 1521-30.

WYKOFF, D. D. & O'SHEA, E. K. 2001. Phosphate transport and sensing in Saccharomyces cerevisiae. *Genetics,* 159**,** 1491-9.

WYKOFF, D. D., RIZVI, A. H., RASER, J. M., MARGOLIN, B. & O'SHEA, E. K. 2007. Positive feedback regulates switching of phosphate transporters in S. cerevisiae. *Mol Cell,* 27**,** 1005-13.

XU, Y. F., AMADOR-NOGUEZ, D., REAVES, M. L., FENG, X. J. & RABINOWITZ, J. D. 2012. Ultrasensitive regulation of anapleurosis via allosteric activation of PEP carboxylase. *Nat Chem Biol,* 8**,** 562-8.

YORK, J. D. 2006. Regulation of nuclear processes by inositol polyphosphates. *Biochim Biophys Acta,* 1761**,** 552-9.

YORK, S. J., ARMBRUSTER, B. N., GREENWELL, P., PETES, T. D. & YORK, J. D. 2005. Inositol diphosphate signaling regulates telomere length. *J Biol Chem,* 280**,** 4264-9.

ZAMAN, S., LIPPMAN, S. I., ZHAO, X. & BROACH, J. R. 2008. How Saccharomyces responds to nutrients. *Annu Rev Genet,* 42**,** 27-81.